

1 List of changes

2	Replaced: Static	13
3	Replaced: Dynamic	13
4	Replaced: Constructing	14
5	Replaced: Producing	14
6	Replaced: Adding	14
7	Replaced: Calculating	14
8	Replaced: Intermediate	15
9	Replaced: Dynamic	15
10	Replaced: Static	16
11	Replaced: Static	20
12	Added: of operation	33
13	Replaced: dynamic	33
14	Replaced: static	33
15	Replaced: static	33
16	Replaced: dynamic	33
17	Replaced: Dynamic	33
18	Added: (see Table 3.1)	33
19	Replaced: Static	33
20	Added: The overall structure...	34
21	Replaced: many hours	34
22	Added: density	34
23	Added: – see Fig. 2-1	34

24	Replaced: Is it stretched out like...	34
25	Replaced: cross-sections	35
26	Replaced: result from a slice acr...	35
27	Added: Their exact usage wit...	35
28	Replaced: essentially parabolas	36
29	Added: density	36
30	Replaced: profiles	37
31	Deleted: profiles	37
32	Added: just	37
33	Added: Although not self-...	37
34	Added: The reason \bar{n} is referr...	38
35	Added: A final point to make...	38
36	Added: Density	38
37	Added: density	38
38	Added: These are derived in A...	39
39	Replaced: The steady current wi...	39
40	Replaced: a density limit that a...	40
41	Replaced: disrupt.	40
42	Added: These conclusions can...	40
43	Added: and	40
44	Added: .	40
45	Deleted: and π has its usual m...	40
46	Replaced: it accurately predicts...	41
47	Deleted: (i.e. the ones we use)	42

48	Replaced: dynamic	42
49	Replaced: static	42
50	Replaced: static	42
51	Replaced: in equilibrium	42
52	Replaced: Its underlying behavi...	42
53	Replaced: Utilizing the surface i...	42
54	Deleted: Here, Q is an arbitrar...	42
55	Deleted: This allows the boots...	43
56	Added: The second definition...	43
57	Deleted: For a more formal loo...	43
58	Added: The instructions to do...	43
59	Deleted: Getting back on track...	43
60	Deleted: Recognizing that the l...	43
61	Deleted: In standardized units,...	43
62	Added: Finally, summarizing...	44
63	Replaced: static	44
64	Deleted: The next segue on our...	44
65	Deleted: The natural place to s...	44
66	Deleted: What this reaction de...	45
67	Deleted: The final point to ma...	45
68	Added: The next segue on our...	45
69	Replaced: Summarized, though,...	45
70	Replaced: the following volume i...	45
71	Added: (f_D). This dilution fa...	45

72	Replaced: dynamic	46
73	Deleted: As mentioned before,	47
74	Replaced: this chapter's	47
75	Replaced: static	47
76	Replaced: static	48
77	Replaced: static	48
78	Replaced: The	48
79	Replaced: chapter	48
80	Added: Further, each temper	49
81	Replaced: static	51
82	Replaced: dynamic	51
83	Replaced: dynamic	51
84	Replaced: Static	51
85	Replaced: static	51
86	Replaced: static	51
87	Replaced: static	51
88	Replaced: static	51
89	Replaced: Dynamic	52
90	Replaced: Dynamic	52
91	Replaced: static	67
92	Replaced: static	68
93	Replaced: static	68
94	Replaced: static	71
95	Replaced: static	72

96	Added: reactor design	77
97	Added: This generalized plas	77
98	Replaced: This is described by t	78
99	Added: During this time, a pl	80
100	Added: The exact definitions f	81
101	Added: – usually measured in	82
102	Added: microhenry-scale	82
103	Replaced: static	87
104	Replaced: Constructing	88
105	Added: – as dictated by cycli	89
106	Added: flattop	89
107	Replaced: expected	89
108	Replaced: Producing	89
109	Added: the	91
110	Added: code	91
111	Replaced: Adding	91
112	Replaced: as much as a 50% im	91
113	Replaced: drifting radially	92
114	Added: (valid for a circular pl	92
115	Replaced: After a few lines of al	92
116	Replaced: spiraled	94
117	Replaced: Calculating	95
118	Deleted: strongly	95
119	Added: mainly	95

120	Deleted: a little	95
121	Deleted: Here, the constant ter	95
122	Replaced: Here, P_W	95
123	Replaced: Section 3.4.3	95
124	Replaced: a previous model	96
125	Replaced: dynamic	96
126	Replaced: static	97
127	Replaced: static	97
128	Replaced: dynamic	97
129	Replaced: static	98
130	Replaced: dynamic	100
131	Replaced: dynamic	101
132	Replaced: resolve a similar problem	102
133	Replaced: intermediate	107
134	Replaced: dynamic	107
135	Replaced: dynamic (D)	107
136	Replaced: intermediate (I)	107
137	Replaced: dynamic	108
138	Replaced: intermediate	108
139	Replaced: dynamic	108
140	Replaced: static	108
141	Replaced: Intermediate	109
142	Replaced: intermediate	109
143	Replaced: Dynamic	109

144	Replaced: dynamic	109
145	Replaced: static	113
146	Replaced: static	113
147	Replaced: dynamic	121
148	Replaced: static	124
149	Replaced: dynamic	128
150	Replaced: static	128
151	Replaced: static	135
152	Replaced: Static	151
153	Replaced: Static	151
154	Replaced: static	156
155	Replaced: static	157
156	Replaced: dynamic	158
157	Replaced: static	158
158	Replaced: dynamic	158
159	Replaced: static	158
160	Replaced: dynamic	158

A Levelized Comparison of Pulsed and Steady-State Tokamaks

by

Daniel Joseph Segal

B.S. Engineering Physics, University of Wisconsin (2014)

Submitted to the Department of Nuclear Science and Engineering
in partial fulfillment of the requirements for the degree of

Master of Science in Nuclear Science and Engineering

at the

MASSACHUSETTS INSTITUTE OF TECHNOLOGY

February 2018

© Massachusetts Institute of Technology 2018. All rights reserved.

Author

Department of Nuclear Science and Engineering

November 11, 2018

Certified by

Jeffrey P. Freidberg

KEPCO Professor Emeritus

Thesis Supervisor

Certified by

Anne E. White

Cecil and Ida Green Associate Professor

Thesis Reader

Accepted by

Ju Li

Battelle Energy Alliance Professor

Chair, Department Committee on Graduate Students

161 **A Levelized Comparison of**
162 **Pulsed and Steady-State Tokamaks**

163 by

164 Daniel Joseph Segal

165 Submitted to the Department of Nuclear Science and Engineering
166 on November 11, 2018, in partial fulfillment of the
167 requirements for the degree of
168 Master of Science in Nuclear Science and Engineering

169 **Abstract**

170 The goal of fusion energy research is to build a profitable reactor. This thesis develops
171 a cost estimate model for fusion reactors from a physicist's perspective. It then applies
172 it to the two main modes of operation for a tokamak reactor: pulsed and steady-state.
173 In the end, an apples-to-apples comparison is developed, which is used to explain:
174 the relative advantages of pulsed and steady-state operation, as well as, the design
175 parameters that provide the most leverage in lowering machine costs. The most
176 notable of these is the magnetic field strength – which should be doubled by ongoing
177 research efforts at MIT using high-temperature superconducting (HTS) tape.

Thesis Supervisor: Jeffrey P. Freidberg
Title: Professor of Nuclear Science and Engineering (Emeritus)

Contents

179	1	Introducing Fusion Reactors	23
180	1.1	Treating Fusion as a Science	23
181	1.2	Treating Fusion as a Business	26
182	1.3	Pricing a Fusion Reactor	28
183	1.4	Modeling a Fusion Reactor	30
184	2	Designing a Steady-State Tokamak	33
185	2.1	Defining Plasma Parameters	34
186	2.1.1	Understanding Tokamak Geometry	34
187	2.1.2	Prescribing Plasma Profiles	36
188	2.2	Solving the Steady Current	39
189	2.2.1	Enforcing the Greenwald Density Limit	40
190	2.2.2	Declaring the Bootstrap Current	42
191	2.2.3	Deriving the Fusion Power	44
192	2.2.4	Using Current Drive	47
193	2.2.5	Completing the Steady Current	48
194	2.3	Handling Current Drive Self-Consistently	49
195	3	Formalizing the Systems Model	51
196	3.1	Explaining StaticFixed Variables	51
197	3.2	Connecting DynamicFloating Variables	52
198	3.3	Enforcing Power Balance	56
199	3.3.1	Collecting Power Sources	56
200	3.3.2	Approximating Radiation Losses	58

201	3.3.3	Estimating Heat Conduction Losses	59
202	3.3.4	Writing the Lawson Criterion	61
203	3.3.5	Finalizing the Primary Constraint	63
204	3.3.6	Exploring the Freidberg Criterion	66
205	3.4	Collecting Secondary Constraints	67
206	3.4.1	Introducing the Beta Limit	68
207	3.4.2	Giving the Kink Safety Factor	69
208	3.4.3	Working under the Wall Loading Limit	70
209	3.4.4	Setting a Maximum Power Cap	72
210	3.4.5	Listing the Heat Loading Limit	73
211	3.5	Summarizing the Fusion Systems Model	74
212	4	Designing a Pulsed Tokamak	77
213	4.1	Modeling Plasmas as Circuits	78
214	4.1.1	Drawing the Circuit Diagram	78
215	4.1.2	Plotting Pulse Profiles	80
216	4.1.3	Specifying Circuit Variables	84
217	4.1.4	Constructing Reasoning the Pulse Length	88
218	4.2	Producing Salvaging Flux Balance	89
219	4.2.1	Rearranging the Circuit Equation	90
220	4.2.2	Adding Importing Poloidal Field Coils	91
221	4.3	Improving Tokamak Geometry	93
222	4.3.1	Defining Central Solenoid Dimensions	93
223	4.3.2	Calculating Measuring Component Thicknesses	95
224	4.3.3	Revisiting Central Solenoid Dimensions	97
225	4.4	Piecing Together the Generalized Current	99
226	4.5	Simplifying the Generalized Current	101
227	4.5.1	Recovering the Steady Current	101
228	4.5.2	Extracting the Pulsed Current	102
229	4.5.3	Rationalizing the Generalized Current	103

230	5	Completing the Systems Model	105
231	5.1	Describing a Simple Algebra	105
232	5.2	Generalizing Previous Equations	107
233	5.2.1	Rehashing the Limits	108
234	5.2.2	Minimizing Intermediate Derived Quantities	109
235	5.2.3	Pinning Dynamic Floating Variables	109
236	5.3	Wrapping up the Logic	113
237	6	Presenting the Code Results	115
238	6.1	Validating Code with other Models	116
239	6.1.1	Comparing with the PSFC Arc Reactor	117
240	6.1.2	Contrasting with the Aries Act Studies	118
241	6.1.3	Benchmarking with the Process DEMO Designs	121
242	6.2	Developing Prototype Reactors	124
243	6.2.1	Navigating around Charybdis	126
244	6.2.2	Pinning down Proteus	127
245	6.3	Learning from the Data	128
246	6.3.1	Picking a Design Point	128
247	6.3.2	Utilizing High Field Magnets	132
248	6.3.3	Looking at Design Alternatives	135
249	7	Planning Future Work	143
250	7.1	Incorporating Stellarator Technology – Ladon	143
251	7.2	Making a Hybrid Reactor – Janus	144
252	7.3	Bridging Confinement Scalings – Daedalus	145
253	7.4	Addressing Model Shortcomings	146
254	7.4.1	Including Pedestal Temperature Profiles	146
255	7.4.2	Expanding the Radiation Loss Term	147
256	7.4.3	Taking Flux Sources Seriously	147
257	8	Concluding Reactor Discussion	149

258	A Presenting StaticFixed Variables	151
259	B Simulating with Fussy.jl	153
260	B.1 Getting the Code to Work	153
261	B.2 Sorting out the Codebase	154
262	B.2.1 Typing out Structures	155
263	B.2.2 Referencing Input Decks and Solutions	157
264	B.2.3 Acknowledging Utility Functions	157
265	B.2.4 Mentioning Base Level Files	157
266	B.3 Delving into Reactor Methods	158
267	B.4 Demonstrating Code Usage	159
268	B.4.1 Initializing the Workspace	160
269	B.4.2 Running a Study	160
270	B.4.3 Extracting Results	161
271	B.4.4 Plotting Curves	162
272	C Discussing Fusion Power	167
273	C.1 Fusion Power – P_F	167
274	C.2 Reactivity – (σv)	169
275	D Selecting Plasma Profiles	173
276	D.1 Density – n	173
277	D.2 Temperature – T	175
278	D.3 Pressure – p	177
279	D.4 Bootstrap Current – f_{BS}	177
280	D.5 Volume Averaged Powers	179
281	E Determining Plasma Flux Surfaces	181
282	E.1 Flux Surface Coordinates	181
283	E.2 Cross-sectional Area and Volume	183
284	E.3 Surface and Volume Integrals	184

285	F Expanding on the Bootstrap Current	187
286	F.1 Summarized Results	187
287	F.2 Detailed Analysis	188

List of Figures

289	1-1	Cut-Away of Tokamak Reactor	24
290	1-2	Comparison of Pulsed and Steady-State Current	25
291	1-3	Fusion Never Funding Timeline	26
292	1-4	H-Mode Confinement Time Scaling	27
293	1-5	Steady State Magnet Components	32
294	1-6	Pulsed Magnet Components	32
295	2-1	Geometry of a Tokamak	35
296	2-2	Geometric Parameters	36
297	2-3	Radial Plasma Profiles	37
298	2-4	Greenwald Density Limit	41
299	3-1	Current Balance in a Tokamak	54
300	3-2	Power Balance in a Reactor	62
301	3-3	Freidberg Triple Product	67
302	4-1	A Simple Plasma Transformer Description	79
303	4-2	Time Evolution of Circuit Profiles	81
304	4-3	Dimensions of Tokamak Cross-Section	94
305	5-1	Minimize Cost Step I – Find Valid Reactor	110
306	5-2	Minimize Cost Step II/III – Optimize Reactor	111
307	6-1	Arc Model Comparison	117
308	6-2	Act Studies Cost Dependence on the H Factor	118
309	6-3	Aries Act I Model Comparison	119
310	6-4	Aries Act II Model Comparison	120

311	6-5 Demo Steady Model Comparison	122
312	6-6 Demo Pulsed Model Comparison	123
313	6-7 How to Build a Fusion Reactor	125
314	6-8 Steady State Prototype Comparison	126
315	6-9 Pulsed Prototype Comparison	127
316	6-10 Limit Regimes as function of B_0	129
317	6-11 Steady State Cost Curves	130
318	6-12 Pulsed Cost Curves	131
319	6-13 Pulsed B_{CS} Sensitivity	133
320	6-14 Pulsed Monte Carlo Sampling	134
321	6-15 Bootstrap Current Monte Carlo Sampling	136
322	6-16 Internal Inductance Sensitivities	137
323	6-17 Pulsed H Sensitivities	139
324	6-18 Steady State Current Drive Efficiency	140
325	6-19 Current Drive Efficiency vs Launch Angle	141
326	7-1 Cut-Away of Stellarator Reactor	144
327	7-2 Current Balance in a Tokamak	145
328	B-1 A Blank Plot	163
329	B-2 An Empty Plot	164
330	B-3 An Unscaled Plot	165
331	B-4 A Scaled Plot	165
332	C-1 Comparing Nuclear Fusion and Fission	168
333	C-2 The D-T Fusion Reaction	169
334	D-1 Radial Plasma Profiles	173
335	E-1 Cut-Away of Tokamak Reactor	181
336	E-2 Dimensions of Tokamak Cross-Section	183

337 List of Tables

338	3.1	Dynamic Variables	52
339	4.1	Piecewise Linear Scheme for Pulsed Operation	81
340	4.2	Example TF Coils and Central Solenoid Critical Values	97
341	5.1	Main Equation Bank	107
342	6.1	Arc Variables	117
343	6.2	Act I Variables	119
344	6.3	Act II Variables	120
345	6.4	Demo Steady Variables	122
346	6.5	Demo Pulsed Variables	123
347	6.6	Charybdis Variables	126
348	6.7	Proteus Variables	127
349	A.1	List of Static Fixed Variables	151

List of Equations

351	1.1	Magnetic Energy – W_M	29
352	1.2	Cost per Watt – C_W	30
353	2.1	Minor Radius – a	35
354	2.2	Density Profile – n	37
355	2.4	Temperature Profile – T	38
356	2.5	Current Profile – J	38
357	2.6	Internal Inductance – l_i	39
358	2.7	Normalized Poloidal Magnetic Field – b_p	39
359	2.8	Current Balance – I	39
360	2.11	Greenwald Density – \bar{n}	42
361	2.15	Bootstrap Current – I_{BS}	44
362	2.20	Dilution Factor – f_D	46
363	2.21	Volume Integral – Q_V	46
364	2.23	Fusion Power – P_F	46
365	2.28	Current Drive – I_{CD}	48
366	2.30	Steady Current – I_P	49
367	2.31	Current Drive Efficiency – η_{CD}	50
368	3.1	Scanned Temperature – \bar{T}	53
369	4.75	Generalized Current – I_P	100
370	C.1	Fusion Energy – E_F	167
371	C.3	Alpha Power – P_α	169
372	C.4	Neutron Power – P_n	169

Chapter 1

Introducing Fusion Reactors

The central goal of fusion energy research is to build a profitable nuclear reactor. It has long been joked though that fusion power will always be 20-50 years away. This paper lays a framework for exploring reactor space for functional, efficient designs – based on world experiments during the last half-century. Due to the speed and simplicity of the model, hundreds of reactors can be explored in minutes (outpacing the domestic program slightly).

With this proposed model, interesting reactors can be pinpointed long before engineers hit the blueprints. This should help shorten the time until a profitable reactor, as well as illuminate ways to improve modern plasma theory. Further, it verifies the reasoning of MIT’s PSFC to invest in high field, high-temperature superconducting (HTS) tape – as this technology would lead to much smaller devices.

1.1 Treating Fusion as a Science

When people talk about fusion, they usually talk about plasma physics, and when people talk about plasma physics, they often talk about things like: the sun, lightning, and the aurora borealis. Of these three, the sun is the only nuclear reactor. However, the sun can stay on all day because the massive gravity of its fuel source helps keep

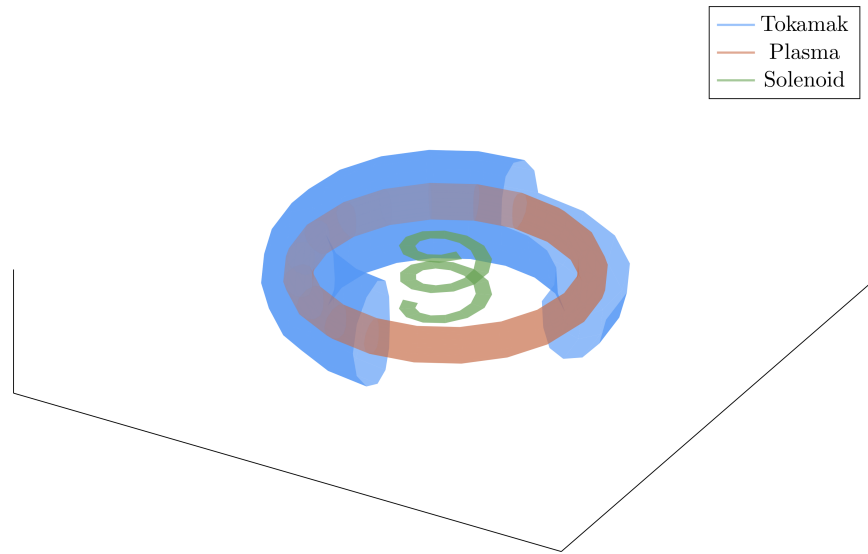


Figure 1-1: Cut-Away of Tokamak Reactor

The three main components of a magnetic fusion reactor are: the tokamak structure, the plasma fuel, and the spring-like solenoid at the center.

391 it self-contained in space. On Earth, this is not possible – the plasma fuel* needs to
392 be contained by other means (i.e. with magnets).

393 A tokamak is one of the leading candidates for a profitable fusion reactor. It shares the
394 shape of a doughnut, using magnets to keep a hula hoop of plasma swirling inside it.
395 The difficulty of keeping this plasma swirling though, is that it does not enjoy being
396 spun too fast or squeezed too hard. Conversely, the tokamak housing the plasma does
397 not like taking too much of a beating or being scaled to T-Rex sized proportions. This
398 sets the stage for tokamak reactor design – building on the various plasma physics
399 and nuclear engineering constraints of the day.

400 One of the most contentious points of building a tokamak, however, is whether it
401 will be run as: pulsed (the European approach⁵) or steady-state (the United States
402 effort⁶). Here, pulsed operation refers to how a reactor is turned on and off periodically
403 – around ten times a day. Whereas, steady state machines are meant to be left on

*Plasmas are the fourth state of matter after: solids, liquids, and gases. Fundamentally they are gaseous fluids that respond to electric and magnetic fields.

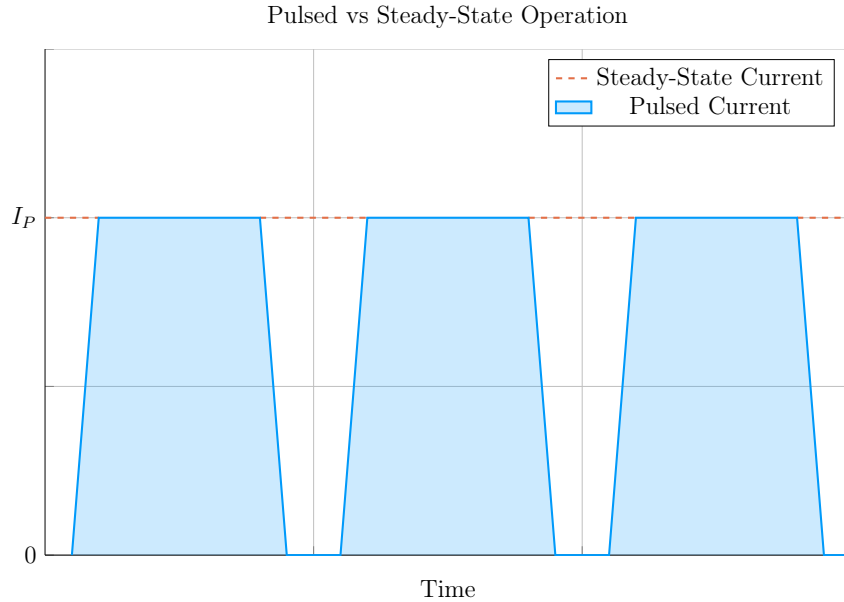


Figure 1-2: Comparison of Pulsed and Steady-State Current

Inside a pulsed reactor, current is ramped up and down several times a day – with breaks in-between. Steady state reactors are meant to stay on for weeks, months, or years.

404 nearly the entirety of their 50-year campaigns. These behaviors are shown in Fig. 1-2.

405 These two modes of operation, *pulsed* and *steady-state*, greatly influence the design
 406 through the current balance equation (derived later). What this means practically is
 407 tokamaks need current to spin their plasma hoops at some required speed and this
 408 current has to come from somewhere. Luckily, the plasma naturally enjoys spinning
 409 and provides some assistance through the bootstrap current. The remaining current
 410 must then be produced by external means.

411 The source of external current drive is what distinguishes pulsed from steady-state
 412 devices. Steady-state devices provide the required current assistance either through
 413 lasers or particle beams – this paper’s model focusing on a type of laser assistance
 414 called lower-hybrid current drive (LHCD).⁷ Pulsed machines, on the other hand, rely
 415 on inductive sources – which by definition require cycles of charging and discharging
 416 several times a day.*

417 The goal of this document is to show that pulsed and steady-state operation are

*These inductive sources are akin to a battery on a laptop that must be recharged every so often.

actually two sides of the same coin. This yields the simple conclusion that a single comprehensive model can run both modes at the flip of a switch. It even opens the opportunity of a hybrid reactor that exists somewhere in between the two.

1.2 Treating Fusion as a Business

Plasmas may be interesting, but that is not why countries build billion dollar research experiments. The ultimate goal of fusion research is to develop an energy resource that competes with coal and other base-load power sources (e.g. from hydroelectric and nuclear fission power plants). The problem is plasmas are chaotic and hard to contain, while tokamaks are expensive and slow to build. This perfect match has long put the field's projected timeline to that of *fusion never*.⁸

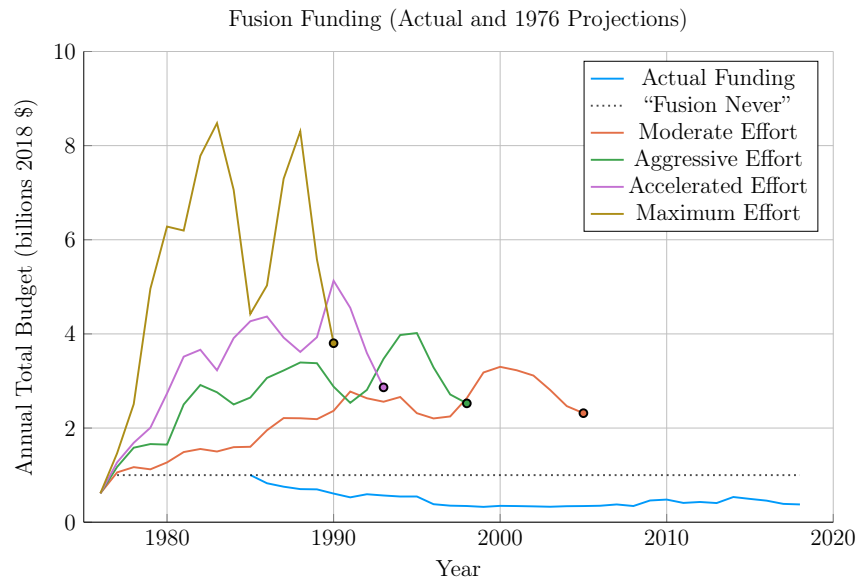


Figure 1-3: Fusion Never Funding Timeline

Comparison of Projected Timelines of Fusion from 1976 with Actual DOE Budgets.^{9,10}
The dotted line is popularly referred to in the community as "Fusion Never."¹¹

The major problem with containing a plasma in a reactor is that a plasma does not want to be contained. Since the early days of fusion research, plasmas have often found escape mechanisms. When presented with a magnetic bottle, they found their

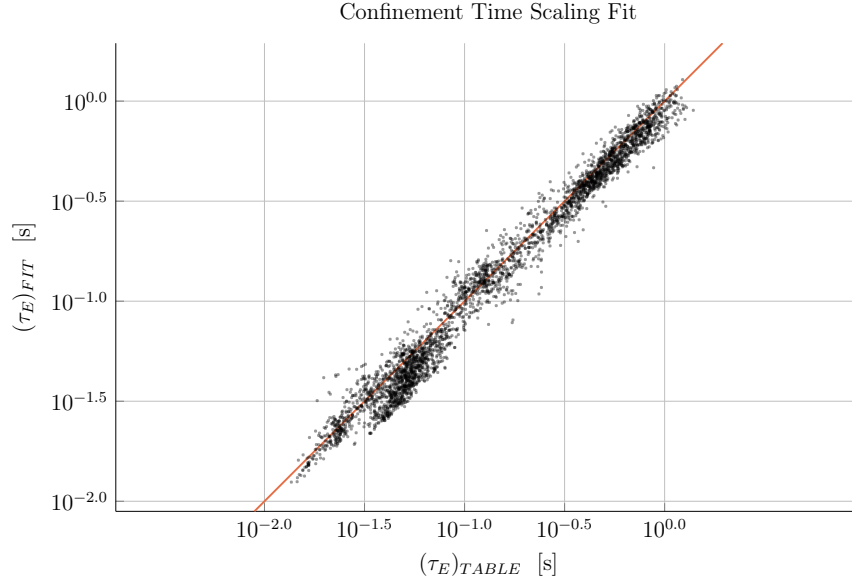


Figure 1-4: H-Mode Confinement Time Scaling

This plot shows how well the ELMy H-Mode Scaling Law does for fitting τ_E to the ITER98 database of global tokamaks. For most values, the fit is at least 80% accurate.

way out the top. In a tokamak, they attack the outer edges like an overinflated tire-tube. Fusion energy has seemed to remain a Tantalizing effort – within arms reach, but staunchly guarded by a shroud of instabilities.

The truth is plasmas are extremely chaotic: they show nonlinear behavior in almost everything they do. As of now, no theory or supercomputer-backed code can predict even something so fundamental to design as the movement of energy and particles within a tokamak. As such, the field has adopted several rules of thumb and empirical scalings – based on the last half century of experiments – which help one navigate around a plasma’s finicky behavior.

The two most widely used rules of thumb within the fusion design community are: the Greenwald density limit and the ELMy H-Mode confinement time scaling law. As such, the model in this document heavily utilizes the two to make a quick running code. These two relations are also why this model – which happens to be zero-dimensional – can reproduce with high fidelity the answers from three-dimensional codes, which can take days, weeks, or even months to run!

446 The use of the ELMy H-Mode scaling law also brings up another subtlety in the field.
447 To measure the movement of energy within a plasma, scaling relations are needed
448 that correlate to specific modes of plasma behavior – i.e. ones that can robustly be
449 found on a device by technicians. Currently, people rank H-Mode scalings over L-
450 Mode ones (because H stands for high confinement and L stands for low). However,
451 people often seek out other modes that can reliably be found on other machines.
452 These go by names like: I-Mode (i.e. intermediate confinement), Enhanced H-Mode,
453 and Reversed Shear modes.^{12–14}

454 Without going into too much detail, these alternate modes can be extremely valu-
455 able, as they often lead to more attractive reactors (than those made under H-Mode
456 scalings). The problem, however, is often not finding a better performing mode on a
457 single machine, but robustly finding it on other ones. This is important, because find-
458 ing a mode on multiple machines is what allows new scaling relations to be produced
459 and refined.*

460 1.3 Pricing a Fusion Reactor

461 To compare tokamaks used as fusion reactors the obvious metrics are costs. ITER –
462 the second most expensive experiment today (only behind the LHC) – has a history
463 rich in countries backing out for high price tags and rejoining only when they finally
464 get lowered.⁷ The problem is \$20B is a lot of money and 20 years is a long time.
465 Moreover, approximating true costs becomes even trickier when designers need to
466 project (or neglect) economies-of-scale for expensive components, such as the magnets
467 and irradiated materials.

468 As such, this paper adopts stand-ins for the conventional capital cost and cost-per-
469 watt metrics. This is done for simplicity, for both: modeling reasons as well as
470 conveying the two metrics to physicists. To begin, the relevant approximation for

*In H-Mode and L-Mode’s favor, they have been found on every machine that should see them.

471 capital cost – how much a tokamak costs to build – is the magnetic energy.¹⁵

$$W_M \propto R^3 B^2 \quad (1.1)$$

472

473 In this magnetic energy proportion relation, the tokamak’s major radius – R – is
474 involved in a volumetric term (R^3) and B is the strength (in Teslas) of the hooped
475 shape magnetic field that lays nested within the plasma’s shell (near its core). This
476 quantity simply states that the two surefire ways to make a machine more expensive
477 to build are: making it larger and using stronger magnets.

478 The next metric, the cost-per-watt, is defined by dividing the capital cost (i.e. the
479 magnetic energy) by the main source of power output. This quantity measures how
480 profitable a reactor will be once it is built. In a tokamak, the main power output is
481 assumed to be fusion power, which relies on light elements (i.e. two Hydrogens) fusing
482 into a heavier one (i.e. one Helium) – hopefully releasing enough energy to offset the
483 expense of causing it to happen in the first place. Although fusion power will not be
484 defined till later, it does highlight the fact that this measure of cost-per-watt actually
485 has units of time!*

486 The final piece of the costing puzzle is a duty factor that levelizes the comparison of
487 pulsed and steady-state tokamaks. As pulsed machines may be off 20% of the time,
488 their fusion power output should be reduced by that percentage. This is accounted
489 for in the duty factor, which is simply the ratio of the flattop – the time when pulsed
490 machines are approximately held at steady-state – to the entire length of the pulse.

491 In pulsed machines, the entire pulse includes charging the inductive sources as well as
492 flushing out the tokamak between runs. These non-flattop portions of time can last
493 around thirty minutes (where the reactor makes no money). As steady-state machines
494 lack these non-flattop portions, their duty factors are rightfully one. Analysis in
495 Section 4.1.4 and discussion with several researchers, however, show that the same

*As energy per unit watt has units of time (i.e seconds).

will probably hold true for a pulsed reactor, too.

Summarizing, the cost-per-watt coupled with the duty factor provides an ad hoc pricing metric, C_W , given by:

$$C_W = \frac{W_M}{f_{Duty} \cdot P_F} \quad (1.2)$$

It serves as a cornerstone for comparing the entire landscape of tokamak reactors – whether they run in pulsed or steady-state operation. Although not a true engineering cost metric (i.e. in dollars per watt), it does provide an obvious physics meaning. Coupled with the magnetic energy stand-in for capital cost, these two costs allow researchers to pinpoint profitable and inexpensive tokamaks within reactor space.

1.4 Modeling a Fusion Reactor

Before reactors can be costed, though, they have to be modeled. Therefore the first half of this thesis is devoted to the theory behind tokamak design. A priority is placed more on a physicist’s intuition than an engineer’s costing rigor. This is justified by the nonlinearities inherent to the fusion systems and rationalized by this paper’s results matching more sophisticated frameworks with high fidelity.

What makes this paper’s model different from others in the field is the generalized handling of both modes of tokamak operation: pulsed and steady-state. This was necessitated by a desire to compare the two modes on a level playing field. What this shows is that both pulsed and steady-state tokamaks could make for profitable fusion reactors – assuming some technological advancements.

One technological advancement that could lead to major wins is improving magnet components. This is why MIT has championed high-field designs for the better part of the last century. In their latest effort, the PSFC team has explored new high-

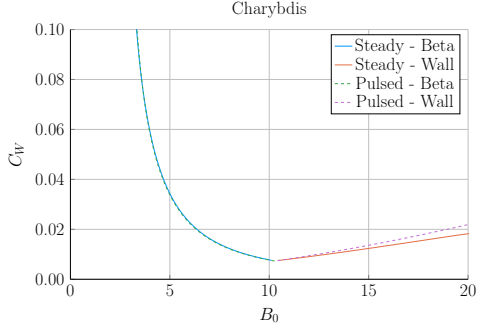
519 temperature superconducting (HTS) tape capable of doubling the maximum achiev-
520 able field strength. What this paper shows is that this logic is indeed correct and
521 that HTS tape is all that is needed to build optimum reactors.

522 More concretely, this paper shows that new HTS tape technology is capable of low-
523 ering both pulsed and steady-state tokamak costs. Further, the benefits of doubling
524 the magnet strength bring the situation to a realm of significantly diminished rates
525 of return. HTS is thus the end goal for the conventional D-T fusion paradigm.

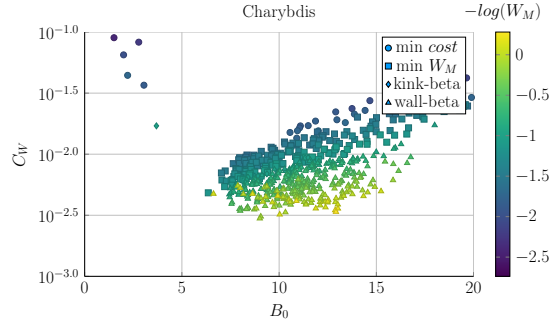
526 Moreover, this model shows that HTS is best utilized in different components for
527 pulsed and steady-state operation. Steady-state tokamaks favor HTS use in the D-
528 shaped magnets that circle the machine (i.e. the TF coils). Whereas pulsed devices
529 would benefit from employing HTS in the central solenoid – that produces most of a
530 reactor’s inductive current. A corollary of this is conventional copper magnets (i.e.
531 inexpensive ones) can be used for pulsed TF coils, as their improved confinement
532 saturates at much lower field strengths.

533 Now that the problem has been thoroughly introduced, we will go over the theory
534 behind steady-state and, then, pulsed tokamaks. A couple segues will be taken along
535 the way to show how the model can be incorporated into a fusion systems code. This
536 code – Fussy.jl – is the topic of an appendix chapter and is freely available at:

537 git.io/tokamak

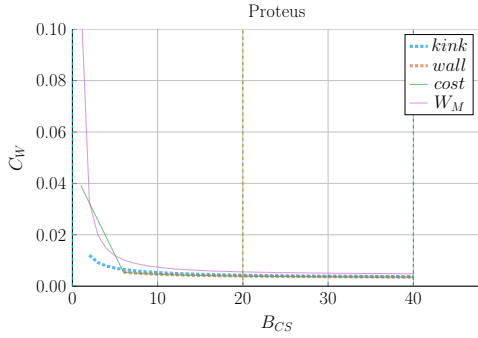


(a) Toroidal Field Sensitivity

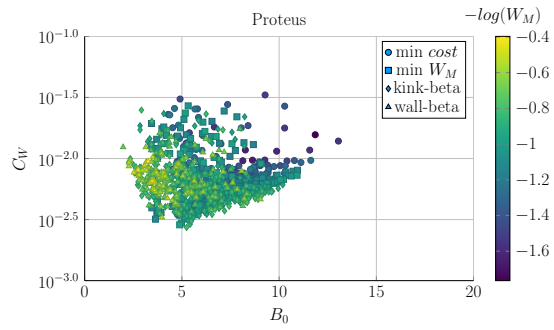


(b) Toroidal Field Samplings

Figure 1-5: Steady State Magnet Components



(a) Solenoid Strength Sensitivity



(b) Toroidal Field Samplings

Figure 1-6: Pulsed Magnet Components

Chapter 2

Designing a Steady-State Tokamak

This chapter explores a simple model for designing steady-state tokamaks. In the next couple chapters, the model is first formalized for use in a systems code and then generalized to handle pulsed operation. These derivations highlight that the only difference between the two modes of operation is how they generate their auxiliary plasma current: LHCD for steady-state operation and inductive sources for when a reactor is purely pulsed.

Along the way, equations will be derived that get rather complicated. To remedy the situation, a distinction between `dynamicfloating` and `staticfixed` values is now given, which will allow splitting most equations into `staticfixed` and `dynamicfloating` parts. `DynamicFixed` values – i.e. the tokamak’s major radius (R_0) and magnet strength (B_0), as well as the plasma’s current (I_P), temperature (\bar{T}), and density (\bar{n}) – are first-class variables in the model (see Table 3.1). Everything is derived to relate them. `StaticFixed` values, on the other hand, can be treated as code inputs, which remain constant throughout a reactor solve. These most obviously include the various geometric and profile parameters introduced next section.

The overall structure of this chapter, then, is built around developing an equation for plasma current in a steady-state tokamak. It is shown that this value arises from balancing current in a reactor using both a plasma’s own bootstrap current (I_{BS}),

as well the tokamak's auxiliary driven current (I_{CD}). These relations necessitate geometric parameters and plasma profiles, which will be given shortly. Along the way, definitions will also be needed for the Greenwald density (N_G) and the fusion power (P_F). What is shown is that the current does not actually depend directly on the major radius (R_0) or magnet strength (B_0) of a tokamak – allowing these variables to be put off until next chapter.

2.1 Defining Plasma Parameters

As mentioned previously, the zero-dimensional model derived here can closely approximate solutions from higher-dimensional codes that might take many hoursweeks to run. The essence of boiling down three-dimensional behaviors to one dimensional profiles – and zero-dimensional averaged values – begins with defining the most important plasma parameters. These are the: current density (J), temperature (T), and density (n) of a plasma.

Solving this problem most generally usually involves decoupling the geometry of the plasma from the shaping of its nearly parabolic radial-profiles – both of which will be explained shortly.

2.1.1 Understanding Tokamak Geometry

The first thing people see when they look at a tokamak is its geometry – see Fig. 2-1. How big is it? Is it stretched out like a bicycle tire or compressed to the point of being nearly spherical? Would a slice across the major radius result in two cross-sections that were: circular, elliptic, or triangular?~~Is it stretched out like a tire or smooshed together like a bagel? If it were torn in two, would the exposed areas look like: circles, ovals, or triangles?~~

These questions lend themselves to the three important geometric variables – the inverse aspect ratio (ϵ), the elongation (κ), and the triangularity (δ). The inverse

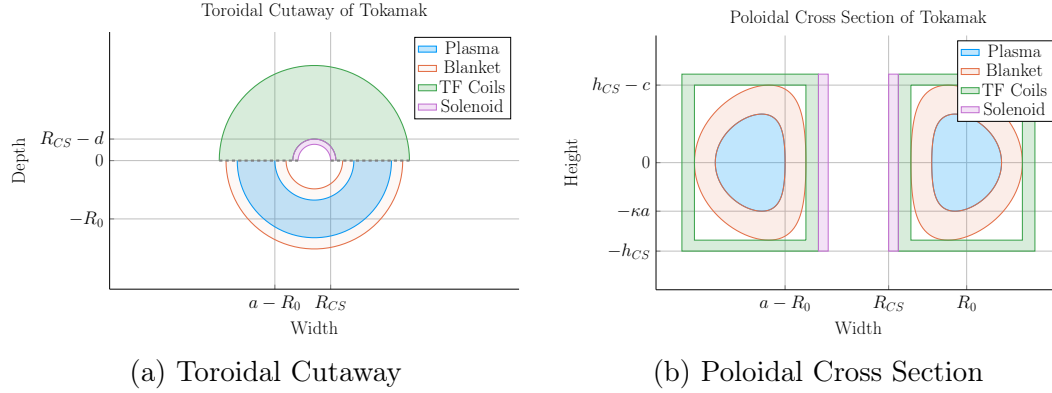


Figure 2-1: Geometry of a Tokamak

This diagram is of a tokamak's toroidal (top) view and the poloidal cross section of a slice across the major axis. Included are the four components of a reactor: the plasma, its metallic blanket, the toroidal field magnets surrounding them, and the central solenoid. These have thicknesses of a , b , c and d , respectively. R_{CS} is where the solenoid starts.

583 aspect ratio is a measure of how stretched out the device is, or formulaically:

$$a = \epsilon \cdot R_0 \quad (2.1)$$

584

585 This says that the minor radius (a), measured in meters, is related to the major radius
 586 of the machine (R_0) through ϵ . Or more tangibly, the minor radius is related to the
 587 two small ~~cross-sections~~ ~~circles~~ that ~~result from a slice across the major radius of the~~
 588 ~~machine come from tearing a bagel in two.~~ Whereas the major radius is related to
 589 ~~the overall circle of the bagel when viewing it from the top.~~

590 The remaining two geometric parameters – κ and δ – are related to the shape of the
 591 torn halves. As the name hints, elongation (κ) is a measure of how stretched out
 592 the tokamak is vertically – is the cross-section a circle or an oval? The triangularity
 593 (δ) is then how much the cross-sections point outward from the center of the device.
 594 All three's effects can be seen in Fig. 2-2. ~~Their exact usage within describing flux~~
 595 ~~surfaces is shown in Appendix E.~~

596 These geometric factors allow the volumetric and surface integrals governing fusion

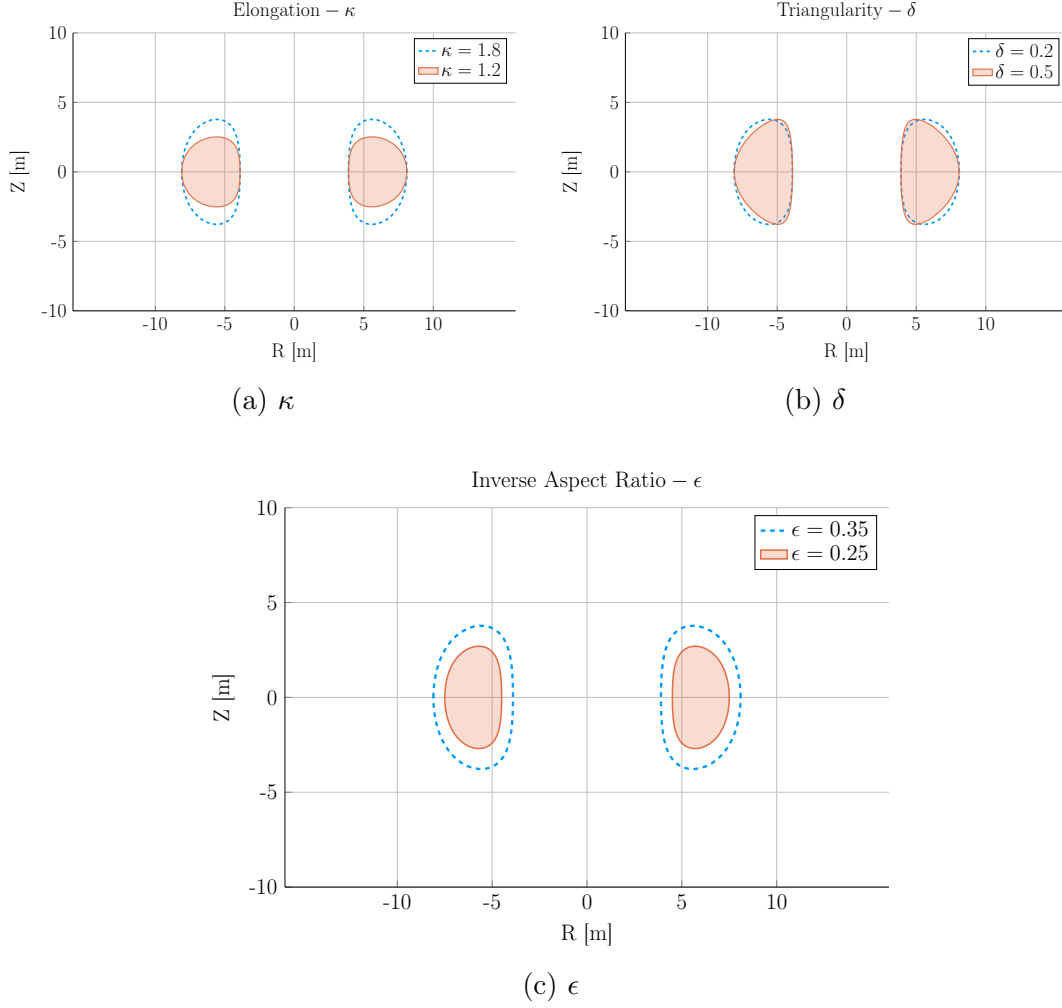


Figure 2-2: Geometric Parameters

These three geometric parameters allow the toroidal cross-sections to scale radially, stretch vertically, and become more triangular – thus improving upon simple circular slices.

power and bootstrap current to be condensed to simple radial ones – see Eqs. (E.24) and (E.25). The only remaining step is to define the radial profiles for: the density, temperature, and current of a plasma.

2.1.2 Prescribing Plasma Profiles

The first step in defining radial profiles is realizing that all three quantities are ~~essentially parabolas~~~~basically parabolas~~ – i.e. the temperature, density and current ~~density~~, shown in Section 2.1.2, are peaked at some radius (usually the center) and

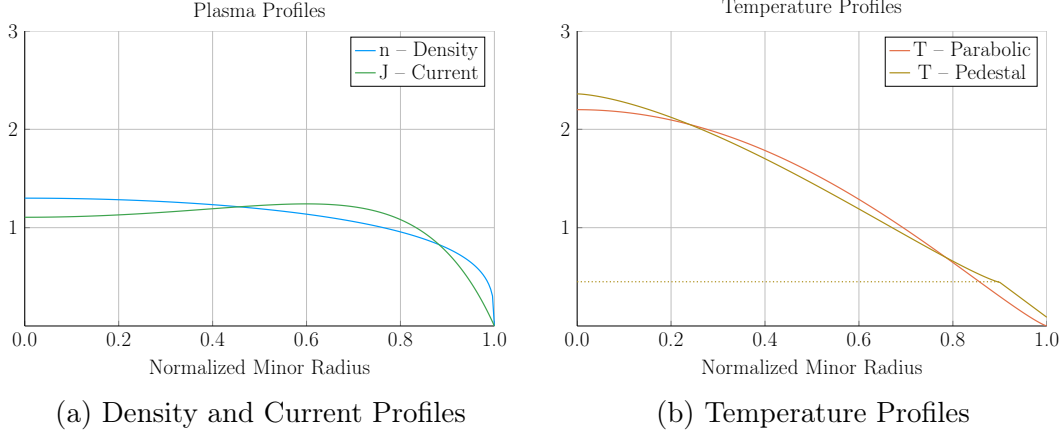


Figure 2-3: Radial Plasma Profiles

The three most fundamental ~~profiles~~^{properties} of a fusion plasma are its temperature, density, and current. These ~~profiles~~ allow the model to reduce from three dimensions to just half of one.

then decay to zero somewhere before the walls of the tokamak enclosure.

Although not self-consistent, these profiles do capture enough of the physics to approximate relevant phenomenon, such as transport and fusion power.¹

The Density Profile

To begin, density has the simplest profile. This is because it is relatively flat, remaining near the average value – \bar{n} – throughout the body of the plasma until quickly decaying to zero near the edge of the plasma.* For this reason, a parabolic profile with a very low peaking factor – ν_n – is well suited.

$$n(\rho) = \bar{n} \cdot (1 + \nu_n) \cdot (1 - \rho^2)^{\nu_n} \quad (2.2)$$

The reason \bar{n} is referred to as the volume-averaged density is because using the volume integral – given by Eq. (E.24) – over the density profile results in that value after

*Even in H-Mode plasmas where density profiles have a pedestal,¹⁶ they usually have much less of a peak than temperatures¹⁷ – especially so in a reactor setting.¹⁸

615 dividing through by the volume (V):

$$\bar{n} = \frac{\int n(\mathbf{r}) d\mathbf{r}}{V} \quad (2.3)$$

616 A final point to make is this parabolic profile allows for a short closed-form relation
617 for the Greenwald density limit – substantially simplifying this fusion systems model.

618 The Temperature Profile

619 The use of a parabolic profile for the plasma temperature is slightly more dubious.
620 This is because H-Mode plasmas are actually highly peaked at the center, decaying
621 to a non-zero pedestal temperature near the edge before finally dropping sharply to
622 zero. This model chooses to forego this pedestal representation for a simple parabolic
623 one – although the pedestal approach is discussed in Appendix D. Analogous to the
624 density, the profile treats \bar{T} as the average value and ν_T as the peaking parameter.

$$T(\rho) = \bar{T} \cdot (1 + \nu_T) \cdot (1 - \rho^2)^{\nu_T} \quad (2.4)$$

625

626 The Current **Density** Profile

627 The plasma current **density** is the third profile and cannot safely be represented by a
628 simple parabola. This is because having an adequate bootstrap current relies heavily
629 on a profile being peaked off-axis – i.e. at some radius not at the center. This hollow
630 profile can then be modeled with the commonly given plasma internal inductance (l_i).
631 Concretely, the current's hollow profile is described by:

$$J(\rho) = \bar{J} \cdot \frac{\gamma^2 \cdot (1 - \rho^2) \cdot e^{\gamma \rho^2}}{e^\gamma - 1 - \gamma} \quad (2.5)$$

632

633 The intermediate γ quantity can then be numerically solved for from the plasma
 634 internal inductance using the following relations – with b_p representing the normalized
 635 poloidal magnetic field. **These are derived in Appendix F.**

$$l_i = \frac{4\kappa}{1 + \kappa^2} \int_0^1 b_p^2 \frac{d\rho}{\rho} \quad (2.6)$$

$$b_p(\rho) = \frac{-e^{\gamma\rho^2}(\gamma\rho^2 - 1 - \gamma) - 1 - \gamma}{\rho(e^\gamma - 1 - \gamma)} \quad (2.7)$$

637
 638 Combined, these three geometric parameters and profiles lay the foundation for this
 639 zero-dimensional fusion systems model.

640 2.2 Solving the Steady Current

641 As suggested, one of the most important equations in a fusion reactor is current
 642 balance. In steady-state operation, all of a plasma's current (I_P) must come from
 643 a combination of its own bootstrap current (I_{BS}), as well as auxiliary current drive
 644 (I_{CD}). This can be represented mathematically as:

$$I_P = I_{BS} + I_{CD} \quad (2.8)$$

645
 646 The goal is then to write equations for bootstrap current and driven current. This
 647 will make heavy use of the Greenwald density limit. **The steady current will then**
 648 **be**~~Without spoiling too much, the steady current is~~ shown to be only a function of
 649 temperature! In other words, this current is independent of a tokamak's geometry
 650 and magnet strength. As will be pointed out then, though, a subtlety arises that will
 651 bring the two back into the picture – self-consistency in the current drive efficiency
 652 (η_{CD}).

2.2.1 Enforcing the Greenwald Density Limit

The Greenwald density limit is a density limit that applies to all tokamaks ~~ubiquitous in the field of fusion energy~~. It sets a hard limit on the density and how it scales with current and reactor size. Although currently lacking a true first-principles theoretical explanation, it does have a real meaning within the design context. Operate at too low a density and run the risk of never entering H-Mode. Run the density too high, and cause the tokamak's plasma to ~~disrupt~~~~disrupt catastrophically!~~ These conclusions can be seen in Fig. 2-4.

As no theoretical backing exists, the Greenwald density limit can simply be written (with citation) as:²

$$\hat{n} = N_G \cdot \left(\frac{I_P}{\pi a^2} \right) \quad (2.9)$$

Here, \hat{n} has units of $10^{20} \frac{\text{particles}}{\text{m}^3}$, N_G is the Greenwald density fraction, and I_P is again the plasma current (measured in mega-amps). ~~and π has its usual meaning (3.141592653...)~~.

The final variable is then the minor radius – a – which was previously defined through:

$$a = \epsilon \cdot R_0 \quad (2.1)$$

The next step is transforming the *line-averaged* density (\hat{n}) into the *volume-averaged* version (\bar{n}) used in this model. Harnessing the simplicity of the density's parabolic profile allows this relation to be written in a closed form as:

$$\hat{n} = \frac{\sqrt{\pi}}{2} \cdot \left(\frac{\Gamma(\nu_n + 2)}{\Gamma(\nu_n + \frac{3}{2})} \right) \cdot \bar{n} \quad (2.10)$$

Where $\Gamma(\dots)$ represents the gamma function: the non-integer analogue of the factorial function.

Combining these pieces allows the volume-averaged density to be written in standard-

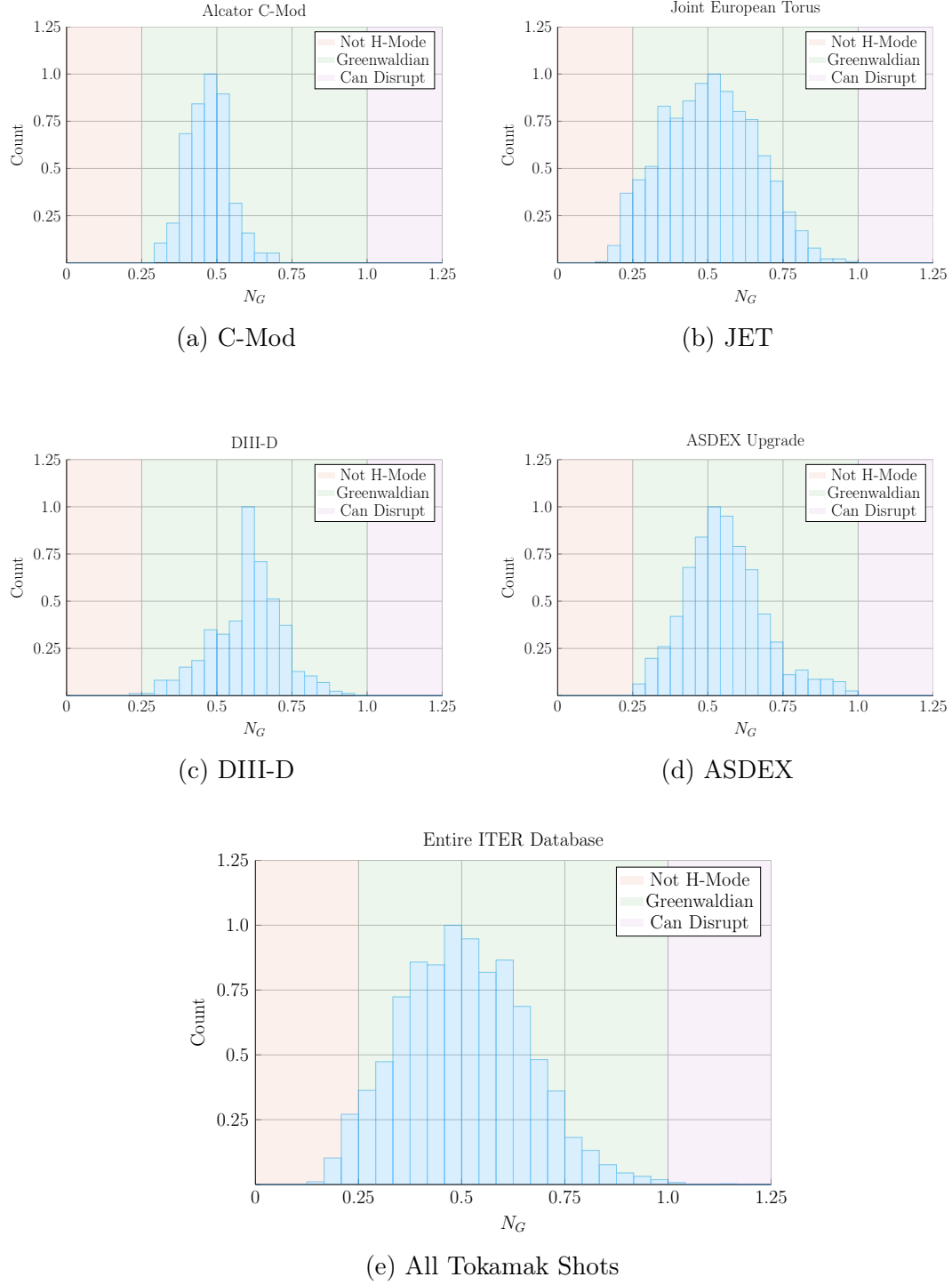


Figure 2-4: Greenwald Density Limit

The Greenwald Density Limit is a robust metric of what densities an H-Mode plasma can attain. Although empirical in nature, it accurately predicts when a tokamak will undergo degraded plasma transport.²~~it is an indicator for good transport regimes.~~

672 ized units ~~(i.e. the ones we use)~~ as:

$$\bar{n} = K_n \cdot \left(\frac{I_P}{R_0^2} \right) \quad (2.11)$$

673

$$K_n = \frac{2N_G}{\epsilon^2 \pi^{3/2}} \cdot \left(\frac{\Gamma(\nu_n + \frac{3}{2})}{\Gamma(\nu_n + 2)} \right) \quad (2.12)$$

674 The format of the previous equation pair will be used throughout the remainder of
 675 the paper. The top equation relates ~~dynamicfloating~~ variables (i.e. \bar{n} , I_P , and R_0),
 676 while the ~~staticfixed~~-value coefficient (K_n) lumps together ~~staticfixed~~ quantities, such
 677 as: N_G , ϵ , 2, π , and ν_n .

678 2.2.2 Declaring the Bootstrap Current

679 The first term to define in current balance, Eq. (2.8), is the bootstrap current. This
 680 bootstrap current is a mechanism of tokamak plasmas that helps supply some of
 681 the current needed to keep a plasma in ~~equilibriumstable~~. Its underlying behavior
 682 stems from particles stuck in banana-shaped orbits on the outer edges of the device
 683 propelling the majority species along their helical trajectories around the tokamak.
 684 ~~From a hand-waving perspective, it involves particles stuck in banana-shaped orbits~~
 685 ~~on the outer edges of a tokamak behaving like racing-game style speed boosts that~~
 686 ~~accelerate charged particles along their hooped-shaped race tracks.~~

687 Utilizing the surface integral from Eq. (E.25), the bootstrap current (I_{BS}) can be
 688 written in terms of the temperature and density profiles: ~~To get an equation for~~
 689 ~~bootstrap current, we must first introduce the surface integral—made possible from~~
 690 ~~our previous choice of geometric parameters:—~~

691 ~~Here, Q is an arbitrary function of the normalized radius (ρ) and g is a geometric~~
 692 ~~factor (of order 1):~~

693 This allows the bootstrap current (I_{BS}) to be written in terms of the temperature
 694 and density profiles:

$$I_{BS} = 2\pi a^2 \kappa g \int_0^1 J_{BS} \rho d\rho \quad (2.13)$$

$$\begin{aligned} J_{BS} &= f\left(n, T, \frac{dn}{d\rho}, \frac{dT}{d\rho}\right) \\ &\equiv 4.88 \cdot \left(\frac{r}{R_0}\right) \cdot \left(\frac{nT}{B_\theta}\right) \cdot \left(\frac{1}{n} \frac{dn}{dr} + 0.055 \frac{1}{T} \frac{dT}{dr}\right) \end{aligned} \quad (2.14)$$

696 The second definition for the bootstrap current density – J_{BS} – comes from using
 697 well known theoretical results plus several simplifying assumptions, including the
 698 large aspect limit.

699 For a more formal look into this J_{BS} function, check the appendix section on pedestal
 700 temperatures. The point to make now is that it depends on the the profiles' derivatives,
 701 leading to one major discrepancy in the model.

702 As shown later in the results, bootstrap fractions are often under-predicted by this
 703 model. This is due to parabolic profiles (i.e. for temperature) having much less steep
 704 declines near the edge (i.e. in their derivatives) than characteristic H-Mode profiles
 705 with pedestals. This implies that the area most positively impacted by a pedestal
 706 profile for temperature would be the bootstrap current derivation. The instructions
 707 to do so are given in Appendix D.4.

708 Getting back on track—and without completeness—the bootstrap current can now
 709 be written in proportionality form as:

710 Recognizing that the last term is basically the inverse of the Greenwald density (see
 711 Eq. 2.11), allows the proportionality to be written in the following form. Note that
 712 this implies the bootstrap current is only a function of temperature!

713 In standardized units, this proportionality can be written as a concrete relation of
 714 the form:

715 Finally, summarizing the results of Appendix F, the bootstrap current is found to be

only a function of temperature! In standardized units, it can be written as:

$$I_{BS} = K_{BS} \cdot \bar{T} \quad (2.15)$$

$$K_{BS} = 4.879 \cdot K_n \cdot \left(\frac{1 + \kappa^2}{2} \right) \cdot \epsilon^{5/2} \cdot H_{BS} \quad (2.16)$$

$$H_{BS} = (1 + \nu_n)(1 + \nu_T)(\nu_n + 0.054\nu_T) \int_0^1 \frac{\rho^{5/2} (1 - \rho^2)^{\nu_n + \nu_T - 1}}{b_p} d\rho \quad (2.17)$$

Quickly noting, this H_{BS} term serves as the analogue of ~~static~~**fixed**-value coefficients (e.g. K_{BS} and K_n) when they contain an integral. And b_p represents the poloidal magnet strength given by Eq. 2.7.

2.2.3 Deriving the Fusion Power

~~The next segue on our journey to solving for the steady current is deriving the fusion power (P_F), which appears in current drive. This requires a more first-principles approach than those used up until now. As such, a quick background is given to motivate the parameters it adds—i.e. the dilution factor (f_D) and the Bosch-Hale fusion reactivity (σv).~~

~~The natural place to start when talking about fusion is the binding energy per nucleon plot (see Fig. N). As can be seen, the function reaches a maximum value around the element Iron ($A=56$). What this means at a basic level is: elements lighter than iron can *fuse* into a heavier one (i.e. hydrogens into helium), whereas heavier elements can *fission* into lighter ones (e.g. uranium into krypton and barium). This is what differentiates fission (uranium-fueled) reactors from fusion (hydrogen-fueled) ones. For fusion reactors, the most common reaction in a first-generation tokamak will be: What this reaction describes is two isotopes of hydrogen—i.e. deuterium and tritium—fusing into a heavier element, helium, while simultaneously ejecting a neutron. The entire energy of the fusion reaction (E_F) is then divvied up 80-20 between the neutron~~

and helium, respectively. Quantitatively, the helium (hereafter referred to as an alpha particle) receives 3.5 MeV.

The final point to make before returning to the fusion power derivation is the main difference between the two fusion products: helium (i.e. the alpha particle) and the neutron. First, neutrons lack a charge — they are neutral. This means they cannot be confined with magnetic fields. As such, they simply move in straight lines until they collide with other particles. As the structure of a tokamak is mainly metal, the neutron is much more likely to collide there than the gaseous plasma, which is orders of magnitude less dense. Conversely, alpha particles are charged — when stripped of their electrons — and can therefore be kept within the plasma using magnets. What this means practically is that of the 17.6 MeV that comes from every fusion reaction, only 3.5 MeV remains inside the plasma (within the helium particle species).

The next segue on our journey to solving for the steady current is deriving the fusion power (P_F), which appears in current drive. A comprehensive introduction to this is given in Appendix C. Summarized, though, a formula for Returning to the problem at hand, the fusion power from a D-T reaction – in megawatts – is given by the following volume integral:[?] –Jeff Freidberg’s textbook through the following volume integral:–

$$P_F = \int E_F n_D n_T \langle \sigma v \rangle d\mathbf{r} \quad (2.18)$$

$$E_F = 17.6 \text{ MeV} \quad (2.19)$$

The n_D and n_T in this equation represent the density of the deuterium and tritium ions, respectively. Assuming a 50-50 mix of the two, they can be related to the electron density – i.e. the one used in this model – through the dilution factor (f_D). This dilution factor represents the decrease in available fuel from part of the plasma actually being composed of non-hydrogen gasses:

$$n_D = n_T = f_D \cdot \left(\frac{n}{2} \right) \quad (2.20)$$

761

762 The fusion reactivity, $\langle\sigma v\rangle$, is then a nonlinear function of the temperature, T , which
 763 the model approximates using the Bosch-Hale tabulation (described in the appendix).
 764 As this tabulated value appears inside an integral, it seems important to point out
 765 that the temperature is now the most difficult ~~dynamic~~~~floating~~ variable to handle –
 766 over R_0 , B_0 , \bar{n} , and I_P . This will come into play when the model is formalized next
 767 chapter.

768 The next step in the derivation of fusion power is transforming the three-dimensional
 769 volume integral (see Eq. 2.18) into a zero-dimension averaged value. First, the volume
 770 analogue of the previously given surface-area integral is:

$$Q_V = 4\pi^2 R_0 a^2 \kappa g \int_0^1 Q(\rho) \rho d\rho \quad (2.21)$$

771 Where again, Q is an arbitrary function of ρ and g is a geometric factor approximately
 772 equal to one. The fusion power can now be rewritten as:

$$P_F = \pi^2 E_F f_D^2 R_0 a^2 \kappa g \int_0^1 n^2 \langle\sigma v\rangle \rho d\rho \quad (2.22)$$

773 In standardized units, this becomes:

$$P_F = K_F \cdot \bar{n}^2 \cdot R_0^3 \cdot (\sigma v) \quad (2.23)$$

774

$$K_F = 278.3 \cdot f_D^2 \cdot (\epsilon^2 \kappa g) \quad (2.24)$$

775 Where the standardized fusion reactivity is now,

$$(\sigma v) = 10^{21} (1 + \nu_n)^2 \int_0^1 (1 - \rho^2)^{2\nu_n} \langle\sigma v\rangle \rho d\rho \quad (2.25)$$

776 ~~As mentioned before, this fusion power is divvied up 80-20 between the neutron and~~

777 ~~alpha particle. These relations will be used shortly. For now, they can be described~~
778 ~~mathematically as:~~

779 At this point, the current drive needed for steady-state can now be defined.

780 2.2.4 Using Current Drive

781 As may have been lost along the way, ~~this chapter's the current~~ mission is to define
782 a formula for steady current – from the current balance equation for steady-state
783 tokamaks:

$$I_P = I_{BS} + I_{CD} \quad (2.8)$$

784 In standardized units, the equation for current drive is often given in the literature
785 as:¹⁹

$$I_{CD} = \eta_{CD} \cdot \left(\frac{P_H}{\bar{n}R_0} \right) \quad (2.26)$$

786 Here, η_{CD} is the current drive efficiency with units $\left(\frac{\text{MA}}{\text{MW-m}^2} \right)$ and P_H is the heating
787 power in megawatts driven by LHCD (and absorbed by the plasma).

788 Let it be known, though, that driving current in a plasma is hard! In fact, pulsed
789 reactor designers (i.e. European fusion researchers) think it is so difficult, they may
790 choose to forego it completely – focusing only on inductive sources that necessitate
791 reactor fatigue and downtime.

792 A common current drive efficiency (η_{CD}) seen in many designs is 0.3 ± 0.1 in the
793 standard units. It is however inherently a function of all the plasma parameters –
794 with subtlety put off until the discussion of self-consistency. For now it assumed to
795 have some constant/~~static~~~~fixed~~ value.

796 The remaining step in deriving an equation for driven current (I_{CD}) is a formula for
797 the heating power (P_H). The way fusion systems models – like this one – handle the
798 heating power is through the physics gain factor, Q. Sometimes referred to as big Q,
799 this value represents how many times over the heating power (P_H) is amplified as it

800 is transformed into fusion power (P_F):

$$P_H = \frac{P_F}{Q} \quad (2.27)$$

801 Now, utilizing the previously defined Greenwald density and fusion power:

$$\bar{n} = K_n \cdot \left(\frac{I_P}{R_0^2} \right) \quad (2.11)$$

802

$$P_F = K_F \cdot \bar{n}^2 \cdot R_0^3 \cdot (\sigma v) \quad (2.23)$$

803 The current from LHCD can be written as:

$$I_{CD} = K_{CD} \cdot I_P \cdot (\sigma v) \quad (2.28)$$

804

$$K_{CD} = (K_F K_n) \cdot \frac{\eta_{CD}}{Q} \quad (2.29)$$

805 As η_{CD} and Q appear within a ~~staticfixed~~ coefficient, it is implied that both re-
806 main constant throughout a solve. This subtlety is lifted when handling η_{CD} self-
807 consistently, which will be discussed shortly. However, even in that context, it proves
808 beneficial to still think of η_{CD} as a sequence of ~~staticfixed~~ variables – set by the model
809 rather than the user.

810 2.2.5 Completing the Steady Current

811 ~~TheAs hinted along the way, the~~ goal of this ~~chaptersection~~ has been to derive a
812 simple formula for steady current (I_P). The problem started with current balance in
813 a steady-state reactor:

$$I_P = I_{BS} + I_{CD} \quad (2.8)$$

814 Two equations were then found for the bootstrap (I_{BS}) and driven (I_{CD}) current:

$$I_{BS} = K_{BS} \cdot \bar{T} \quad (2.15)$$

815

$$I_{CD} = K_{CD} \cdot I_P \cdot (\sigma v) \quad (2.28)$$

816 Combining these three equations and solving for the total plasma current (I_P) – in
817 mega-amps – yields:

$$I_P = \frac{K_{BS} \bar{T}}{1 - K_{CD}(\sigma v)} \quad (2.30)$$

818

819 This is the answer we have been seeking!

820 As mentioned before, this simple formula appears to only depend on temperature!*

821 Apparently, the plasma should have the same current at some temperature (i.e. $\bar{T} =$
822 15 keV), regardless of the size of the machine or the strength of its magnets. This
823 has the important corollary that each temperature maps to only one current value.
824 Further, each temperature would then map to a single magnet strength, capital cost,
825 etc. (as shown next chapter).

826 As has become a mantra, though, the subtlety of this behavior lies in the self-
827 consistency of the current-drive efficiency – η_{CD} .

828 2.3 Handling Current Drive Self-Consistently

829 Although a thorough description of the wave theory behind lower-hybrid current
830 drive (LHCD) is well outside the scope of this text, it does motivate the solving of
831 a tokamak's major radius (R_0) and field strength (B_0). It also shows how what was
832 once a simple problem has now transformed into a rather complex one – a common
833 occurrence with plasmas.

*This dependence only on temperature refers to dynamic variables. The plasma current can still be highly volatile to many of the static variables, such as: ϵ , κ , N_G , f_D , ν_n , l_i , etc.

834 The logic behind finding a self-consistent current-drive efficiency is starting at some
835 plausible value (i.e. $\eta_{CD} = 0.3$), solving for the steady current – i.e. $I_P = f(\bar{T})$ – and
836 then somehow iteratively creeping towards a value deemed self-consistent. What this
837 means is that in addition to the solver described in the last section, there needs to be
838 a black-box function that solutions are piped through to get better guesses at η_{CD} .
839 The black-box function we use is a variation of the Ehst-Karney model.²⁰

840 As mentioned, a self-consistent η_{CD} is found once a trip through the Ehst-Karney
841 black-box results in the same η_{CD} as was piped in – to some tolerable level of error.
842 This consistency incorporates an explicit dependence on the tokamak configuration.
843 Mathematically,

$$\tilde{\eta}_{CD} = f(R_0, B_0, \bar{n}, \bar{T}, I_P) \quad (2.31)$$

844

845 As such, to recalculate it after every solution of the steady current requires a value
846 for both B_0 and R_0 – the targets of this model’s primary and secondary constraints.
847 These will be the highlight of the next chapter.

Chapter 3

Formalizing the Systems Model

The goal of this chapter is to take a step back from the steady current derivation and see the larger picture behind reactor design. As such, a more in-depth description of `staticfixed` and `dynamicfloating` variables is given. This discussion of `dynamicfloating` variables will then lend itself to a description of the framework underpinning the fusion systems model. As such, we will now need formulas for the radius and magnet strength of the tokamak. Moving forward, the current will then remain a connecting piece as we switch gears to pulsed tokamaks and compare the two schemes' underlying solvers.

3.1 Explaining `StaticFixed` Variables

In this model, `staticfixed` variables are ones that remain constant while solving for a reactor. These include geometric scalings (i.e. ϵ , δ , κ), profile parameters (i.e. ν_n , ν_T , l_i), and a slew of physics constants related to pulsed and steady-state design (e.g. Q , N_G , f_D). For a complete list of `staticfixed` variables, consult the appendix. The point to make now is that this model treats `staticfixed` variables as second-class objects. As such they often reside in `staticfixed` coefficients – K_\square – which are treated as constants.

865 3.2 Connecting **DynamicFloating** Variables

866 **DynamicFloating** variables – \bar{T} , \bar{n} , I_P , R_0 , B_0 – are the first-class variables of this
 867 fusion systems model. They represent the fundamental properties of a plasma and
 868 tokamak (which constitute a fusion reactor). As such, they will be reintroduced one
 869 at a time, explaining how they fit into the model – and which equation is capable of
 870 representing it.

Table 3.1: Dynamic Variables

Symbol	Name	Units
I_P	Plasma Current	MA
\bar{T}	Plasma Temperature	keV
\bar{n}	Electron Density	10^{20} m^{-3}
R_0	Major Radius	m
B_0	Magnetic Field	T

871 Bluntly, this fusion systems model is a simple algebra problem: solve five equations
 872 with five unknowns (i.e. \bar{T} , \bar{n} , I_P , R_0 , B_0). Although this naive approach would work,
 873 we can do a little better by wrangling these five equations down to just one. This was
 874 already done while deriving the steady current. It just happened that the current
 875 was not directly dependent on the tokamak size (R_0) or magnet strength (B_0).

876 This will prove more challenging for the generalized current needed for pulsed oper-
 877 ation. Even so, this equation will still be boiled down to one equation with a single
 878 unknown – I_P . A solution to which can be solved much faster than the naive 5
 879 equation approach. This is one reason the model is so fast.

880 The Plasma Temperature – \bar{T}

881 The plasma temperature, measured in keV (kilo-electron-volts), is one of the most
 882 finicky variables in the fusion systems model. It first proved troublesome when it was
 883 shown that a pedestal profile – not a parabolic one used here – would be needed for
 884 an accurate calculation of bootstrap current. The unusual tabulation for reactivity –
 885 (σv) – which appeared in fusion power only further exposed this nonlinearity.

Acknowledging that temperature is the most difficult to handle parameter prompts its use as the scanned variable. What this means practically is scanning temperatures produces curves of reactors. By example, a scan may be run over the average temperatures (\bar{T}): 10, 15, 20, 25, and 30 keV – each corresponding to its own reactor. In equation form, this becomes:

$$\bar{T} = \text{const.} \quad (3.1)$$

Where the constant happens to be 10 in one run, 15 for the next, and 30 in the fifth.

The Plasma Density – \bar{n}

The cornerstone of this fusion systems model has always been the application of the Greenwald density limit from square one. It is for this reason – as well as being a good approximation – that a parabolic profile was rationalized over a pedestal (H-Mode) one. Repeated, the Greenwald density limit is:

$$\bar{n} = K_n \cdot \frac{I_P}{R_0^2} \quad (2.11)$$

This is an exceptionally simple relationship and why it guided the model. Unlike the next three variables, it is actually used in their derivations. Therefore, any reactor found through this model is considered a *Greenwaldian Reactor* – one held at the Greenwald density limit.

The Plasma Current – I_P

The plasma current is what separates steady-state from pulsed operation. From before, the steady current was found to be:

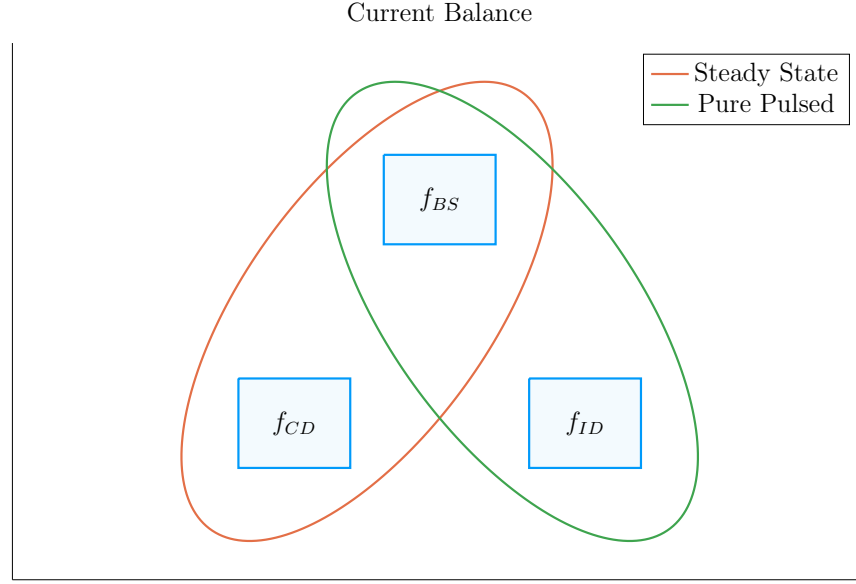


Figure 3-1: Current Balance in a Tokamak

In a tokamak, there needs to be a certain amount of current – and that current has to come from somewhere. All good reactors have an adequate bootstrap current. What provides the remaining current is what distinguishes steady state from pulsed operation.

$$I_P = \frac{K_{BS}\bar{T}}{1 - K_{CD}(\sigma v)} \quad (2.30)$$

905 This was derived by setting the total current equal to the two sources of current:
 906 bootstrap and current drive. Or in fractional form,

$$I_P = I_{BS} + I_{CD} \rightarrow 1 = f_{BS} + f_{CD} \quad (3.2)$$

907 This says that the current fractions of bootstrap and current drive must sum to one.
 908 As shown next chapter, inductive sources can be included into this current balance:

$$1 = f_{BS} + f_{CD} + f_{ID} \quad (3.3)$$

909 This equation shows how steady-state and pulsed operation can coexist (see Fig. 3-1).
 910 The final point to make is reducing the model to being purely pulsed – i.e. neglecting

911 the current drive:

$$1 = f_{BS} + f_{ID} \tag{3.4}$$

912 Therefore, the next chapter will generalize the steady current to allow pulsed oper-
913 ation, and then simplify it to the purely pulsed case. Just as steady current faced
914 self-consistency issues with η_{CD} , this current will also involve its own root solving
915 conundrum – the description of which will be given in the following two chapters.

916 **The Tokamak Magnet Strength – B_0**

917 The tokamak magnet strength has no obvious equation to eliminate it. With foresight,
918 the one this model chooses to use is power balance in a reactor. Similar to current
919 balance, power balance is what separates a reactor from a toaster. As such, it is
920 referred throughout this document as: the primary constraint. It will be derived
921 later this chapter.

922 **The Tokamak Major Radius – R_0**

923 Much like the magnet strength, the major radius has no obvious relation to express it.
924 This is convenient, because the model still has yet to resolve one of its most pressing
925 issues: physical and engineering-based constraints. This laundry list of requirements
926 further restricts reactor space to the curves shown in the results section. Collectively,
927 these are referred to as the secondary constraints – discussed later this chapter. By
928 miracle, these constraints all just happen to depend on the size of the reactor – the
929 reason they are chosen to substitute out the radius.

3.3 Enforcing Power Balance

What separates a reactor from a toaster is power balance. It accounts for how the power going into a plasma's core exactly matches the power coming out of it. To approximate this conservation equation, two sets of power will be introduced: the sources and the sinks.

The sources have mainly been introduced at this point – they include the alpha power (P_α) and the heating power (P_H), as well as a new ohmic power term (P_Ω). The remaining two powers – the sinks – then appear through the radiation and heat conduction losses, which will be given shortly. In equation form, power balance becomes:

$$\sum_{sources} P = \sum_{sinks} P \quad (3.5)$$

or expanded to fit this model:

$$P_\alpha + P_H + P_\Omega = P_{BR} + P_\kappa \quad (3.6)$$

For clarity, the left-hand side of this equality are the sources. Whereas the remaining two are sinks, i.e. Bremsstrahlung radiation (P_{BR}) and heat conduction losses (P_κ).

3.3.1 Collecting Power Sources

As suggested, the two dominant sources of power in a tokamak are: alpha power (P_α) and auxiliary heating (P_H). From earlier, it was determined that alpha particles (i.e. helium nuclei) carry around 20% of the total fusion power; or as we put it mathematically:

$$P_\alpha = \frac{P_F}{5} \quad (3.7)$$

948 Additionally, it was determined that the heating power is what was eventually am-
 949 plified into fusion power – or through equation:

$$P_H = \frac{P_F}{Q} \quad (3.8)$$

950 The final source term then is the ohmic power (P_Ω). This is identical to how copper
 951 wires in a home heat up as current runs through them. From a simple circuits
 952 picture, the power across the plasma is related to its current and resistance – in our
 953 standardized units – through:

$$P_\Omega = 10^6 \cdot I_P^2 \cdot R_P \quad (3.9)$$

954 Here, the resistance of the plasma is unlike any material humans encounter on a daily
 955 basis – actually decreasing with temperature. The fusion systems model handles the
 956 plasma resistance (R_P) with the neoclassical Spitzer resistivity. Through equation,

$$R_P = \frac{K_{RP}}{R_0 \bar{T}^{3/2}} \quad (3.10)$$

$$K_{RP} = 5.6e-8 \cdot \left(\frac{Z_{eff}}{\epsilon^2 \kappa} \right) \cdot \left(\frac{1}{1 - 1.31\sqrt{\epsilon} + 0.46\epsilon} \right) \quad (3.11)$$

957 Combined with the Greenwald limit, ohmic power can be written more compactly as,

$$P_\Omega = K_\Omega \cdot \left(\frac{\bar{n}^2 R_0^3}{\bar{T}^{3/2}} \right) \quad (3.12)$$

$$K_\Omega = 10^6 \cdot \frac{K_{RP}}{K_n^2} \quad (3.13)$$

958 With the sources defined, we are now in a position to discuss the two sink terms used
 959 in this model's power balance.

3.3.2 Approximating Radiation Losses

All nuclear reactors emit radiation. From a power balance perspective, this means some power has to always be reserved to recoup from its losses – measured in megawatts. In a fusion reactor, the three most important types of radiation are: Bremsstrahlung radiation, line radiation, and synchrotron radiation.

Without going into too much detail, this model chooses to only model Bremsstrahlung radiation – as it usually dominates within the plasma’s core. However, adding the effects of line-radiation and synchrotron radiation would drive results closer to real-world experiments. For example, line-radiation would better account for the heavy impurities that appear as pieces of a tokamak fall into the plasma.

For clarity, Bremsstrahlung – or breaking – radiation is what occurs when a charged particle (e.g. an electron) is accelerated by some means. In a tokamak, this happens all the time as charged particles are flung around and around the machine.* As given in Jeff Freidberg’s book, this term is described by the volume integral:

$$P_{BR} = \int S_{BR} d\mathbf{r} \quad (3.14)$$

Here, the radiation power density (S_{BR}) is given by:

$$S_{BR} = \left(\frac{\sqrt{2}}{3\sqrt{\pi^5}} \cdot \frac{e^6}{\epsilon_0^2 c^3 h m_e^{3/2}} \right) \cdot (Z_{eff} n^2 T^{1/2}) \quad (3.15)$$

The constants in the left set of parentheses all have their usual physics meanings (i.e. c is the speed of light and m_e is the mass of an electron). What is new is the effective charge: Z_{eff} .

The effective charge is a scheme for collapsing the charge that each particle has to a collective value. Fundamental charge, here, is what: neutrons lack, electrons and hydrogen have one of, and helium has two. As such, a plasma with a purely deuterium

*This centripetal acceleration is akin to a child spinning a bucket as fast as they can without spilling a drop of water.

and tritium fuel would have an effective charge of one. This value would then quickly rise if a Tungsten tile – with 74 units of charge – were to fall into the plasma core from the walls of the tokamak.

Using the volume integral – seen in the derivation of fusion power – allows the Bremsstrahlung power to be written in standardized units as:

$$P_{BR} = K_{BR} \bar{n}^2 \bar{T}^{1/2} R_0^3 \quad (3.16)$$

$$K_{BR} = 0.1056 \frac{(1 + \nu_n)^2 (1 + \nu_T)^{1/2}}{1 + 2\nu_n + 0.5\nu_T} Z_{eff} \epsilon^2 \kappa g \quad (3.17)$$

This power term represents the radiation power losses involved in power balance. All that is needed now is a formula for heat conduction losses – the hardest plasma behavior to model to date.

3.3.3 Estimating Heat Conduction Losses

Heat is energy that lacks direction on a microscopic level. Macroscopically, it generally moves from hotter areas to colder ones. As hinted by the plasma profile for temperature, heat emanates from the center of a plasma and migrates towards the walls of its tokamak enclosure. It therefore seems an important quantity to calculate when balancing power in a plasma's core.

The difficulty of estimating heat conduction, though, lies in the chaotic nature of plasmas – no theory or computation today can properly model it. As such, reactor designers have turned towards experimentalists for empirical scaling laws based on the dozen or so strongest tokamaks in the world. These are collectively referred to as confinement time scalings, i.e. the ELMy H-Mode Scaling Law.

The derivation of this heat conduction loss term (P_κ) starts in a manner similar to the previous powers. To begin, an equation for P_κ is given in Jeff Freidberg's book

1002 as:

$$P_{\kappa} = \frac{1}{\tau_E} \int U d\mathbf{r} \quad (3.18)$$

1003 This volume integral includes two new terms: the confinement time (τ_E) and the
1004 internal energy (U). Before explaining these terms, a qualitative description is in
1005 order. As mentioned previously, the heat – or microscopically random – energy is
1006 captured by the internal energy (U). Then the confinement time (τ_E) is how long it
1007 would take for the heat to completely leave the device if the system were suddenly
1008 turned off.

1009 A formula for confinement time will be delayed till the end of this section, when it is
1010 needed to solve for the magnetic field (B_0). The internal energy (U), however, can be
1011 given now as it has its typical physics meaning. This assumes that all three plasma
1012 species are held nearly at the same temperature (T) as the electrons:

$$U = \frac{3}{2} (n + n_D + n_T) T \quad (3.19)$$

1013 Here again, n_D and n_T – the density of deuterium and tritium, respectively – are
1014 related to the electron density (used in this model) through the dilution factor, which
1015 assumes a 50-50 mix of D-T fuel:

$$n_D = n_T = f_D \cdot \left(\frac{n}{2} \right) \quad (3.20)$$

1016 Foregoing the mathematical rigor of previous sections, the equations here can be
1017 combined to form an equation for P_{κ} – the heat conduction losses – in standardized
1018 units:

$$P_{\kappa} = K_{\kappa} \frac{R_0^3 \bar{n} \bar{T}}{\tau_E} \quad (3.21)$$

$$K_{\kappa} = 0.4744 (1 + f_D) \frac{(1 + \nu_n)(1 + \nu_T)}{1 + \nu_n + \nu_T} (\epsilon^2 \kappa g) \quad (3.22)$$

Now that all five terms have been defined in power balance, the next step is expanding it and solving for the tokamak's toroidal magnetic field strength: B_0 .

3.3.4 Writing the Lawson Criterion

Before locking in the primary constraint – i.e. the magnet strength (B_0) equation from power balance – it seems appropriate to take a detour and explain an intermediate solution: the Lawson Criterion. Within the fusion community, the Lawson Criterion is the cornerstone in any argument on the possibility of a design being used as a reactor (and not just some grandiose toaster).

An equation for the Lawson Criterion – sometimes referred to as the *triple product* – is easily found in the literature as:

$$n \cdot T \cdot \tau_E = \frac{60}{E_F} \cdot \frac{T^2}{\langle \sigma v \rangle} \quad (3.23)$$

Similar to the steady current derived earlier, the right-hand side is only dependent on temperature. Further, as the left-hand side is a measure of difficult to achieve parameters, the goal is to minimize both sides. This occurs when the plasma temperature is around 15 keV – a fact memorized by many fusion engineers. As will be seen, this is a simplified result of our model. This is why $\bar{T} = 15$ keV is not always the optimum temperature – but usually is in the right neighborhood for reasonable reactor designs.

As all the terms in power balance have already been defined, the starting point will be simply repeating the standardized equations for all five included powers.

$$P_{\alpha} = \frac{P_F}{5} \quad (3.7)$$

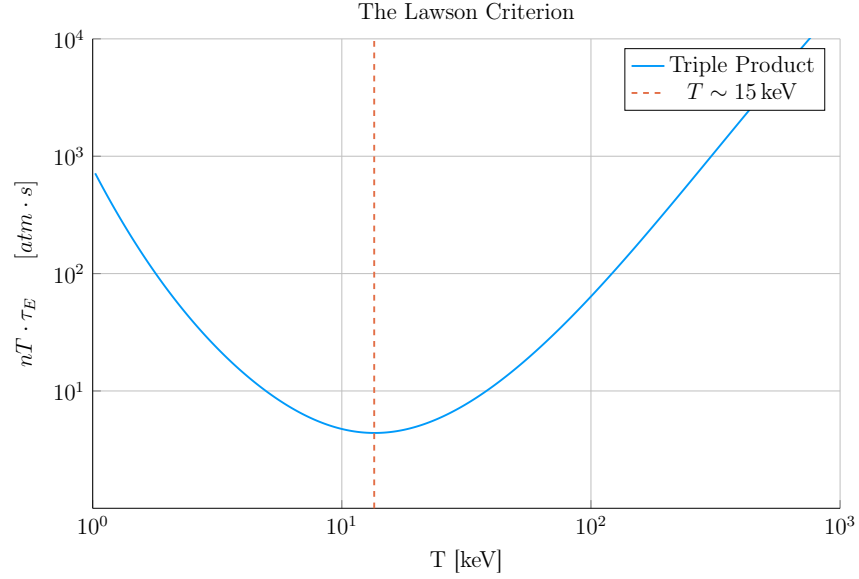


Figure 3-2: Power Balance in a Reactor

Power balance is what differentiates a reactor from a toaster. When cast as the Lawson Criterion for fusion, it explains why D-T plasmas often have a temperature around 15 keV.

$$P_H = \frac{P_F}{Q} \quad (3.8)$$

$$P_\Omega = K_\Omega \cdot \left(\frac{\bar{n}^2 R_0^3}{\bar{T}^{3/2}} \right) \quad (3.12)$$

$$P_{BR} = K_{BR} \bar{n}^2 \bar{T}^{1/2} R_0^3 \quad (3.16)$$

$$P_\kappa = K_\kappa \frac{R_0^3 \bar{n} \bar{T}}{\tau_E} \quad (3.21)$$

¹⁰³⁸ With the fusion power again being,

$$P_F = K_F \cdot \bar{n}^2 \cdot R_0^3 \cdot (\sigma v) \quad (2.23)$$

¹⁰³⁹ These can then be substituted into power balance:

$$P_\alpha + P_H + P_\Omega = P_{BR} + P_\kappa \quad (3.6)$$

1040 After a couple lines of algebra, power balance can be rewritten in a form analogous
1041 to the triple product:

$$\bar{n} \cdot \bar{T} \cdot \tau_E = \frac{K_\kappa \bar{T}^2}{\left(K_P (\sigma v) + K_{OH} \bar{T}^{-3/2}\right) - K_{BR} \bar{T}^{1/2}} \quad (3.24)$$

$$K_P = K_F \cdot \left(\frac{5 + Q}{5 \times Q}\right) \quad (3.25)$$

1042 As can be seen, this is remarkably similar to the simple Lawson Criterion:

$$n \cdot T \cdot \tau_E = \frac{60}{E_F} \cdot \frac{T^2}{\langle \sigma v \rangle} \quad (3.23)$$

1043 The main difference is this model does not ignore ohmic power and radiation losses
1044 completely. The inclusion of radiation for example sometimes bars a range of temper-
1045 atures from being physically realizable.* With this intermediate relation in place, the
1046 goal is now to give a formula for the confinement time and solve it for the magnetic
1047 field strength (B_0) – thus giving the Primary Constraint.

1048 3.3.5 Finalizing the Primary Constraint

1049 The goal now is to transform the Lawson Criterion into an equation for magnet
1050 strength (B_0). This choice to solve the equation for B_0 was completely arbitrary,
1051 only motivated by the foresight of how it fits into the fusion systems model. To solve
1052 the primary constraint, the confinement time scaling law will need to be introduced.
1053 At the end, a messy – albeit highly useful – relation will be the reward.

*The denominator of Eq 3.24 has discontinuities when the $K_{BR} \bar{T}^{1/2}$ term exactly equals the parenthesised one. Therefore, valid reactors only exist outside the discontinuities, when the entire triple product is finite and positive.

1054 The energy confinement time – τ_E – is one of the most elusive terms in all of fusion
 1055 energy. It is an attempt to boil down all the chaotic nature of plasmas into a simple
 1056 measure of how fast its internal energy would be ejected from the tokamak if the
 1057 device was instantaneously shut down. As such, reactor designers have turned toward
 1058 experimentalists for empirical scalings based on the world’s tokamaks. These all share
 1059 a form similar to:

$$\tau_E = K_\tau H \frac{I_P^{\alpha_I} R_0^{\alpha_R} a^{\alpha_a} \kappa^{\alpha_\kappa} \bar{n}^{\alpha_n} B_0^{\alpha_B} A^{\alpha_A}}{P_L^{\alpha_P}} \quad (3.26)$$

1060 This mouthful of a formula is how the field actually designs machines (i.e. ITER). Let
 1061 it be known, though, that these fits often do remarkable well, having relative errors
 1062 less than 20% on interpolated data. The new terms in this equation are: P_L , K_τ , H ,
 1063 A , and the α_\square factors.

1064 First, the loss power is a metric used in the engineering community to quantify the
 1065 power being transported out of the “core” of the plasma by charged particles (i.e. not
 1066 the neutrons).³ To optimize fits, experimentalists have defined this as a combination
 1067 of the source power terms:

$$P_L = P_\alpha + P_H + P_\Omega \quad (3.27)$$

1068 However, many have argued that the term should actually be replaced by its correct
 1069 physics meaning – the conductive heat loss power. As this model uses the ELMy
 1070 H-Mode scaling law, which is standard in the field, this alternative definition will not
 1071 be used:

$$\tilde{P}_L \approx P_\kappa = P_\alpha + P_H + P_\Omega - P_{BR} \quad (3.28)$$

1072 Moving on, K_τ is simply a constant fit-makers use in their scalings. Whereas H is
 1073 the (H-Mode) scaling factor – the analogue of K_τ used by reactor designers. This
 1074 H factor can be used to artificially boost the confinement of a machine (i.e. it adds

1075 a little bit of magic). Continuing, A is the average mass number of the fuel source,
 1076 in atomic mass units. For a 50-50 D-T fuel, this is 2.5, as deuterium weighs two
 1077 amus and tritium weighs three. Lastly, the alpha factors (e.g. α_n , α_a , α_P) are fitting
 1078 parameters that represent each variable's relative importance in the scaling.

1079 For ELMy H-Mode, this confinement scaling law can be written as:

$$\tau_E = 0.145 H \frac{I_P^{0.93} R_0^{1.39} a^{0.58} \kappa^{0.78} \bar{n}^{0.41} B_0^{0.15} A^{0.19}}{P_L^{0.69}} \quad (3.29)$$

1080 Where similar ones can be given for L-Mode, I-Mode, etc. One final remark to make
 1081 before moving on is that even these fits have subtleties. The value of κ , for example,
 1082 may have a slightly different geometric meaning from tokamak to tokamak. And the
 1083 exact definition of loss power – P_L – introduces an even larger area of discrepancy.
 1084 Although not actually used, a better fit for our model might be one from the author:

$$\tilde{\tau}_E = 0.08 H \frac{(R_0^{1.49} B_0^{0.3} I_P^{0.93}) \cdot (\epsilon^{0.17} A^{0.23} \kappa^{0.56})}{\tilde{P}_L^{0.54}} \quad (3.30)$$

1085 Returning to the problem at hand, though, this model's Lawson Criterion (eq. 3.24)
 1086 can be simplified after expanding the left-hand side using the Greenwald density and
 1087 substituting in a confinement time scaling law. Albeit a little cumbersome, this can
 1088 be wrangled into an equation for B_0 !

$$B_0 = \left(\frac{G_{PB}}{K_{PB}} \cdot \left(I_P^{\alpha_I} R_0^{\alpha_R} \right)^{-1} \right)^{\frac{1}{\alpha_B}} \quad (3.31)$$

$$G_{PB} = \frac{\bar{T} \cdot \left(K_P(\sigma v) + K_\Omega \bar{T}^{-3/2} \right)^{\alpha_P}}{\left(K_P(\sigma v) + K_\Omega \bar{T}^{-3/2} - K_{BR} \bar{T}^{1/2} \right)} \quad (3.32)$$

$$K_{PB} = H \cdot \left(\frac{K_\tau K_n^{\alpha_n^*}}{K_\kappa} \right) \cdot (\epsilon^{\alpha_a} \kappa^{\alpha_\kappa} A^{\alpha_A}) \quad (3.33)$$

Where we have added new starred alpha values for the density, current, and major radius:

$$\alpha_n^* = 1 + \alpha_n - 2\alpha_P \quad (3.34)$$

$$\alpha_I^* = \alpha_I + \alpha_n^* \quad (3.35)$$

$$\alpha_R^* = \alpha_R + \alpha_a - 2\alpha_n^* - 3\alpha_p \quad (3.36)$$

Again, if the alternate definition for heat loss (\tilde{P}) were used, another definition for \tilde{G}_{PB} would arise. Quickly reemphasizing, though, these tilded values are not actually used in the model:

$$\tilde{G}_{PB} = \frac{\bar{T}}{\left(K_P(\sigma v) + K_\Omega \bar{T}^{-3/2} - K_{BR} \bar{T}^{1/2} \right)^{(1-\alpha_P)}} \quad (3.37)$$

This equation for B_0 – derived from power balance – is thus the primary constraint for reactor designs. It is the first step in connecting the plasma (i.e. \bar{n} , \bar{T} , and I_P) to its tokamak enclosure (i.e. B_0 and R_0). The remaining step is finding an equation – or in this case, equations – for the major radius of the device. These radius equations will collectively be referred to as: the Secondary Constraints.

3.3.6 Exploring the Freidberg Criterion

Before moving onto the Secondary Constraint, it is worth noting that this power balance equation can be written in a triple product form analogous to the Lawson Criterion. For this reason, we will refer to it as the Freidberg Triple Product:

$$R_0^{\alpha_R^*} \cdot B_0^{\alpha_B} \cdot I_P^{\alpha_I^*} = \frac{G_{PB}}{K_{PB}} \quad (3.38)$$

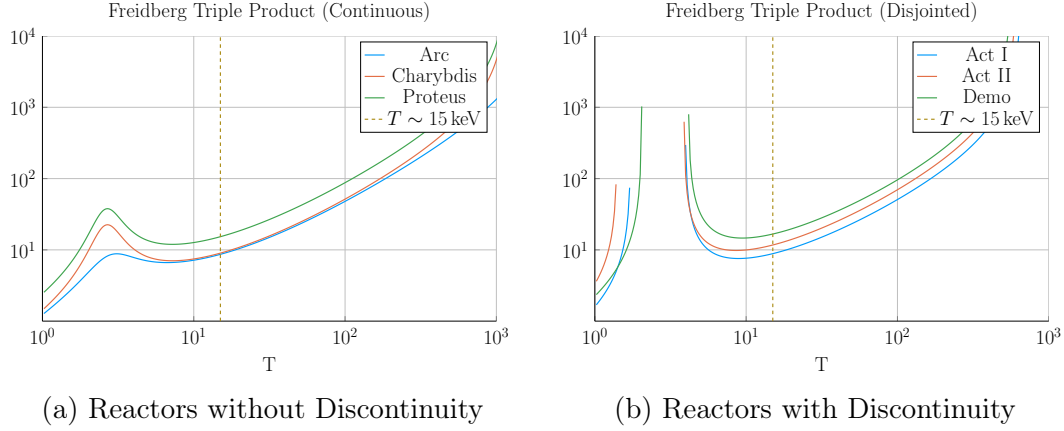


Figure 3-3: Freidberg Triple Product

The Freidberg Triple Product builds on the original Lawson Criterion by incorporating empirical scalings, such as confinement time and the Greenwald density.

As is readily apparent, this has a shape similar to the Lawson Criterion. Again, the goal is operate when the right-hand side reaches an approximate minimum. This corresponds to when the left-hand side is also minimized – where each term represents one of the difficult to achieve quantities of a tokamak fusion reactor.

3.4 Collecting Secondary Constraints

As of now, the only missing equation within our list of ~~static~~~~fixed~~ variables – i.e. R_0 , B_0 , \bar{T} , \bar{n} , and I_P – is for the major radius of the tokamak. This equation will come from around five potential limits, each either physical or engineering-based. These limits will then correspond to different curves through reactor space. As will be shown, many of these reactors will be invalid (as they violate at least one of the other limits).

Before tackling the subject of finding reactors that exist on the fine line of satisfying every secondary constraints, though, it is essential to collect them one-by-one. These are: the Troyon Beta Limit, the Kink Safety Factor, the Wall Loading Limit, the Power Cap Constraint, and the Heat Loading Limit.

1118 The goal of this section is to solve for each of these constraints on the major radius.
 1119 As with the primary constraint, this choice of solving for R_0 was completely arbitrary.
 1120 It just so happens that each limit described here depends on the size of a reactor –
 1121 which is not true for the magnetic field strength.

1122 3.4.1 Introducing the Beta Limit

1123 The Beta Limit is the most important secondary constraint – especially for steady-
 1124 state reactors. It sets a maximum on the amount of pressure a plasma is willing
 1125 to tolerate. As with future secondary constraints, literature-based equations will be
 1126 transformed into formulas for R_0 . Each will then contain some limiting quantity that
 1127 can be handled by a ~~static~~fixed variable – as β_N will be used shortly.

1128 The starting point for the beta limit is to define the important plasma physics quan-
 1129 tity: β – the plasma beta. This value is a ratio between a plasma’s internal pressure
 1130 and the pressure exerted on it by the tokamak’s magnetic configuration. Mathemat-
 1131 ically,⁷

$$\beta = \frac{\text{plasma pressure}}{\text{magnetic pressure}} = \frac{\bar{p}}{\left(\frac{B_0^2}{2\mu_0}\right)} \quad (3.39)$$

1132 Using this model’s temperature and density profiles, the volume-averaged pressure
 1133 (\bar{p}) can be written in units of atmospheres (i.e. atm) as:

$$\bar{p} = 0.1581 (1 + f_D) \frac{(1 + \nu_n)(1 + \nu_T)}{1 + \nu_n + \nu_T} \bar{n} \bar{T} \quad (3.40)$$

1134 Moving forward, the final step is plugging this definition for plasma beta into the
 1135 physics-based Troyon Beta Limit. Although outside the scope of this text, it is a
 1136 stability limit set by treating plasmas as charge-carrying fluids. This equation can
 1137 be written in the following form, where β_N is the normalized plasma beta – i.e. a
 1138 ~~static~~fixed variable usually set between 2% and 4%.²¹

$$\beta = \beta_N \frac{I_P}{aB_0} \quad (3.41)$$

1139 Substituting the plasma β from eq. 3.39, into this relation results in the model's first
1140 equation for tokamak radius:

$$R_0 = \frac{K_{TB}\bar{T}}{B_0} \quad (3.42)$$

$$K_{TB} = 4.027e-2 (K_n) \left(\frac{\epsilon}{\beta_N} \right) (1 + f_D) \frac{(1 + \nu_n)(1 + \nu_T)}{1 + \nu_n + \nu_T} \quad (3.43)$$

1141 As mentioned, this is often the dominating constraint in a steady-state reactor. The
1142 often dominating constraint for pulsed designs – the kink safety factor – will be the
1143 focus of the next subsection.

1144 3.4.2 Giving the Kink Safety Factor

1145 Just like how the Troyon Beta Limit set a fluids-based maximum on plasma pressure,
1146 the Kink Safety Factor sets one on the plasma's current. This constraint usually
1147 only appears in pulsed designs, as it is assumed that getting to this high a current in
1148 steady-state (with only LHCD) would prove extremely unpractical.

1149 The starting point, again, is an equation from the literature for the kink condition:³

$$q_{95} = 5\epsilon^2 f_q \cdot \frac{R_0 B_0}{I_P} \quad (3.44)$$

1150 Here the safety factor – q_{95} – is subscripted by 95, an identifier that this value is
1151 taken at the 95% flux surface (i.e. near the statistically drawn edge of the plasma).
1152 It typically has values around 3. Next, the f_q variable is a geometric scaling factor:

$$f_q = \frac{1.17 - 0.65\epsilon}{2(1 - \epsilon^2)^2} \cdot (1 + \kappa^2 * (1 + 2\delta^2 - 1.2\delta^3)) \quad (3.45)$$

1153 Combined, the kink safety factor can now be written in standardized units as:

$$R_0 = \frac{K_{SF} I_P}{B_0} \quad (3.46)$$

$$K_{SF} = \frac{q_{95}}{5\epsilon^2 f_q} \quad (3.47)$$

1154 This relation is the secondary constraint important for most pulsed reactor designs.
1155 As with the Beta Limit, the two are derived through plasma physics alone. The
1156 remaining secondary constraints, however, are engineering-based in origin – these
1157 include: the Wall Loading Limit, the Power Cap Constraint, and the Heat Loading
1158 Limit. Each will be defined shortly.

1159 3.4.3 Working under the Wall Loading Limit

1160 The first engineering-based secondary constraint – the wall loading limit – will prove
1161 to be an important quantity when determining the magnet strength at which reactor
1162 costs first start to increase. As hinted, its definition originates from nuclear engineer-
1163 ing concerns: it is a measure of the maximum neutron damage a tokamak’s walls can
1164 take over the lifetime of the machine.

1165 The first step in deriving a secondary constraint for wall loading is a description of the
1166 problem it models. In a reactor, fusion reactions typically make high-energy neutrons
1167 – with around 14.1 MeV of kinetic energy – that continually blast the inner wall of
1168 the tokamak. Therefore a quick-and-dirty metric would be limiting the amount of
1169 neutron power that can be unloaded on the surface area of a tokamak. This can be
1170 written as:

$$P_W = \frac{P_n}{S_P} \quad (3.48)$$

1171 Here, S_P is the surface area of the tokamak’s inner wall and P_n is the neutron power

1172 derived in the subsection on fusion power. The quantity, P_W , then serves a role
 1173 analogous to β_N for the beta limit and q_{95} for the kink safety factor – it is a ~~static~~**fixed**
 1174 variable representing the maximum allowed wall loading. For fusion reactors, P_W is
 1175 assumed to be around 2-4 $\frac{\text{MW}}{\text{m}^2}$. It will be shown that the wall loading limit is important
 1176 in any tokamak – regardless of operating mode (i.e. steady-state or pulsed).

1177 For completeness, the surface area can be defined through:

$$S_P = 4\pi^2 a_P R_0 \cdot \frac{\left(1 + \frac{2}{\pi} (\kappa_P^2 - 1)\right)}{\kappa_P} \quad (3.49)$$

1178 In this formula, the various dimensions subscripted with P's are:

$$a_P = 1.04 a \quad (3.50)$$

$$\kappa_P = 1.3 \kappa \quad (3.51)$$

$$\epsilon_P = \frac{a_P}{R_0} \quad (3.52)$$

1179 Finishing this secondary constraint, the Wall Loading limit can be written in stan-
 1180 dardized units as:

$$R_0 = K_{WL} \cdot I_P^{\frac{2}{3}} \cdot (\sigma v)^{\frac{1}{3}} \quad (3.53)$$

$$K_{WL} = \left(\frac{K_F K_n^2}{5\pi^2 P_W} \cdot \frac{\kappa_P}{\epsilon_P} \cdot \frac{1}{1 + \frac{2}{\pi} \cdot (\kappa_P^2 - 1)} \right)^{\frac{1}{3}} \quad (3.54)$$

1181 3.4.4 Setting a Maximum Power Cap

1182 As opposed to the previous three secondary constraints, the maximum power cap is
1183 more of a rule of thumb. Because no reactor – coal, solar, or otherwise – has a 4000
1184 MW reactor, neither should fusion. It makes sense from a practical position after
1185 realizing the long history of tokamaks being delayed, underfunded, or completely
1186 canceled. Mathematically, this has the simple form:

$$P_E \leq P_{CAP} \quad (3.55)$$

1187 Here, P_{CAP} is the maximum allowed power output of the reactor. Similar to the other
1188 limiting quantities, P_{CAP} is treated as a ~~static~~~~fixed~~ variable (i.e. set to 4000 MW).
1189 The electrical power output of the reactor (P_E) is then related to the fusion power
1190 through:⁷

$$P_E = 1.273 \eta_T \cdot P_F \quad (3.56)$$

1191 The constant in front (i.e. 1.273) represents some extra power the reactor makes as
1192 more fuel is bred when the fusion neutrons pass through a tokamak (inside its still-
1193 undiscussed blanket region). The variable η_T is the thermal efficiency of the reactor
1194 – which is usually found to be around 40%.

1195 Substituting in fusion power and solving for the major radius results in:

$$R_0 = K_{PC} \cdot I_P^2 \cdot (\sigma v) \quad (3.57)$$

$$K_{PC} = K_F K_n^2 \cdot \left(\frac{1.273 \eta_T}{P_{max}} \right) \quad (3.58)$$

1196 This secondary constraint can be used to create curves of reactors, although it is
1197 mainly used as a stopping point for designs – i.e. if you get to the power-cap regime,

1198 you have gone too far. This is different than the next constraint, which is basically a
 1199 glorified warning sign in the contemporary tokamak design paradigm.

1200 3.4.5 Listing the Heat Loading Limit

1201 Plasmas are hot. The commonly given fact is one electron volt is around 20,000 °F.
 1202 Although a tad deceptive, melting a tokamak is an all too real concern. The problem
 1203 is there is currently no solution to the problem. Although researchers have explored
 1204 various types of heat divertors, none have been shown to withstand the gigawatts
 1205 of heat emitted from a reactor-size tokamak. Further, as it is not as glamorous as
 1206 plasma physics, attempts to tackle the problem head-on have often gone unfunded.²²

1207 As such, this model takes the approach that we are no worse than the rest of the
 1208 field. We almost completely ignore the heat loading limit and just refer to it at the
 1209 end, saying "and then this magic divertor will have to deal with solar corona levels
 1210 of heat." After which, discussion will quickly be redirected to happier concerns.

1211 For thoroughness though, a secondary constraint will still be derived. The first step
 1212 is giving the heat load limit commonly found in the literature:²³

$$q_{DV} = \frac{K_{DV}}{K_F} \cdot \frac{P_F I_P^{1.2}}{R_0^{2.2}} \quad (3.59)$$

$$K_{DV} = \frac{18.31e-3}{\epsilon^{1.2}} \cdot K_P \cdot \left(\frac{2}{1 + \kappa^2} \right)^{0.6} \quad (3.60)$$

1213 After a simple rearrangement and substitution for fusion power, this becomes:

$$R_0 = K_{DH} \cdot I_P \cdot (\sigma v)^{\frac{1}{3.2}} \quad (3.61)$$

$$K_{DH} = \left(\frac{K_{DV} K_n^2}{q_{DV}} \right)^{\frac{1}{3.2}} \quad (3.62)$$

At this point all the secondary constraints have been defined. The next step is taking a step back and motivating the derivation of a current equation suitable for pulsed tokamaks.

3.5 Summarizing the Fusion Systems Model

This chapter focused on the bigger picture behind designing a zero-dimension fusion systems model. It started with a description of various design parameters and then segued into explaining the five relations needed to close the model – i.e. for \bar{T} , \bar{n} , I_P , B_0 , and R_0 .

Before moving onto generalizing the steady current to model pulsed reactors, a quick recap of the equations will prove beneficial. The first variable tackled was temperature – i.e. scan five evenly-spaced \bar{T} values between 10 and 30 keV. This was then quickly followed by the Greenwald density limit – the cornerstone of this framework. Through equations, these two were written as:

$$\bar{T} = \text{const.} \quad (3.1)$$

$$\bar{n} = K_n \cdot \frac{I_P}{R_0^2} \quad (2.11)$$

The next variable handled was the steady current:

$$I_P = \frac{K_{BS}\bar{T}}{1 - K_{CD}(\sigma v)} \quad (2.30)$$

As was mentioned then, this only directly depends on temperature, but is strongly affected by a tokamak's configuration – R_0 and B_0 - through the current drive efficiency (η_{CD}). For pulsed reactors, this equation proves too simple as it ignores inductive current. To remedy the situation, current balance will be revisited next chapter. The

1232 main point to make now, though, is that the R_0 and B_0 dependence will be made
 1233 explicit.

1234 Moving on, the remaining equations were the primary and secondary constraints for
 1235 B_0 and R_0 , respectively. It was through these relations that a tokamak's configuration
 1236 was brought back into the fold. The choice of solving the two constraints for their
 1237 respective variables was completely arbitrary – motivated only by the foresight of
 1238 how they fit into the model. Repeated below, they served as the proper vehicles for
 1239 closing the system of equations. The next step now is to learn how to generalize the
 1240 current formula and design a pulsed tokamak reactor.

$$B_0 = \left(\frac{G_{PB}}{K_{PB}} \cdot \left(I_P^{\alpha_I^*} R_0^{\alpha_R^*} \right)^{-1} \right)^{\frac{1}{\alpha_B}} \quad (3.31)$$

$$R_0 = \frac{K_{TB} \bar{T}}{B_0} \quad (3.42)$$

$$R_0 = \frac{K_{SF} I_P}{B_0} \quad (3.46)$$

$$R_0 = K_{WL} \cdot I_P^{\frac{2}{3}} \cdot (\sigma v)^{\frac{1}{3}} \quad (3.53)$$

$$R_0 = K_{PC} \cdot I_P^2 \cdot (\sigma v) \quad (3.57)$$

$$R_0 = K_{DH} \cdot I_P \cdot (\sigma v)^{\frac{1}{3.2}} \quad (3.61)$$

1241 Chapter 4

1242 Designing a Pulsed Tokamak

1243 Pulsed tokamaks are the flagship of the European fusion reactor design effort. As such,
1244 this paper's model will now be generalized to accommodate this mode of operation.
1245 Fundamentally, this involves transforming current balance into flux balance – adding
1246 inductive (pulsed) sources to stand alongside the LHCD (steady-state) ones.

1247 The first step in generalizing current balance will be understanding the problem from
1248 a basic electrical engineering perspective – i.e. with circuit analysis. The resulting
1249 equation will then be transformed into the flux balance seen in other models from
1250 the literature. All that will need to be done then is solving the problem for plasma
1251 current (I_P) and simplifying it for various situations – e.g. steady-state operation.

1252 This generalized plasma current will then be found to be a function of the other
1253 dynamic variables (i.e. R_0 , B_0 , and \bar{T}). This, of course, is more difficult to handle
1254 computationally than the steady current, which only directly depended on tempera-
1255 ture (\bar{T}). Discussion about solving this new root solving problem will be the topic of
1256 the next chapter.

1257 4.1 Modeling Plasmas as Circuits

1258 Although it may have been lost along the way, what makes plasmas so interesting and
1259 versatile – in comparison to gases – is their ability to respond to electric and magnetic
1260 fields. It seems natural then to model plasma current from a circuits perspective (i.e.
1261 with resistors, voltage sources, and inductors). By name, this circuit is referred to as
1262 a transformer where: the plasma is the secondary and the yet-to-be discussed central
1263 solenoid (of the tokamak) is the primary.

1264 The first step in deriving a current equation is to determine the circuit equations
1265 that govern pulsed operation in a tokamak. This will be done in two steps. First, we
1266 will draw a circuit diagram and write the equations that describe it. Next, we will
1267 use a simple schematic for how current evolves in a transformer to boil the resulting
1268 differential equations into simple algebraic ones – as is the hallmark of our model.

1269 4.1.1 Drawing the Circuit Diagram

1270 Understanding a circuit always starts with drawing a simple diagram, see Fig. 4-1.
1271 This figure depicts the transformer governing pulsed reactor. The left sub-circuit
1272 is the transformer’s primary – the central solenoid component of the tokamak that
1273 provides most of the inductive current. Whereas, the right sub-circuit is the plasma
1274 acting as the transformer’s secondary. The central solenoid, here, is then a helically-
1275 spiraled metal coil that fits within the inner ring of the doughnut. For now, every
1276 other flux source (besides this central solenoid) is neglected.

1277 This is described by the standard circuits involving voltage sources, resistors, and
1278 inductors: ~~Hopefully without scaring the reader too much, the circuit equations –~~
1279 ~~when only modeling voltage sources, resistors, and inductors – are described by:~~

$$V_i = \sum_j^n \frac{d}{dt} (M_{ij} I_j) + I_i R_i \quad , \quad \forall i = 1, 2, \dots, n \quad (4.1)$$

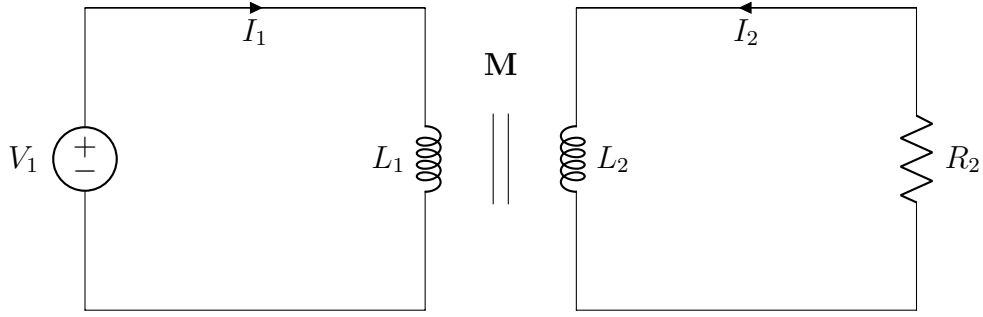


Figure 4-1: A Simple Plasma Transformer Description

Without going into the inductances (M) and resistances (R), the variable n is the number of sub-circuits, here being 2. Whereas, the variables i and j are the indices of sub-circuits (i.e. 1 for the primary, 2 for the secondary). For illustrative purposes, this would boil down to the following relation for a battery attached to a lightbulb:

$$V = IR \quad (4.2)$$

Back to the transformer diagram, the equations for the two subcircuits can be expanded and greatly simplified. Besides ignoring every inductive source other than the central solenoid, the next powerful assumption is treating the solenoid as a superconductor (i.e. with negligible resistance). Lastly, the inductances between components and themselves are held constant – independent of time. This allows the coupled transformer equations to be written as:

$$V_1 = L_1 \dot{I}_1 - M \dot{I}_2 \quad (4.3)$$

$$-I_2 R_P = L_2 \dot{I}_2 - M \dot{I}_1 \quad (4.4)$$

With I_1 and I_2 going in opposite directions. Note, here, that the subscript on M has been dropped, as there are only two components. This was done in conjunction to adding internal (self-)inductance terms. Mathematically, the mapping between variables is:

$$M = M_{12} = M_{21} \quad (4.5)$$

$$L_1 = M_{11} \quad (4.6)$$

$$L_2 = M_{22} \quad (4.7)$$

1294 Repeated, the one subscript represents the primary – the central solenoid – and the
 1295 two stands for the plasma as the transformer’s secondary. Exact definitions for the
 1296 inductances will be put off till the end of the next subsection.

1297 4.1.2 Plotting Pulse Profiles

1298 Up until now, little has been discussed that has a time dependence. For steady-state
 1299 tokamaks, this did not occur because it is an extreme case where pulses basically last
 1300 the duration of the machine’s lifespan (i.e. around 50 years). By definition, though,
 1301 a pulsed machine has pulses – with around ten scheduled per day. For this reason, a
 1302 fusion pulse is now investigated in detail.

1303 Transformer pulses between the central solenoid and the plasma occur on the timescale
 1304 of hours. During this time, a plasma is brought up to some quasi-steady-state current
 1305 (I_P^*) for around an hour and then ramped back down using the available flux in the
 1306 solenoid (measured in volt-seconds). For clarity, each pulse is subdivided into four
 1307 phases: ramp-up, flat-top, ramp-down, and dwell. Pictorially represented in Fig. 4-2,
 1308 these divisions allow a simple scheme for transforming the coupled circuit differential
 1309 equations – from Eqs. (4.3) and (4.4) – into simple algebraic formulas.

1310 Along the way, we will approximate derivatives with linear piecewise functions. Using
 1311 t_i to represent the initial time and t_f as the final one, these can be written as:

Tokamak Circuit Profiles

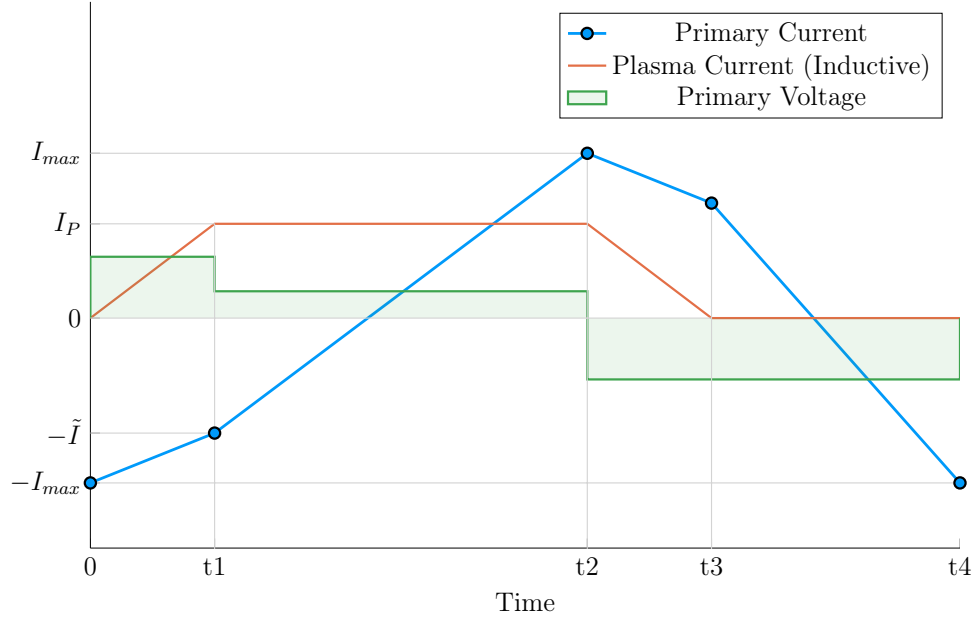


Figure 4-2: Time Evolution of Circuit Profiles

$$\dot{I} = \frac{I(t_f) - I(t_i)}{t_f - t_i} \quad (4.8)$$

1312 In tabular form, the data from Fig. 4-2 can be written in this piecewise fashion as:

Table 4.1: Piecewise Linear Scheme for Pulsed Operation

(a) Currents			(b) Voltage			
Time	I_1	I_2	Phase	t_i	t_f	V_1
0	$-I_{max}$	0	Ramp-Up	0	t_1	$+V_{max}$
t1	$-\tilde{I}$	I_P^*	Flat-top	t_1	t_2	$+\tilde{V}$
t2	$+I_{max}$	I_P^*	Ramp-Down	t_2	t_3	$-V_{max}$
t3	$+\tilde{I}$	0	Dwell	t_3	t_4	$-V_{max}$
t4	$-I_{max}$	0				

1313 The exact definitions for the plasma's inductive current (I_P^*) and the maximum volt-
 1314 age in the central solenoid (V_{max}) will be put off until the end of the section.

1315 The Ramp-Up Phase – RU

1316 The first phase in every plasma pulse is the ramp-up. During ramp-up, the central
 1317 solenoid starts discharging from its fully charged values, as the plasma is brought to
 1318 its quasi-steady-state current. As this occurs on the timescale of minutes – not hours
 1319 – resistive effects of the plasma can safely be ignored. This results in the ramp-up
 1320 equations becoming:

$$V_{max} = \frac{1}{\tau_{RU}} \cdot \left(L_1 \cdot (I_{max} - \tilde{I}) - M \cdot I_{ID} \right) \quad (4.9)$$

$$0 = \frac{1}{\tau_{RU}} \cdot \left(M \cdot (I_{max} - \tilde{I}) - L_2 \cdot I_{ID} \right) \quad (4.10)$$

1321 Simplifying these equations will be done shortly, for now the new terms are what
 1322 is important. The maximum voltage of the solenoid is V_{max} – usually measured in
 1323 kilovolts. Next, I_{max} is the solenoid’s current at the beginning of ramp-up. Whereas
 1324 \tilde{I} is the magnitude of the current once the plasma is at its flattop inductive-drive
 1325 current – I_{ID} . The τ_{RU} quantity, then, is the duration of time it takes to ramp-up
 1326 (i.e. RU). Again, L_1 and L_2 are the microhenry-scale internal inductances of the
 1327 solenoid and plasma, respectively, and M is the mutual inductance between them.

1328 The last step in discussing ramp-up is giving the two important formulas that come
 1329 from it:

$$\tilde{I} = I_{max} - I_{ID} \cdot \left(\frac{L_2}{M} \right) \quad (4.11)$$

$$\tau_{RU} = \frac{I_{ID}}{V_{max}} \cdot \left(\frac{L_1 L_2 - M^2}{M} \right) \quad (4.12)$$

1330 The Flattop Phase – FT

1331 The most important phase in any reactor’s pulse is flattop – the quasi-steady-state
1332 time when the tokamak is making electricity (and money). Flattops are assumed
1333 to last a couple of hours for a profitable machine, during which the central solenoid
1334 completely discharges to overcome a plasma’s resistive losses – keeping it in a quasi-
1335 steady-state mode of operation. In a steady-state reactor, this phases constitutes the
1336 entirety of the pulse.

1337 Although the resistance cannot be safely neglected for flattop – as it was for ramp-up –
1338 the plasma’s inductive current (I_{ID}) is assumed constant. This leads to its derivative
1339 in equations cancelling out! Mathematically,

$$\tilde{V} = \frac{L_1}{\tau_{FT}} \cdot (I_{max} + \tilde{I}) \quad (4.13)$$

$$I_{ID}R_P = \frac{M}{\tau_{FT}} \cdot (I_{max} + \tilde{I}) \quad (4.14)$$

1340 As with ramp-up, the simplifications will be given shortly. The new terms here,
1341 however, are an intermediate voltage for the central solenoid (\tilde{V}), and the duration
1342 of the flattop (τ_{FT}). The resistance term was given in Eq. (3.10). Solutions can then
1343 be found by substituting \tilde{I} – from Eq. (4.11) – into the flattop equations:

$$\tilde{V} = I_{ID}R_P \cdot \left(\frac{L_1}{M} \right) \quad (4.15)$$

$$\tau_{FT} = \frac{I_{max} \cdot 2M - I_{ID} \cdot L_2}{I_{ID}R_P} \quad (4.16)$$

1344 The Ramp-Down Phase – RD

1345 Due to the simplicity – and symmetry – of this model’s reactor pulse, ramp-down is
1346 the exact mirror of ramp-up. It takes the same amount of time and results in the

1347 same algebraic equations. For brevity, this will just be represented as:

$$\tau_{RD} = \tau_{RU} \quad (4.17)$$

1348 For clarity, this is the time when a plasma's current is brought down from its flattop
1349 value to zero.

1350 **The Dwell Phase – DW**

1351 Where the first three phases had little ambiguity, the dwell phase changes definition
1352 from model to model. For now, it is assumed to be the time it takes the central
1353 solenoid to reset after a plasma has been completely ramped-down to an off-mode.
1354 To get a more realistic duty factor for cost estimates, it could include an evacuation
1355 time, set to last around thirty minutes. During this evacuation, a plasma is vacuumed
1356 out of a device as it undergoes some inter-pulse maintenance.

1357 Ignoring evacuation for now, the dwell phase involves resetting the central solenoid
1358 when the plasma's current is negligible. This fundamentally means the secondary of
1359 the transformer is nonexistent – the central solenoid is the entire circuit. In equation
1360 form,

$$V_{max} = \frac{L_1}{\tau_{DW}} \cdot (I_{max} + \tilde{I}) \quad (4.18)$$

1361 Or substituting in \tilde{I} and solving for τ_{DW} ,

$$\tau_{DW} = \frac{L_1}{M} \cdot \frac{(I_{max} \cdot 2M - I_{ID} \cdot L_2)}{V_{max}} \quad (4.19)$$

1362 **4.1.3 Specifying Circuit Variables**

1363 The goal now is to collect the results from the four phases and introduce the induc-
1364 tance, resistance, voltage, and current terms relevant to our model. This will motivate

1365 recasting the problem as flux balance in a reactor – the form commonly used in the
 1366 literature (and discussed next section).

1367 First, collecting the phase durations in one place:

$$\tau_{RU} = \frac{I_{ID}}{V_{max}} \cdot \left(\frac{L_1 L_2 - M^2}{M} \right) \quad (4.12)$$

$$\tau_{FT} = \frac{I_{max} \cdot 2M - I_{ID} \cdot L_2}{I_{ID} R_P} \quad (4.16)$$

$$\tau_{RD} = \tau_{RU} \quad (4.17)$$

$$\tau_{DW} = \frac{L_1}{M} \cdot \frac{(I_{max} \cdot 2M - I_{ID} \cdot L_2)}{V_{max}} \quad (4.19)$$

1368 These can be used in the definition of the duty-factor: the fraction of time a reactor
 1369 is putting electricity on the grid. Formulaically,

$$f_{duty} = \frac{\tau_{FT}}{\tau_{pulse}} \quad (4.20)$$

$$\tau_{pulse} = \tau_{RU} + \tau_{FT} + \tau_{RD} + \tau_{DW} \quad (4.21)$$

1370 As will turn out, the solving of pulsed current actually only involves Eq. (4.16).
 1371 What is interesting about this, is that there is no explicit dependence on ramp-down
 1372 or dwell! Whereas ramp-up passes \tilde{I} to the flattop phase, the other two are just
 1373 involved in calculating the duty factor.

1374 The remainder of this subsection will then be defining the following circuit variables:
 1375 I_{ID} , I_{max} , V_{max} , L_1 , L_2 , and M . Again, the resistance was defined last chapter as:

$$R_P = \frac{K_{RP}}{R_0 \bar{T}^{3/2}} \quad (3.10)$$

1376 The Inductive Current – I_{ID}

1377 The inductive current is the source of current that separates pulsed from steady-state
 1378 operation. Quickly fitting it into the previous definitions of current balance – see
 1379 Eq. (3.3):

$$I_{ID} = I_P - (I_{BS} + I_{CD}) \quad (4.22)$$

1380 As before, I_P is the total plasma current in mega-amperes, I_{BS} is the bootstrap current,
 1381 and I_{CD} is the current from LHCD (i.e. lower hybrid current drive). For this model,
 1382 the relation can be rewritten as:

$$I_{ID} = I_P \cdot \left(1 - K_{CD}(\sigma v)\right) - K_{BS} \bar{T} \quad (4.23)$$

1383 The Central Solenoid Maximums – V_{max} and I_{max}

1384 For this simple model, the central solenoid has two maximum values: the voltage and
 1385 current. The voltage is the easier to give value. Literature values have this around:²⁴

$$V_{max} \approx 5 \text{ kV} \quad (4.24)$$

1386 The maximum current, on the other hand, can be defined through Ampere's Law on
 1387 a helically-shaped central solenoid:¹⁵

$$I_{max} = \frac{B_{CS} h_{CS}}{N \mu_0} \quad (4.25)$$

1388 Here, B_{CS} is a magnetic field strength the central solenoid is assumed to operate at
 1389 (i.e. 12 T), h_{CS} is the height of the solenoid, N is the number of loops, and μ_0 has its
 1390 usual physics meaning (i.e. $40 \pi \frac{\mu\text{H}}{\text{m}}$). As will be seen, the value of N does not directly
 1391 affect the model, as it cancels out in the final flux balance. The height of the central

1392 solenoid will be the focus of an upcoming section on improving tokamak geometry.

1393 **The Central Solenoid Inductance – L_1**

1394 For a central solenoid with circular cross-sections of finite thickness (d), the inductance
1395 can be written as:²¹

$$L_1 = G_{LT} \cdot \left(\frac{\mu_0 \pi N^2}{h_{CS}} \right) \quad (4.26)$$

$$G_{LT} = \frac{R_{CS}^2 + R_{CS} \cdot (R_{CS} + d) + (R_{CS} + d)^2}{3} \quad (4.27)$$

1396 Note that R_{CS} is the inner radius of the central solenoid and $(R_{CS} + d)$ is the outer
1397 one. In the limit where d is negligible, this says that the inductance is quadratically
1398 dependent on the radius of the central solenoid:

$$\lim_{d \rightarrow 0} G_{LT} = G_{LT}^\dagger = R_{CS}^2 \quad (4.28)$$

1399 The formulas for both R_{CS} and d will be defined in a few sections.

1400 **The Plasma Inductance – L_2**

1401 The plasma inductance is a composite of several different terms, but overall scales
1402 with radius. Through equation,

$$L_2 = K_{LP} R_0 \quad (4.29)$$

1403 This ~~static~~~~fixed~~ coefficient – K_{LP} – then combines three inductive behaviors of the
1404 plasma. The first is its own self inductance (through l_i).⁷ The next is a resistive
1405 component through the Ejima coefficient, C_{ejima} , which is usually set to $\sim \frac{1}{3}$.³ And
1406 lastly, a geometric component – involving ϵ and κ – is given by the Hirshman-Neilson

1407 model.²⁵ Mathematically,

$$K_{LP} = \mu_0 \cdot \left(\frac{l_i}{2} + C_{ejima} + \frac{(b_{HN} - a_{HN})(1 - \epsilon)}{(1 - \epsilon) + \kappa d_{HN}} \right) \quad (4.30)$$

1408 Here the HN values come from the 1985 Hirshman-Neilson paper:

$$a_{HN}(\epsilon) = 2.0 + 9.25\sqrt{\epsilon} - 1.21 \epsilon \quad (4.31)$$

$$b_{HN}(\epsilon) = \ln(8/\epsilon) \cdot (1 + 1.81\sqrt{\epsilon} + 2.05 \epsilon) \quad (4.32)$$

$$d_{HN}(\epsilon) = 0.73\sqrt{\epsilon} \cdot (1 + 2\epsilon^4 - 6\epsilon^5 + 3.7\epsilon^6) \quad (4.33)$$

1409 **The Mutual Inductance – M**

1410 The mutual inductance – M – represents the coupling between the solenoid primary
1411 and the plasma secondary. A common method for treating this mutual inductance is
1412 through a coupling coefficient, k, that links the two self-inductances. Formulaically,

$$M = k\sqrt{L_1 L_2} \quad (4.34)$$

1413 The value of the coupling coefficient, k, is always less than (or equal to) 1, but usually
1414 has a value around one-third. With all the equations defined, we are now at a position
1415 to explain one of the larger nuances of this fusion systems framework: declaring the
1416 pulse length of a tokamak.

1417 **4.1.4 ConstructingReasoning the Pulse Length**

1418 This subsection focuses on a quantitative estimate for how to select a pulse length.
1419 As no fusion reactor exists in the world today, the writers believe this is an acceptable

1420 calculation. Further, the resulting length of two hours matches the durations of other
1421 studies in the literature.

1422 Starting at the end, our goal is to find the pulse length of a tokamak reactor in seconds
1423 – as dictated by cyclical stress concerns. The first piece of information is the expected
1424 lifetime of the central solenoid, $N \approx 10$ years. The next is the desired number of shots
1425 the machine will likely have, $M \approx 50,000$ shots.* This gives the ballpark estimate of
1426 around 10 pulses a day – or a **flattop** pulse length of two hours.

1427 With the pulse length defined, we are now in a position to justify neglecting the duty
1428 factor for pulsed reactors in this model. Using **expectedballpark** reactor values – while
1429 assuming the central solenoid has around 4000 turns – leads to the following scalings:

$$\tau_{FT} \sim \tau_{pulse} \sim \text{O}(\text{hours}) \quad (4.35)$$

$$\tau_{RU} \sim \tau_{RD} \sim \tau_{DW} \sim \text{O}(\text{mins}) \quad (4.36)$$

1430 As such, even pulsed tokamak reactors should have a duty factor of around unity:

$$f_{duty} \approx 1 \quad (4.37)$$

1431 Now that all the terms in a pulsed circuit have been explored, we will move on to
1432 rearranging the flattop equation to reproduce flux balance. This will then naturally
1433 lead to a generalized current equation – which is the main result of the chapter.

1434 4.2 ProducingSalvaging Flux Balance

1435 The goal of this section is to arrive at a conservation equation for flux balance that
1436 mirrors the ones in the literature. The fusion systems model this one attempts to

*This 50,000 shots comes from multiplying the number of pulses run at Diii-D per year by the expected lifetime of the central solenoid (10 years).²⁶

1437 follow most is the PROCESS code.³ In a manner similar to power balance, flux
 1438 balance can be written as:

$$\sum_{sources} \Phi = \sum_{sinks} \Phi \quad (4.38)$$

1439 4.2.1 Rearranging the Circuit Equation

1440 The way to arrive at flux balance from the circuit equation is to rearrange the flattop
 1441 phase's duration equation:

$$\tau_{FT} = \frac{I_{max} \cdot 2M - I_{ID} \cdot L_2}{I_{ID} R_P} \quad (4.16)$$

1442 Multiplying by the right-hand side's denominator and moving the negative term over
 1443 yields:

$$2MI_{max} = I_{ID} \cdot (L_2 + R_P \tau_{FT}) \quad (4.39)$$

1444 This equation is flux balance, where the left-hand side are the sources (e.g. the central
 1445 solenoid), and the other terms are the sinks (i.e. ramp-up and flattop). The source
 1446 term can currently be encapsulated in:

$$\Phi_{CS} = 2MI_{max} \quad (4.40)$$

1447 The sinks, namely the ramp-up inductive losses (Φ_{RU}) and the flattop resistive losses
 1448 (Φ_{FT}), are what drain up the flux. Again, ramp-down and dwell are not included as
 1449 sinks because flux balance only tracks till the end of flattop. They come into play
 1450 when measuring the cost of electricity – through the duty factor from Eq. (4.20).

1451 Relabeling terms, flux balance can now be rewritten as:

$$\Phi_{CS} = \Phi_{RU} + \Phi_{FT} \quad (4.41)$$

1452 With the ramp-up and flattop flux given respectively by:

$$\Phi_{RU} = L_2 \cdot I_{ID} \quad (4.42)$$

$$\Phi_{FT} = (R_P \tau_{FT}) \cdot I_{ID} \quad (4.43)$$

1453 On comparing these quantities to the ones from the PROCESS team, Φ_{RU} and Φ_{FT}
 1454 are exactly the same. The source terms, on the other hand, are off for two reasons
 1455 – both related to the central solenoid being the only source term in flux balance.
 1456 This can partially be remedied by adding the second most dominant source of flux
 1457 a posteriori – i.e. the PF coils. The second, and inherently limiting factor, is the
 1458 simplicity of the current model. All that can be shown to this regard is that the Φ_{CS}
 1459 terms does reasonably predict the values from the PROCESS code.

1460 4.2.2 AddingImporting Poloidal Field Coils

1461 Adding the effect of PF coils – belts of current driving plates on the outer edges of
 1462 the tokamak – leads to as much as a 50% improvement^{3,4}~~a second-order improvement~~
 1463 over relying solely on the central solenoid for flux generation. From the literature,
 1464 this can be modeled as:²¹

$$\Phi_{PF} = \pi B_V \cdot (R_0^2 - (R_{CS} + d)^2) \quad (4.44)$$

1465 Where again R_{CS} and d are the inner radius and thickness of the central solenoid,
 1466 respectively. These will be the topic of the next section.

1467 Moving forward, the vertical field – B_V – is a magnetic field oriented up-and-down

1468 with the ground. It is needed to prevent a tokamak plasma from drifting radially spinning
 1469 out of the machine. From the literature, the magnitude of this vertical field (valid for
 1470 a circular plasma) is given by:³

$$|B_V| = \frac{\mu_0 I_P}{4\pi R_0} \cdot \left(\ln \left(\frac{8}{\epsilon} \right) + \beta_p + \frac{l_i}{2} - \frac{3}{2} \right) \quad (4.45)$$

1471 Analogous to the previously covered plasma beta, the poloidal beta can be represented
 1472 by:²⁷

$$\beta_p = \frac{\bar{p}}{\left(\frac{\overline{B_p}^2}{2\mu_0} \right)} \quad (4.46)$$

1473 Where the average poloidal magnetic field comes from a simple application of Am-
 1474 pere's law:

$$\overline{B_p} = \frac{\mu_0 I_P}{l_p} \quad (4.47)$$

1475 The variable l_p is then the perimeter of the tokamak's cross-sectional halves:

$$l_p = 2\pi a \cdot \sqrt{g_p} \quad (4.48)$$

1476 Here, g_p is another geometric scaling factor,

$$g_p = \frac{1 + \kappa^2(1 + 2\delta^2 - 1.2\delta^3)}{2} \quad (4.49)$$

1477 After a few lines of algebraBoiled-down, this relation for the magnitude of the vertical
 1478 magnetic field can be written in standardized units as:

$$|B_V| = \left(\frac{1}{10 \cdot R_0} \right) \cdot (K_{VI} I_P + K_{VT} \overline{T}) \quad (4.50)$$

$$K_{VT} = K_n \cdot (\epsilon^2 g_P) \cdot (1 + f_D) \frac{(1 + \nu_n)(1 + \nu_T)}{1 + \nu_n + \nu_T} \quad (4.51)$$

$$K_{VI} = \ln \left(\frac{8}{\epsilon} \right) + \frac{l_i}{2} - \frac{3}{2} \quad (4.52)$$

1479 For clarity, this will be plugged into the new PF coil flux contribution (Φ_{PF}):

$$\Phi_{PF} = \pi B_V \cdot (R_0^2 - (R_{CS} + d)^2) \quad (4.44)$$

1480 Which then gets plugged into a more complete flux balance:

$$\Phi_{CS} + \Phi_{PF} = \Phi_{RU} + \Phi_{FT} \quad (4.53)$$

1481 The R_{CS} and d terms found in Φ_{PF} will now be discussed as they are needed for this
1482 more sophisticated tokamak geometry.

1483 4.3 Improving Tokamak Geometry

1484 From before, this fusion systems model has been said to depend on the major and
1485 minor radius – R_0 and a , respectively – and along the way, various geometric param-
1486 eters have been defined (e.g. ϵ , κ , δ) to describe the geometry further. Now three
1487 more thicknesses will be added: b , c , and d . Additionally, two fundamental dimension
1488 corresponding to the solenoid will be given: the radius (R_{CS}) and height (h_{CS}). These
1489 are the topics of this section.

1490 4.3.1 Defining Central Solenoid Dimensions

1491 The best way to conceptualize tokamak geometry is through cartoon – see Fig. E-2.
1492 What this says is there is a gap at the very center of a tokamak. This gap extends

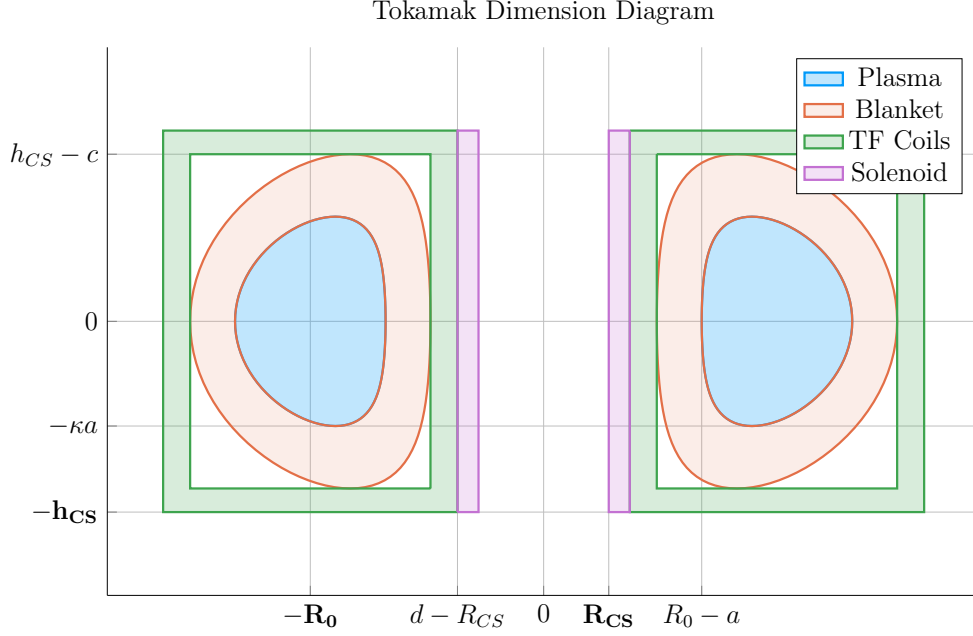


Figure 4-3: Dimensions of Tokamak Cross-Section

1493 radially outwards to R_{CS} meters where the ~~spiraledslinky-shaped~~ central solenoid –
 1494 of thickness d – begins. Between the outer edge of the solenoid and the wall of the
 1495 torus (i.e. the doughnut) are the blanket and toroidal field (TF) coils.

1496 The blanket and TF coils have thicknesses of b and c , respectively. Before defining
 1497 b , c , and d , though, it proves fruitful to relate all the quantities in equations for the
 1498 inner radius (R_{CS}) and height (h_{CS}) of the central solenoid.

$$R_{CS} = R_0 - (a + b + c + d) \quad (4.54)$$

$$h_{CS} = 2 \cdot (\kappa a + b + c) \quad (4.55)$$

1499 Again, this relation is pictorially represented in Fig. E-2. The next step is defining:
 1500 b , c , and d – to close the variable loop.

1501 4.3.2 ~~Calculating~~Measuring Component Thicknesses

1502 In between the inner surface of the central solenoid and the major radius of the
1503 tokamak are four thicknesses: a , b , c , and d . This subsection will go over them
1504 one-by-one.

1505 The Minor Radius – a

1506 The minor radius was the first of these thicknesses we encountered. To calculate it,
1507 we introduced the inverse aspect ratio (ϵ) to relate it to the major radius (R_0):

$$a = \epsilon \cdot R_0 \quad (2.1)$$

1508 The Blanket Thickness – b

1509 The blanket is an area between the TF coils and the torus that is ~~strongly~~ composed
1510 ~~mainly~~ of lithium. It serves to both: protect the superconducting magnet structures
1511 from neutron damage, as well as breed ~~a little~~ more tritium fuel from stray fusion
1512 neutrons. In equation form, the blanket thickness is given by:²³

$$b = 1.23 + 0.074 \ln P_W \quad (4.56)$$

1513 ~~Here, the constant term (i.e. 1.23) is approximately the mean-free-path of fusion~~
1514 ~~neutrons through lithium-7—the thickness of lithium needed to reduce the population~~
1515 ~~of neutrons by $\sim 65\%$. Here, P_W While the second term, which includes P_W , is a~~
1516 correction to account for extra wall loading (as discussed in ~~Section 3.4.3~~the secondary
1517 ~~constraint section~~).

1518 Moving forward, the remaining two thicknesses – c and d – are handled differently,
1519 estimating structural steel portions as well as magnetic current-carrying ones.

1520 The Toroidal Field Coil Thickness – c

1521 The thickness of the TF coils – c – is a little beyond the scope of this paper. It does,
 1522 however, have a form that combines a structural steel component with a magnetic
 1523 portion. From ~~a previous model~~~~one of Jeff's previous models~~, this can be given as:²³

$$c = G_{CI}R_0 + G_{CO} \quad (4.57)$$

$$G_{CI} = \frac{B_0^2}{4\mu_0\sigma_{TF}} \cdot \frac{1}{(1 - \epsilon_b)} \cdot \left(\frac{4\epsilon_b}{1 + \epsilon_b} + \ln \left(\frac{1 + \epsilon_b}{1 - \epsilon_b} \right) \right) \quad (4.58)$$

$$G_{CO} = \frac{B_0}{\mu_0 J_{TF}} \cdot \frac{1}{(1 - \epsilon_b)} \quad (4.59)$$

1524 The critical stress – σ_{TF} in G_{CI} implies it depends on the structural component,
 1525 whereas the maximum current density – J_{TF} – implies a magnetic predisposition
 1526 in G_{CO} . The use of G_{\square} in these quantities, instead of K_{\square} is because they include
 1527 the toroidal magnetic field strength – B_0 . For this reason, they are referred to as
 1528 ~~dynamic floating~~ coefficients. Lastly, the term ϵ_b represents the blanket inverse aspect
 1529 ratio that combines the minor radius with the blanket thickness:

$$\epsilon_b = \frac{a + b}{R_0} \quad (4.60)$$

1530 The Central Solenoid Thickness – d

1531 Finishing this discussion where we started, the central solenoid's thickness – d – has
 1532 a form similar to the TF coil's (i.e. c). In mathematical form, this can be represented
 1533 as:²³

$$d = K_{DR}R_{CS} + K_{DO} \quad (4.61)$$

$$K_{DR} = \frac{3B_{CS}^2}{6\mu_0\sigma_{CS} - B_{CS}^2} \quad (4.62)$$

$$K_{DO} = \frac{6B_{CS}\sigma_{CS}}{6\mu_0\sigma_{CS} - B_{CS}^2} \cdot \left(\frac{1}{J_{OH}} \right) \quad (4.63)$$

Here, the use of K_{\square} for the coefficients signifies their use as ~~static~~~~fixed~~ coefficients. Therefore, B_{CS} must be treated as a ~~static~~~~fixed~~ variable representing the magnetic field strength in the central solenoid. For prospective solenoids using high temperature superconducting (HTS) tape, B_{CS} may be around 20 T. The values of σ_{CS} and J_{CS} have similar meanings to the ones for TF coils. These are collected in a table below with example values representative of our model.

Table 4.2: Example TF Coils and Central Solenoid Critical Values

(a) Stresses [MPa]			(b) Current Densities [MA/m ²]		
Item	Symbol	Limit	Item	Symbol	Limit
Solenoid	σ_{CS}	300	Solenoid	J_{CS}	50
TF Coils	σ_{TF}	600	TF Coils	J_{TF}	200

Before moving on, it seems important to say that although K_{DI} and K_{DO} do not depend on ~~dynamic~~~~floating~~ variables, R_{CS} most definitely does. This is what makes the central solenoid's thickness difficult.

4.3.3 Revisiting Central Solenoid Dimensions

Now that the various thicknesses have been defined (i.e. a , b , c , and d), the equations for the solenoid's dimensions (i.e. R_{CS} and h_{CS}), can now be revisited and simplified. From before,

$$R_{CS} = R_0 - (a + b + c + d) \quad (4.54)$$

$$h_{CS} = 2 \cdot (\kappa a + b + c) \quad (4.55)$$

1547 Utilizing the four thicknesses from before, these can now be expanded to simple
 1548 formulas. Repeating the thicknesses:

$$a = \epsilon \cdot R_0 \quad (2.1)$$

$$b = 1.23 + 0.074 \ln P_W \quad (4.56)$$

$$c = G_{CI}R_0 + G_{CO} \quad (4.57)$$

$$d = K_{DR}R_{CS} + K_{DO} \quad (4.61)$$

1549 Plugging these into the central solenoid's dimensions results in:

$$h_{CS} = 2 \cdot (R_0 \cdot (\epsilon\kappa + G_{CI}) + (b + G_{CO})) \quad (4.64)$$

$$R_{CS} = \frac{1}{1 + K_{DR}} \cdot (R_0 \cdot (1 - \epsilon - G_{CI}) - (K_{DO} + b + G_{CO})) \quad (4.65)$$

1550 These are the complete central solenoid dimension formulas. To make them more
 1551 tractable to the reader, they will now be simplified one step at a time. (The same
 1552 simplification exercise will be done again after the generalized current is derived later
 1553 this chapter.)

1554 The first simplification to make while estimating central solenoid dimensions is to
 1555 neglect the magnetic current-carrying portions of the central solenoid and TF coils.

1556 This results in:

$$\lim_{\substack{G_{CO} \rightarrow 0 \\ K_{DO} \rightarrow 0}} h_{CS} = h_{CS}^{\dagger} = 2R_0 \cdot (K_{EK} + \epsilon_b + G_{CI}) \quad (4.66)$$

$$\lim_{\substack{G_{CO} \rightarrow 0 \\ K_{DO} \rightarrow 0}} R_{CS} = R_{CS}^{\dagger} = \frac{R_0}{1 + K_{DR}} \cdot (1 - \epsilon_b - G_{CI}) \quad (4.67)$$

1557 The new ~~static~~~~fixed~~ coefficient, here, is:

$$K_{EK} = \epsilon \cdot (\kappa - 1) \quad (4.68)$$

1558 The next simplification is ignoring the TF coil thickness – and thus magnetic field
1559 dependence – altogether:

$$\lim_{G_{CI} \rightarrow 0} h_{CS}^{\dagger} = h_{CS}^{\ddagger} = 2R_0 \cdot (K_{EK} + \epsilon_b) \quad (4.69)$$

$$\lim_{G_{CI} \rightarrow 0} R_{CS}^{\dagger} = R_{CS}^{\ddagger} = \frac{R_0}{1 + K_{DR}} \cdot (1 - \epsilon_b) \quad (4.70)$$

1560 These oversimplifications will be used later this chapter while simplifying the gener-
1561 alized current equation to something more tractable. For now, they highlight how the
1562 dimensions change as different components are neglected. The next step is bringing
1563 plasma physics back into the flux balance equation and solving for the generalized
1564 current.

1565 4.4 Piecing Together the Generalized Current

1566 The goal of this section is to quickly expand flux balance using all the defined quan-
1567 tities and then massage it into an equation for plasma current – which is suitable for
1568 root solving. This starts with a restatement of flux balance in a reactor:

$$\Phi_{CS} + \Phi_{PF} = \Phi_{RU} + \Phi_{FT} \quad (4.53)$$

$$\Phi_{CS} = 2MI_{max} \quad (4.40)$$

$$\Phi_{PF} = \pi B_V \cdot (R_0^2 - (R_{CS} + d)^2) \quad (4.44)$$

$$\Phi_{RU} = L_2 \cdot I_{ID} \quad (4.42)$$

$$\Phi_{FT} = (R_P \tau_{FT}) \cdot I_{ID} \quad (4.43)$$

1569 The first step is realizing that the central solenoid flux can now be rewritten using
1570 the new geometry in a standardized form:

$$\Phi_{CS} = K_{CS} \cdot \sqrt{R_0 G_{LT} h_{CS}} \quad (4.71)$$

$$K_{CS} = 2k B_{CS} \cdot \sqrt{\frac{\pi K_{LP}}{\mu_0}} \quad (4.72)$$

1571 Next, we will slightly simplify the PF coil flux using a ~~dynamic~~~~floating~~ variable coef-
1572 ficient:

$$\Phi_{PF} = G_V \cdot \frac{K_{VI} I_P + K_{VT} \bar{T}}{R_0} \quad (4.73)$$

$$G_V = \frac{\pi}{10} \cdot (R_0^2 - (R_{CS} + d)^2) \quad (4.74)$$

1573 This allows us to rewrite the generalized current as:

$$I_P = \frac{(K_{BS} + G_{IU}/G_{IP}) \cdot \bar{T}}{1 - K_{CD}(\sigma v) - G_{ID}/G_{IP}} \quad (4.75)$$

1574

$$G_{IU} = K_{VT} G_V + K_{CS} R_0^{3/2} \cdot \frac{\sqrt{h_{CS} G_{LT}}}{\bar{T}} \quad (4.76)$$

$$G_{ID} = K_{VI} G_V \quad (4.77)$$

$$G_{IP} = K_{LP} R_0^2 + \frac{K_{RP} \tau_{FT}}{\bar{T}^{3/2}} \quad (4.78)$$

As we will show in the next section, this form not only has a form remarkably similar to the steady current – it reduces to it in the limit of infinitely long pulses!

4.5 Simplifying the Generalized Current

This section focuses on making various simplifications to the generalized current:

$$I_P = \frac{(K_{BS} + G_{IV}/G_{IP}) \cdot \bar{T}}{1 - K_{CD}(\sigma v) - G_{ID}/G_{IP}} \quad (4.75)$$

As promised, this will start with the trivial simplification of the generalized current into steady state. Next it will move on to a basic simplification for the purely pulsed case. These two activities should shed some light on how to interpret the equation in the more complicated hybrid case.

4.5.1 Recovering the Steady Current

The place to start with the steady current is the ~~dynamic~~~~floating~~ coefficient, G_{IP} :

$$G_{IP} = K_{LP} R_0^2 + \frac{K_{RP} \tau_{FT}}{\bar{T}^{3/2}} \quad (4.78)$$

As can be seen, as $\tau_{FT} \rightarrow \infty$, so does the coefficient,

$$\lim_{\tau_{FT} \rightarrow \infty} G_{IP} = \infty \quad (4.79)$$

1586 Because G_{IU} and G_{ID} remain constant, their contribution to plasma current becomes
 1587 insignificant in this limit. Concretely,

$$\lim_{\tau_{FT} \rightarrow \infty} I_P = \frac{K_{BS} \bar{T}}{1 - K_{CD}(\sigma v)} \quad (4.80)$$

1588 This is precisely the steady current given by Eq. (2.30)! The generalized current
 1589 automatically works when modeling steady-state tokamaks.*

1590 4.5.2 Extracting the Pulsed Current

1591 For pulsed reactors, we have to ~~resolve a similar problem~~~~play a similar game~~ – except
 1592 now τ_{FT} is expected to be a reasonably sized number (i.e. 2 hours).

1593 With an aim at intuition, the reactor is first treated as purely pulsed – having no
 1594 current drive assistance:

$$\lim_{\eta_{CD} \rightarrow 0} I_P = \frac{(K_{BS} + G_{IU}/G_{IP}) \cdot \bar{T}}{1 - (G_{ID}/G_{IP})} \quad (4.81)$$

1595 Next, for simplicity-sake, the PF coil contribution to flux balance is assumed negligi-
 1596 ble, as it was always just a correction term:

$$\lim_{\Phi_{PF} \ll \Phi_{CS}} G_{IU} = K_{CS} R_0^{3/2} \cdot \frac{\sqrt{h_{CS} G_{LT}}}{\bar{T}} \quad (4.82)$$

$$\lim_{\Phi_{PF} \ll \Phi_{CS}} G_{ID} = 0 \quad (4.83)$$

1597 Piecing this altogether, we can write a new current for this highly simplified case,

$$I_P^\dagger = K_{BS} \bar{T} + \frac{K_{CS} R_0^{3/2} \cdot \sqrt{h_{CS} G_{LT}}}{K_{LP} R_0^2 + K_{RP} \tau_{FT} \bar{T}^{-3/2}} \quad (4.84)$$

*It should be noted that this is much harder when setting τ_{FT} to a large, but finite number – as η_{CD} still needs to be solved self-consistently.

1598 As this is not quite simple enough, these previous simplifications will be incorporated:

$$G_{LT}^\dagger = R_{CS}^2 \quad (4.28)$$

$$h_{CS}^\dagger = 2R_0 \cdot (K_{EK} + \epsilon_b) \quad (4.69)$$

$$R_{CS}^\dagger = \frac{R_0}{1 + K_{DR}} \cdot (1 - \epsilon_b) \quad (4.70)$$

1599 Taking these into consideration results in the following current formula:

$$I_P^\dagger = K_{BS} \bar{T} + \left(\frac{K_{CS} R_0^3}{K_{LP} R_0^2 + K_{RP} \tau_{FT} \bar{T}^{-3/2}} \cdot \frac{(1 - \epsilon_b) \cdot \sqrt{2(K_{EK} + \epsilon_b)}}{1 + K_{DR}} \right) \quad (4.85)$$

1600 In the limit that the pulse length drops to zero (and bootstrap current is negligible),

$$\lim_{\tau_{FT} \rightarrow 0} I_P^\dagger = R_0 \cdot \left(\frac{K_{CS}}{K_{LP}} \cdot \frac{(1 - \epsilon_b) \cdot \sqrt{2(K_{EK} + \epsilon_b)}}{1 + K_{DR}} \right) \quad (4.86)$$

1601 This implies that a purely pulsed current scales with major radius to leading order.

1602 4.5.3 Rationalizing the Generalized Current

1603 From the previous two subsections, we arrived at equations for infinitely large and
1604 infinitely small pulse lengths:

$$\lim_{\tau_{FT} \rightarrow \infty} I_P = \frac{K_{BS} \bar{T}}{1 - K_{CD}(\sigma v)} \quad (4.80)$$

$$\lim_{\tau_{FT} \rightarrow 0} I_P^\dagger = R_0 \cdot \left(\frac{K_{CS}}{K_{LP}} \cdot \frac{(1 - \epsilon_b) \cdot \sqrt{2(K_{EK} + \epsilon_b)}}{1 + K_{DR}} \right) \quad (4.86)$$

1605 What these imply at an intuitive level is that at small pulses, current scales with the
1606 major radius. While for long pulses, current scales with plasma temperature. In the
1607 general case, of course, the problem becomes much harder to predict.

1608 Chapter 5

1609 Completing the Systems Model

1610 As opposed to previous chapters, this one will focus on the numerics behind the
1611 fusion systems model. This will then naturally segue into a discussion of how plots
1612 are made and should be interpreted. The remaining chapters will then decouple the
1613 dissemination of results from their analytic conclusions.

1614 5.1 Describing a Simple Algebra

1615 Boiled down, the systems model used here is a simple algebra problem – given five
1616 equations, solve for five unknowns. The goal is then to pick the five equations that
1617 best represent modern fusion reactor design. This selection should also be done in
1618 such a way that actually reduces the system of equations to a simple univariate root
1619 solving equation (i.e. one equation with one unknown). As will be shown in the
1620 results, this model does remarkably well: matching year-long modeling campaigns in
1621 seconds.

1622 The logical place to start in a discussion of this algebra problem is with the three equa-
1623 tions fundamental to all reactor-grade tokamaks – both in steady-state and pulsed
1624 operation. These are: the Greenwald density limit, power balance, and current bal-
1625 ance. The Greenwald density’s importance was hinted early on when it was used to

1626 simplify every equation derived thereafter.

$$\bar{n} = K_n \cdot \frac{I_P}{R_0^2} \quad (2.11)$$

1627 The two balance equations prove slightly more dubious. As was shown previously,
 1628 current balance – the stability requirement for tokamaks – was most peculiar. It
 1629 brought forth the notion of self-consistency for steady-state machines and a highly-
 1630 coupled multi-root equation for pulsed ones. As such, this equation stands as the one
 1631 everything else will be substituted into to setup for a univariate root solve.

$$I_P = \frac{(K_{BS} + G_{IW}/G_{IP}) \cdot \bar{T}}{1 - K_{CD}(\sigma v) - G_{ID}/G_{IP}} \quad (4.75)$$

1632 Although slightly buried in Eq. (4.75), the right-hand side actually depends on all
 1633 the quantities (including I_P through the blanket thickness). Through equation,

$$I_P = f(I_P, \bar{T}, R_0, B_0) \quad (5.1)$$

1634 The remaining equation common to all reactor-grade tokamaks is power balance –
 1635 the relation that separates power plants from toasters. Due to the use of the ELMy
 1636 H-Mode scaling law for modeling the diffusion coefficient, this had the complicated
 1637 form of:

$$R_0^{\alpha_R^*} \cdot B_0^{\alpha_B} \cdot I_P^{\alpha_I^*} = \frac{G_{PB}}{K_{PB}} \quad (3.38)$$

1638 Although being rather cumbersome, this equation actually remains relatively simple
 1639 in that all three quantities on the left-hand side are separable. To close the system,
 1640 two more equations of this form are needed. These have the following form and will
 1641 be described next.

$$R_0^{\gamma_R} \cdot B_0^{\gamma_B} \cdot I_P^{\gamma_I} = G(\bar{T}) \quad (5.2)$$

1642 5.2 Generalizing Previous Equations

1643 Where the equations defined up to this point in the chapter are shared among all
 1644 fusion reactors, the remaining two equations – needed to close the system – must
 1645 be chosen by the user. These user-supplied equations come in three flavors: limits,
 1646 ~~intermediatederived~~ quantities, and ~~dynamicfloating~~ variables. By convention, we
 1647 enforce that at least one limit must be used. The other constraint can then come
 1648 from any of the three defined collections, which we will refer to as the closure equation.

Table 5.1: Main Equation Bank

To close the system of equations for potential reactors, different equations can be used to lock down tokamak designs. These include physics and engineering limits (L), as well as ways to set ~~dynamic (D)floating (F)~~ or ~~intermediate (I)derived (D)~~ variables to constant values.

Variable	Category	$G(\bar{T})$	γ_R	γ_B	γ_I
Power Balance	-	G_{PB}/K_{PB}	α_R^*	α_B	α_I^*
Beta (β_N)	L	$K_{TB}\bar{T}$	1	1	0
Kink (q_{95})	L	K_{KF}	1	1	-1
Wall Loading (P_W)	L	$K_{WL}(\sigma v)^{1/3}$	1	0	-2/3
Power Cap (P_E)	L	$K_{PC}(\sigma v)$	1	0	-2
Heat Loading (q_{DV})	L	$K_{DV}(\sigma v)^{1/3.2}$	1	0	-1
Major Radius (R_0)	D	$(R_0)_{const}$	1	0	0
Magnet Strength (B_0)	D	$(B_0)_{const}$	0	1	0
Plasma Current (I_P)	D	$(I_P)_{const}$	0	0	1
Plasma Temperature (\bar{T})	D	$(\bar{T})_{const}/\bar{T}$	0	0	0
Electron Density (\bar{n})	D	$(\bar{n})_{const}/K_n$	-2	0	1
Plasma Pressure (\bar{p})	I	$(\bar{p})_{const}/K_n K_{nT} \bar{T}$	-2	0	1
Bootstrap Current (f_{BS})	I	$(f_{BS})_{const}/K_{BS} \bar{T}$	0	0	-1
Fusion Power (P_F)	I	$(P_F)_{const}/K_F K_n^2(\sigma v)$	-1	0	2
Magnetic Energy (W_M)	I	$(W_M)_{const}/K_{WM}$	3	2	0
Cost per Watt (C_W)	I	$(C_W)_{const} \cdot (K_F K_n^2(\sigma v)/K_{WM})$	4	2	-2

1649 5.2.1 Rehashing the Limits

1650 The limits category is simply a rebranding of the secondary constraints given previ-
1651 ously. These include the physics derived limits from MHD theory – i.e. the beta limit
1652 (β_N) and the kink safety factor (q_{95}) – which for clarity, set maximums on the allowed
1653 plasma pressure and velocity, respectively. Additionally, there were several engineer-
1654 ing limits also described: wall loading, heat loading, and maximum power capacity.
1655 For this paper, wall loading from neutrons (P_W) is assumed to be important, whereas
1656 the other two engineering limits are not allowed to explicitly guide designs.

1657 Combined all these limits, as well as the yet to be defined ~~dynamicfloat~~ and ~~intermediatederived~~
1658 equations, are given in Table 5.1. These share a remarkably similar form to power
1659 balance when put into a generalized, separable state. This hints at why the major
1660 radius (R_0), the toroidal field strength (B_0), and the plasma current (I_P) can easily
1661 be separated and substituted out of the current balance equation.

1662 Before moving on, it proves useful to explain the two limits not used to explicitly guide
1663 reactor design – divertor heat loading and the maximum power capacity. The simpler
1664 of the two to reason is the heat loading limit. Although removing the gigawatts of
1665 heat is extremely difficult, it remains an unsolved problem worthy of its own research
1666 machine, but currently neglected financially. As such, it is only kept to provide a
1667 human-interpreted measure of difficulty. The power cap, on the other hand, is just
1668 handled informally. If a reactor surpasses it (i.e. $P_E > 4000MW$), it is considered
1669 invalid.

1670 While the maximum power cap informally sets a maximum major radius for a ma-
1671 chine, there also exists an implicit minimum major radius. This minimum occurs due
1672 to the hole-size constraint – i.e. at some point there is no longer enough room on the
1673 inside of the machine to store the central solenoid, blanket, and TF coils.

1674 At this point, we can now explain how various quantities in the systems model
1675 can be set to user-given constant values. This basically allows users to treat one
1676 ~~dynamicfloating~~ variable as a ~~staticfixed~~ one (e.g. the temperature and bootstrap

1677 fraction).

1678 5.2.2 Minimizing **IntermediateDerived** Quantities

1679 Whereas the limits from the previous section represented constraints with real physics
1680 and engineering repercussions, the **intermediatederived** quantities here are just used
1681 to find when reactors reach certain user-supplied values. Most notable are the capital
1682 cost (through the magnetic energy – W_M) and the cost-per-watt (C_W). The model
1683 also, however, allows easily setting values for the bootstrap fraction, plasma pressure,
1684 and fusion power. As mentioned previously, they are given in Table 5.1 through a
1685 generalized representation of the form:

$$R_0^{\gamma_R} \cdot B_0^{\gamma_B} \cdot I_P^{\gamma_I} = G(\bar{T}) \quad (5.2)$$

1686 What this collection of variables is really useful for, though, is finding minimum cost
1687 reactors – both in a capital context as well as a cost-per-watt one. Without boring
1688 the reader, this is done in a three stage process. First, some valid reactor is found: it
1689 does not matter if it is good, just valid. This of course can be found by systematically
1690 throwing darts at a dart board – see Fig. 5-1

1691 After a valid reactor is found, its cost is recorded leading to a drill-down stage. In
1692 this step, the cost is continuously halved until a valid reactor cannot be found. Once
1693 this invalid reactor is reached, it sets a bound on the minimum cost reactor. As such,
1694 the final stage is a simple bisection step where the minimum cost is honed down to
1695 some acceptable margin of error – see Fig. 5-2.

1696 5.2.3 Pinning **DynamicFloating** Variables

1697 The remaining collection of closure equations is for the five **dynamicfloating** variables
1698 in the systems model: R_0 , B_0 , \bar{n} , \bar{T} , and I_P . As we are making equations of the
1699 following form, the formulas for R_0 , B_0 , and I_P are trivial.

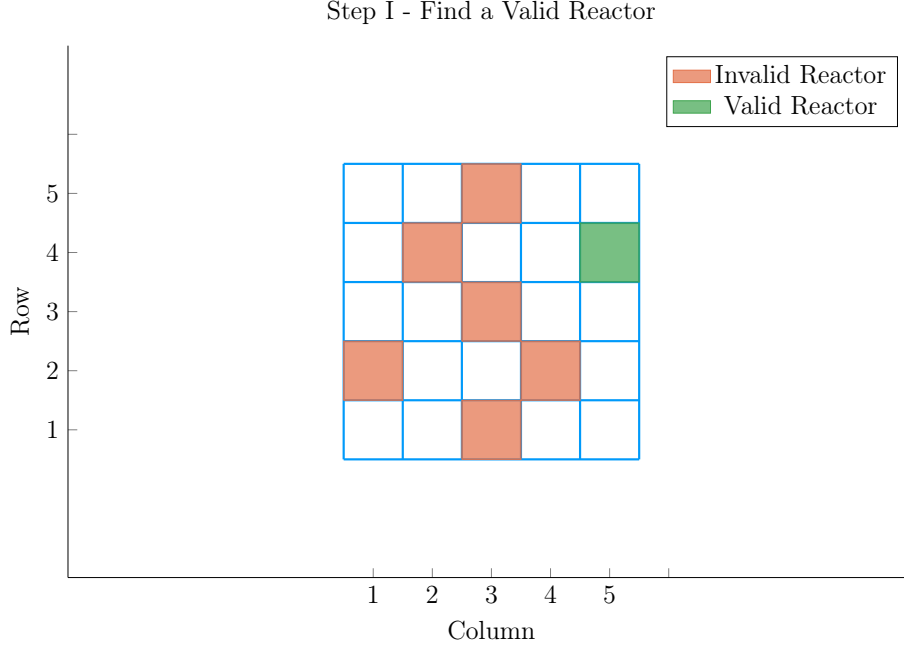


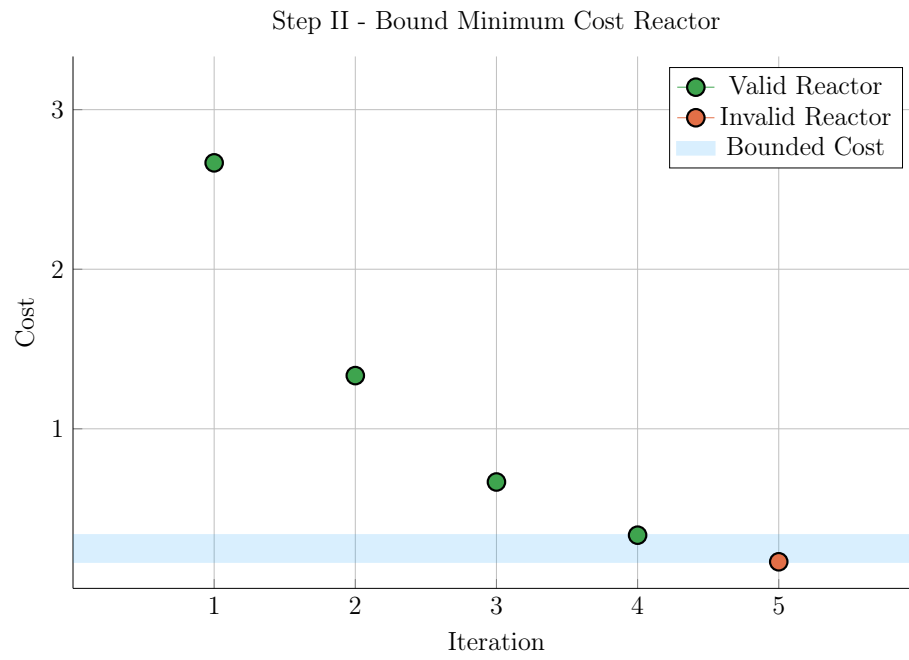
Figure 5-1: Minimize Cost Step I – Find Valid Reactor

$$R_0^{\gamma_R} \cdot B_0^{\gamma_B} \cdot I_P^{\gamma_I} = G(\bar{T}) \quad (5.2)$$

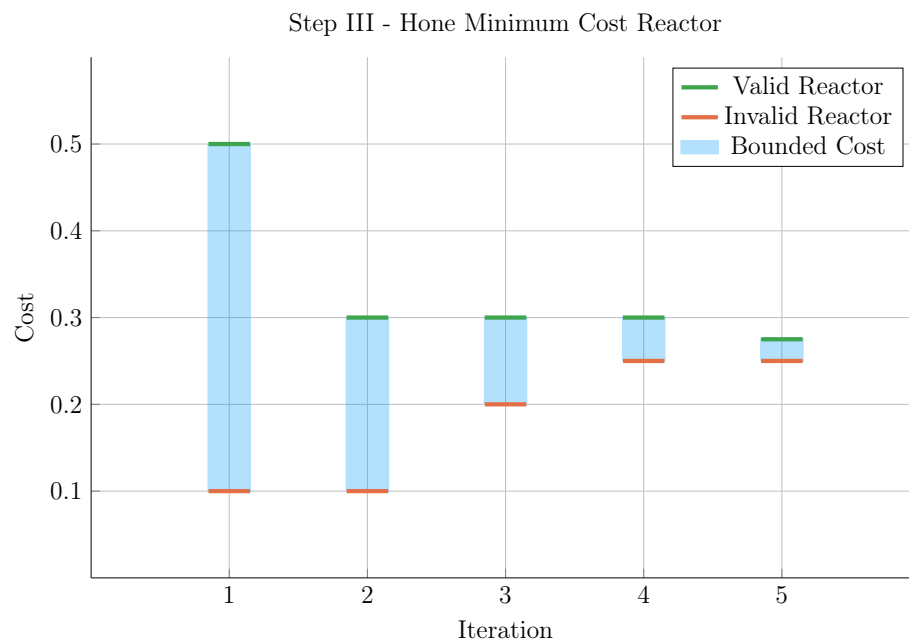
1700 Next, the equation for \bar{n} – shown in Table 5.1 – is just a simple undoing of the Green-
 1701 wald density limit. The remaining equation is then from the original temperature
 1702 equation:

$$\bar{T} = \text{const.} \quad (3.1)$$

1703 As was assumed earlier, this is sort of a default equation for the systems model. By
 1704 this, we mean reactor curves can be created by scanning over temperatures, i.e. set
 1705 $\bar{T} = 5$ keV in one run, 10 in the next, etc. This temperature equation also brings up
 1706 a subtlety of the model, as it does not depend on current, radius, or magnet strength.
 1707 The algorithm that motivated this generalized equation approach most notably bi-
 1708 furcates in the situation where the closure equation does not depend on R_0 , B_0 , or I_P
 1709 (i.e. the temperature equation). The two scenarios are given in Eqs. (5.3) to (5.9) –



(a) Minimize Step II



(b) Minimize Step III

Figure 5-2: Minimize Cost Step II/III – Optimize Reactor

1710 where at least R_0 and B_0 are substituted out of the system. In the temperature case,
 1711 I_P is not needed to be explicitly removed.

1712 Concretely, the root solve for the temperature scenario is for the current, whereas it
 1713 is for the temperature in all other cases. The nomenclature in the code is a *match*
 1714 for Scenario I (i.e. root solving for plasma temperature), and a *solve* for Scenario II
 1715 (i.e. root solving for plasma current).

1716 **Scenario I – Match for \bar{T}**

$$R_0(\bar{T}) = \left(G_1^{(\gamma_{B,2} \gamma_{I,3} - \gamma_{B,3} \gamma_{I,2})} \cdot G_2^{(\gamma_{B,3} \gamma_{I,1} - \gamma_{B,1} \gamma_{I,3})} \cdot G_3^{(\gamma_{B,1} \gamma_{I,2} - \gamma_{B,2} \gamma_{I,1})} \right)^{\frac{1}{\gamma_{RBI}}} \quad (5.3)$$

$$B_0(\bar{T}) = \left(G_1^{(\gamma_{I,2} \gamma_{R,3} - \gamma_{I,3} \gamma_{R,2})} \cdot G_2^{(\gamma_{I,3} \gamma_{R,1} - \gamma_{I,1} \gamma_{R,3})} \cdot G_3^{(\gamma_{I,1} \gamma_{R,2} - \gamma_{I,2} \gamma_{R,1})} \right)^{\frac{1}{\gamma_{RBI}}} \quad (5.4)$$

$$I_P(\bar{T}) = \left(G_1^{(\gamma_{R,2} \gamma_{B,3} - \gamma_{R,3} \gamma_{B,2})} \cdot G_2^{(\gamma_{R,3} \gamma_{B,1} - \gamma_{R,1} \gamma_{B,3})} \cdot G_3^{(\gamma_{R,1} \gamma_{B,2} - \gamma_{R,2} \gamma_{B,1})} \right)^{\frac{1}{\gamma_{RBI}}} \quad (5.5)$$

$$\begin{aligned} \gamma_{RBI} = & (\gamma_{R,1} \gamma_{B,2} \gamma_{I,3} + \gamma_{R,2} \gamma_{B,3} \gamma_{I,1} + \gamma_{R,3} \gamma_{B,1} \gamma_{I,2}) - \\ & (\gamma_{R,1} \gamma_{B,3} \gamma_{I,2} + \gamma_{R,2} \gamma_{B,1} \gamma_{I,3} + \gamma_{R,3} \gamma_{B,2} \gamma_{I,1}) \end{aligned} \quad (5.6)$$

1717 **Scenario II – Solve for I_P**

$$R_0(\bar{T}) = \left(G_1^{\gamma_{B,2}} \cdot G_2^{-\gamma_{B,1}} \cdot I_P^{(\gamma_{B,1} \gamma_{I,2} - \gamma_{B,2} \gamma_{I,1})} \right)^{\frac{1}{\gamma_{RBT}}} \quad (5.7)$$

$$B_0(\bar{T}) = \left(G_1^{-\gamma_{R,2}} \cdot G_2^{\gamma_{R,1}} \cdot I_P^{(\gamma_{I,1} \gamma_{R,2} - \gamma_{I,2} \gamma_{R,1})} \right)^{\frac{1}{\gamma_{RBT}}} \quad (5.8)$$

$$\gamma_{RBT} = \gamma_{R,1} \gamma_{B,2} - \gamma_{R,2} \gamma_{B,1} \quad (5.9)$$

1718 5.3 Wrapping up the Logic

1719 As stated at the beginning of the chapter, this systems model basically boils down to a
 1720 simple 5 equation/5 unknown algebra problem. The Greenwald density was implicitly
 1721 used in the initial derive to simplify the logic. The current balance was then delegated
 1722 to be the root solve equation. Lastly, three equations were needed to remove the major
 1723 radius and magnet strength, as well as either the current or temperature. These 16
 1724 equations were given in Table 5.1 with the generalized solution given in Eqs. (5.3)
 1725 to (5.9).

1726 This now sets the stage for the most interesting part of the document – the results.
 1727 In true Dickens fashion, they will come in several forms. The first result type we
 1728 will encounter will be temperature scans. These allow us to validate the model by
 1729 comparing it to several designs from the literature. These will use the Scenario II
 1730 solver.

1731 Moving onto examples of the Scenario I matcher are sensitivity studies and Monte
 1732 Carlo samplings. The simple one variable sensitivities will reveal local trends from
 1733 sweeping various ~~staticfixed~~ (i.e. input) variables – namely H, κ , B_{CS} , etc. Whereas
 1734 the samplings will highlight global trends as many ~~staticfixed~~/input variables are
 1735 allowed to vary simultaneously.

1736 These Scenario I flavors are further subdivided in regards to the nature of their closure
 1737 equation. The first flavor comes from finding so called two limit solutions, which live
 1738 at the point where the beta and kink (or wall) limits are just marginally satisfied.
 1739 The second main type is then minimum cost reactors – measured in either a capital
 1740 cost or cost-per-watt context. These will be used in depth next chapter.

1741 Chapter 6

1742 Presenting the Code Results

1743 Now that our fusion systems model has been formulated and completed, the next
1744 logical step is to code it up and run it to produce interesting data. To this, the code
1745 for this document – Fussy.jl – is available at git.io/tokamak (with a short guide given
1746 in the Appendix). The results will be given shortly.

1747 Before accosting the reader with some twenty plots and tables, though, it makes sense
1748 to first warn them what they are getting into. This chapter has three sections. The
1749 first is an attempt to test how good the model is by comparing it with other codes
1750 in the field.^{3,5,24} Next, we will develop two prototype reactors that pit steady-state
1751 against pulsed operation on a leveled playing field.

1752 This chapter will then conclude with a discussion on how best to lower the costs
1753 of a tokamak reactor. In line with the MIT mission, this will highlight how using
1754 stronger magnets leads to more compact, efficient machines. The new piece of insight,
1755 then, is how to optimally incorporate high-temperature superconducting (HTS) tape
1756 technology – the miracle found in the ARC design family.

1757 Without spoiling too much for the reader, we will show that HTS tape should be used
1758 in the TF coils for steady-state tokamaks (i.e. B_0), whereas it should only be appear
1759 in the central solenoid (i.e. B_{CS}) for pulsed ones. This is a fundamentally new result!

1760 6.1 Validating Code with other Models

1761 When you develop a new model, the first thing you have to do is check that it makes
1762 sensical results. The goal is not to go overboard, though, by: comparing it with
1763 too many models or requiring perfect matches with all their results. To this, we
1764 will compare Fussy.jl with five designs coming from three separate research teams
1765 – hopefully casting a wide enough net through reactor-space to prove sufficient. It
1766 should be noted that for how simple this model is, it does a remarkable job matching
1767 these more sophisticated frameworks. It also highlights how discrepancies arise in
1768 this highly non-linear computational problem.

1769 The first reactor design that will provide a basis for comparison is the ARC reactor.
1770 As it was also designed by MIT researchers, the fit is shown to be almost exact. This
1771 of course probably involves a fair amount of inherent biases stemming from how this
1772 ecosystem operates and produces engineers – most notably as the core of this code
1773 comes from Jeff’s ongoing interest in the problem.

1774 The next set of reactor designs come from the ARIES four-act study. This ARIES
1775 team is a United States effort to reevaluate the problem of designing a fusion reac-
1776 tor around once a decade. The most recent study focused on how tokamaks shape
1777 up as you assume optimistic and conservative physics and engineering parameters.
1778 Although our model recovers their results, it does highlight one peculiarity of their
1779 algorithm – reliance on the minimum achievable value of H .

1780 The final series of reactors comes from the major codebase used among European
1781 fusion systems experts: PROCESS. As such, this group actually gives an example for
1782 pulsed vs. steady-state tokamaks. Although these designs have the most discrepancies
1783 with our model, discussion will be given that remedy some of the shortcomings. These
1784 basically boil down to: alternative definitions for heat loss appearing in the ELMy
1785 H-Mode Scaling, as well as the simplified nature of our flux balance equation – which
1786 only accounts for central solenoid and PF coil source terms.

6.1.1 Comparing with the PSFC Arc Reactor

As mentioned, this model matches the results from the ARC design almost perfectly. This probably stems from how both models were developed within the MIT community. The points to make now, though, is even with how well the results match, there are two notable discrepancies: the fusion power (P_F) and bootstrap current fraction (f_{BS}). These mainly arise from the use of simple parabolic profiles for temperature.

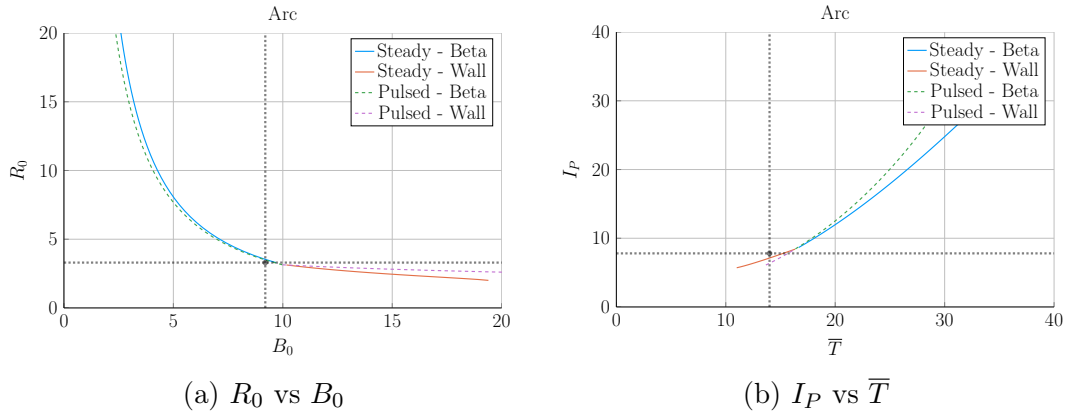


Figure 6-1: Arc Model Comparison

Table 6.1: Arc Variables

(a) Input Variables

Input	Value
H	1.8
Q	13.6
N_G	0.67
ϵ	0.333
κ_{95}	1.84
δ_{95}	0.333
ν_n	0.385
ν_T	0.929
l_i	0.67
A	2.5
Z_{eff}	1.2
f_D	0.9
τ_{FT}	1.6e9
B_{CS}	12.77

(b) Output Variables

Output	Original	Fussy.jl
R_0	3.3	3.4
B_0	9.2	9.5
I_P	7.8	8.8
\bar{n}	1.3	1.3
\bar{T}	14.0	16.8
β_N	0.026	-
q_{95}	7.2	6.1
P_W	2.5	2.2
f_{BS}	0.63	0.56
f_{CD}	0.37	0.44
f_{ID}	-	-
V	141	157
P_F	525	726
η_{CD}	0.321	0.316

1793 6.1.2 Contrasting with the Aries Act Studies

1794 Moving on, the Aries Act study focuses on how steady-state reactors would look under
 1795 both a conservative and optimistic perspective. This is highlighted in Fig. 6-2, which
 1796 shows how costs decrease as the H factor is allowed to increase. Notice that for every
 1797 value of H, the ACT I study (i.e. the optimistic act) has a lower cost than the design
 1798 from ACT II (i.e. the conservative one).

1799 This figure also highlights another peculiarity of the ARIES study – a reliance on the
 1800 minimum possible value of H. Note that just left of the reactor point on both plots
 1801 is a highly erratic portion of the curve. As such, if even a slightly smaller value of H
 1802 were used in either case, a quite distinct reactor would occur. This is not a robust
 1803 way to design machines. A better approach would be to build with some safety factor
 1804 – i.e at a slightly more magical version of H. This can be seen in ARC’s H-Sweep.

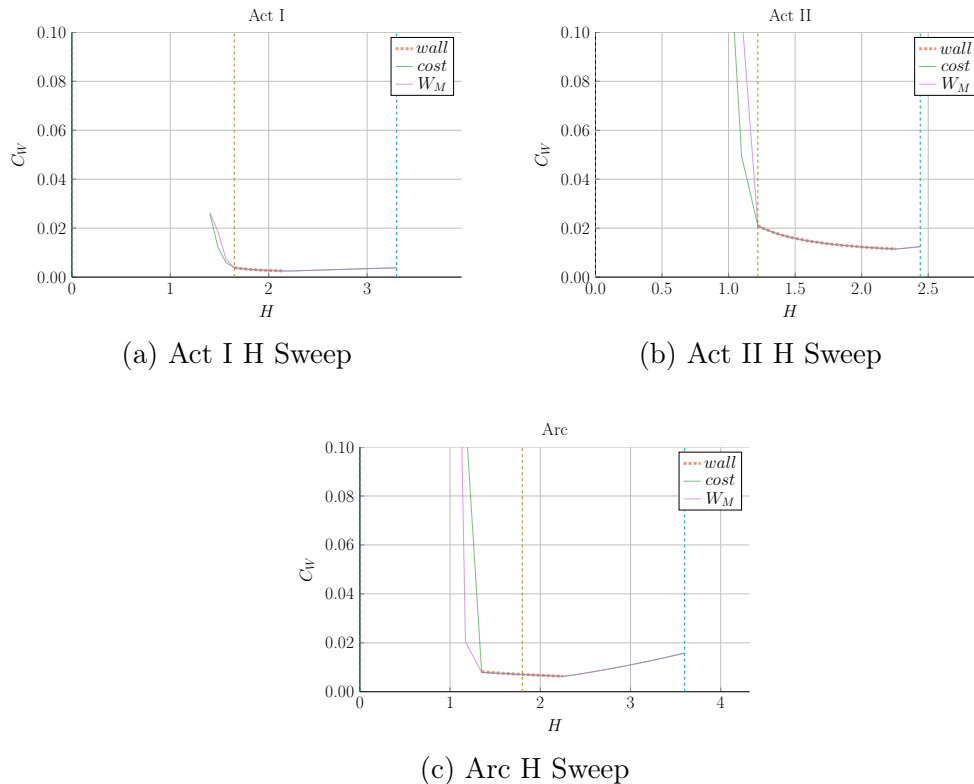


Figure 6-2: Act Studies Cost Dependence on the H Factor

1805 Act I – Advanced Physics and Engineering

1806 Act 1 is the ARIES study that assumes advanced physics and engineering design
 1807 parameters. Although this paper’s model does a good job matching the results from
 1808 their paper, it does show what optimistic design really means. As can be seen, this
 1809 design actually only surpasses the minimum possible toroidal field strength by as less
 1810 than a Tesla! Practically, this means the reactor is barely realizable.

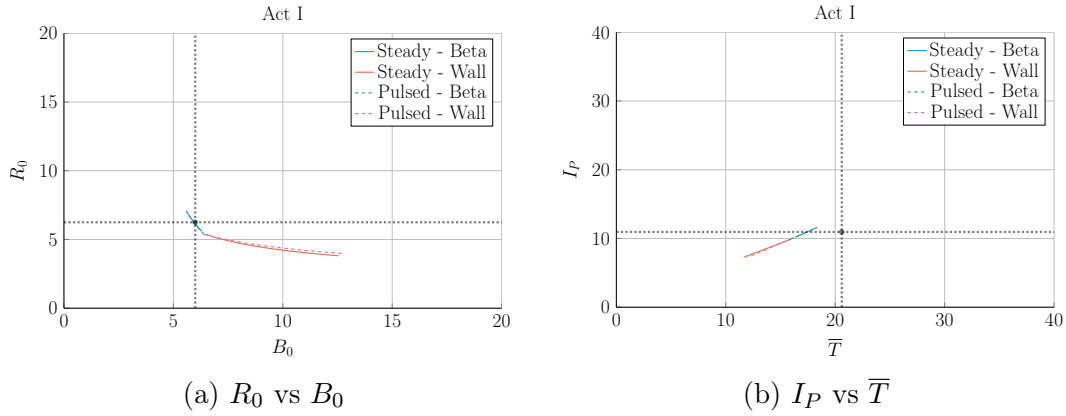


Figure 6-3: Aries Act I Model Comparison

Table 6.2: Act I Variables

(a) Input Variables

Input	Value
H	1.65
Q	42.5
N_G	1.0
ϵ	0.25
κ_{95}	2.1
δ_{95}	0.4
ν_n	0.27
ν_T	1.15
l_i	0.359
A	2.5
Z_{eff}	2.11
f_D	0.75
τ_{FT}	1.6e9
B_{CS}	12.77

(b) Output Variables

Output	Original	Fussy.jl
R_0	6.25	6.23
B_0	6.0	6.0
I_P	10.95	10.78
\bar{n}	1.3	1.3
\bar{T}	20.6	17.2
β_N	0.0427	-
q_{95}	4.5	4.0
P_W	2.45	2.00
f_{BS}	0.91	0.91
f_{CD}	0.09	0.09
f_{ID}	-	-
V	582.0	621.4
P_F	1813	1865
η_{CD}	0.188	0.185

1811 **Act II – Conservative Physics and Engineering**

1812 ARIES more conservative design – Act II – is much more like ARC in nature. From
 1813 the plots, it is obvious the paper’s model is basically right on top of the reactor curve
 1814 made using Fussy.jl. Much like ARC, too, it shows how the model overestimates fusion
 1815 power and underestimates bootstrap fraction due to their selection of a pedestal profile
 1816 for plasma temperature.

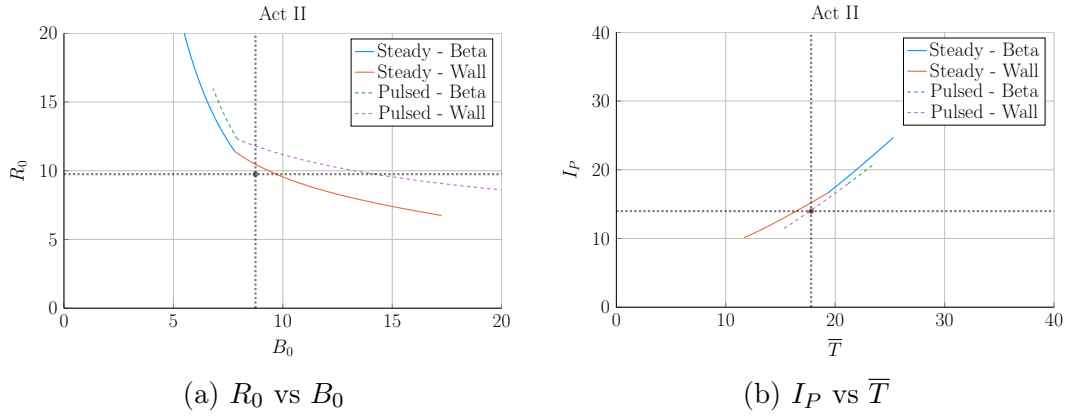


Figure 6-4: Aries Act II Model Comparison

Table 6.3: Act II Variables

(a) Input Variables

Input	Value
H	1.22
Q	25.0
N_G	1.3
ϵ	0.25
κ_{95}	1.964
δ_{95}	0.42
ν_n	0.41
ν_T	1.15
l_i	0.60275
A	2.5
Z_{eff}	2.12
f_D	0.74
τ_{FT}	1.6e9
B_{CS}	12.77

(b) Output Variables

Output	Original	Fussy.jl
R_0	9.75	10.22
B_0	8.75	9.05
I_P	13.98	14.84
\bar{n}	0.86	0.82
\bar{T}	17.8	17.4
β_N	0.026	0.023
q_{95}	8.0	6.6
P_W	1.46	-
f_{BS}	0.77	0.66
f_{CD}	0.23	0.34
f_{ID}	-	-
V	2209	2559
P_F	2637	3460
η_{CD}	0.256	0.307

1817 6.1.3 Benchmarking with the Process DEMO Designs

1818 The PROCESS team’s prospective designs for successors to ITER constitute the final
1819 set of model comparisons: the steady-state and pulsed DEMO reactors. As this paper
1820 is designed to compare these modes of operation, this study proves most fruitful. It
1821 also highlights how common model decisions can dramatically alter what reactors
1822 come out of the solvers.

1823 The first discrepancy is how the PROCESS team defines the loss term in the ELMy H-
1824 Mode scaling law. As shown in their paper, they actually subtract out a Bremsstrahlung
1825 component, while leaving the fitting coefficients the same.³ After modifying Fussy.jl
1826 to incorporate this definition, the steady-state reactor is easily reproducible in $R_0 -$
1827 B_0 slice of reactor space.

1828 Unlike the steady-state case, however, the modified power loss term does not fix the
1829 pulsed case, as it actually draws the reactor curves further from the design in their
1830 paper. As such, it is flux balance that is now the main culprit for discrepancies
1831 between the two models. This makes sense, as this model uses highly simplified
1832 source terms – namely neglecting anything but the central solenoid and PF coils (as
1833 well as ignoring crucial physics for these two components). Even acknowledging the
1834 differences between the two models, Fussy.jl still does remarkably well at reproducing
1835 their much more sophisticated coding framework.

1836 The final point to make is about selecting optimum points to build as the ~~dynamic~~floating
1837 variables are allowed to make curves through reactor space. Up to this point, only
1838 steady-state tokamak designs have been explored. In every single one of these, though,
1839 the paper values have been very close to the point where the beta curves and wall
1840 loading curves cross. This is because they all result in the minimum cost-per-watt.

1841 For pulsed designs, on the other hand, kink curves start to appear for low magnetic
1842 field strengths. Just as beta-wall intersections were optimum places to design for low
1843 cost-per-watt (C_W) reactors, these beta-kink intersections will prove to be the place
1844 where minimum capital cost (W_M) reactors usually occur.

1845 DEMO Steady – A Steady-State ITER Successor

1846 Hands down, this DEMO Steady reactor is the worst modeled reactor using Fussy.jl.
 1847 As mentioned previously, though, some of the discrepancy was removed by using the
 1848 PROCESS team’s modified version of heat loss. This heavily corrected the $R_0 - B_0$
 1849 curve, but had no effect on the $I_P - \bar{T}$ one. An interesting aside is that these curves
 1850 actually show how steady current is independent of secondary constraint (as noted).

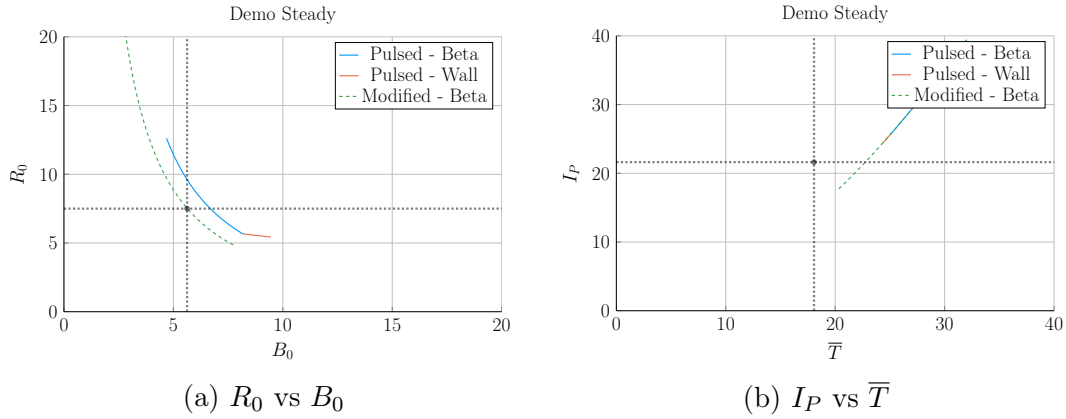


Figure 6-5: Demo Steady Model Comparison

Table 6.4: Demo Steady Variables

(a) Input Variables

Input	Value
H	1.4
Q	24.46
N_G	1.2
ϵ	0.385
κ_{95}	1.8
δ_{95}	0.333
ν_n	0.3972
ν_T	0.9187
l_i	0.9
A	2.856
Z_{eff}	4.708
f_D	0.7366
τ_{FT}	1.6e9
B_{CS}	12.85

(b) Output Variables

Output	Original	Fussy.jl
R_0	7.5	8.2
B_0	5.627	6.307
I_P	21.63	30.93
\bar{n}	0.8746	1.048
\bar{T}	18.07	27.83
β_N	0.038	-
q_{95}	4.405	3.761
P_W	1.911	4.151
f_{BS}	0.611	0.424
f_{CD}	0.389	0.576
f_{ID}	-	-
V	2217	2879
P_F	3255	8971
η_{CD}	0.4152	-

1851 DEMO Pulsed – A Pulsed ITER Successor

1852 This pulsed version of DEMO is the only reactor in our collection that is not run
 1853 in steady-state. As such, it may be the most important one. The first thing that is
 1854 abundantly clear is that this design actually has no valid wall loading portion – only a
 1855 kink and beta curve exist! Even so, the results match pretty well. It should be noted,
 1856 though, that this current drive is treated as an input and not solved self-consistently.

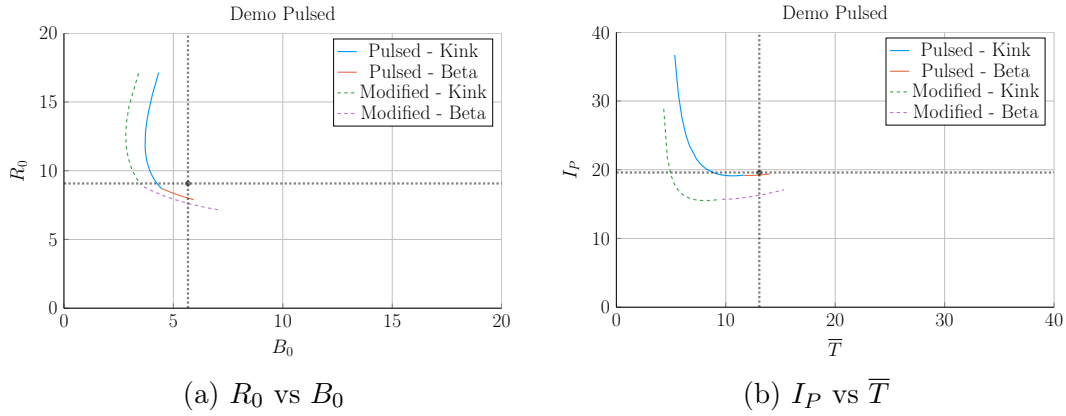


Figure 6-6: Demo Pulsed Model Comparison

Table 6.5: Demo Pulsed Variables

(a) Input Variables

Input	Value
H	1.1
Q	39.86
N_G	1.2
ϵ	0.3226
κ_{95}	1.59
δ_{95}	0.333
ν_n	0.27
ν_T	1.094
l_i	1.155
A	2.735
Z_{eff}	2.584
f_D	0.7753
τ_{FT}	7273
B_{CS}	12.77

(b) Output Variables

Output	Original	Fussy.jl
R_0	9.07	8.10
B_0	5.67	5.48
I_P	19.6	19.3
\bar{n}	0.7983	0.9795
\bar{T}	13.06	13.28
β_N	0.0259	-
q_{95}	3.247	2.853
P_W	1.05	1.47
f_{BS}	0.348	0.164
f_{CD}	0.096	0.106
f_{ID}	0.557	0.730
V	2502	1751
P_F	2037	2376
η_{CD}	0.2721	-

1857 6.2 Developing Prototype Reactors

1858 Now that the model used in Fussy.jl has been tested against other fusion systems
1859 codes in the field, we will develop our own prototype reactors. Because this paper
1860 is about making a levelized comparison of pulsed and steady-state tokamaks, we will
1861 develop middle-of-the-road reactors that only differ by operating mode.

1862 The steady-state prototype, Charybdis, is the obvious choice to start with – as the
1863 model was tested against four of these typed reactors. It was also pointed out that
1864 the model did remarkably well when recreating ARC. As the authors share many of
1865 the ARC team’s philosophies, Charybdis uses ~~static~~fixed parameters very similar to
1866 them.

1867 Next, although led to believe Charybdis’ pulsed twin reactor – Proteus – would be
1868 created by a simple flip of the switch, it was a slight oversimplification. The first
1869 difference is that the pulsed twin, Proteus, is assumed to be purely pulsed: $\eta_{CD} = 0$.
1870 Further, the bootstrap current is much less important than it was for steady-state
1871 tokamaks. This corresponds to a current profile peaked at the origin – i.e. a parabola.
1872 Numerically, this is done by raising l_i from around 5.5 to 6.

1873 The final difference creates the largest change in the twin reactors: the choice of
1874 miracle. As hinted several times before, the H factor is a common way designers
1875 artificially boost the confinement of their machines. This H value will thus be the
1876 miracle for Charybdis, the steady-state prototype. Next, as the main conclusion of
1877 this paper is to state the advantages of high magnetic field, a free way to boost a
1878 central solenoid – through B_{CS} – will be employed using HTS coils.

1879 Opposite the order of how they were designed, the goal now is to lock down a value
1880 of B_{CS} for Proteus and then use it to set the H factor for Charybdis. This selection
1881 algorithm is depicted in Fig. 6-7. For Proteus, the point locked down was $B_{CS} = 20$ T,
1882 which occurred at a fusion power (P_F) of around 1250 MW. As shown in the cost
1883 curve, this was at a point where the ratio between the minimum capital cost and
1884 the minimum cost-per-watt saturated. This choice of a 1250 MW reactor then led to

1885 Charybdis having an H factor of 1.7.

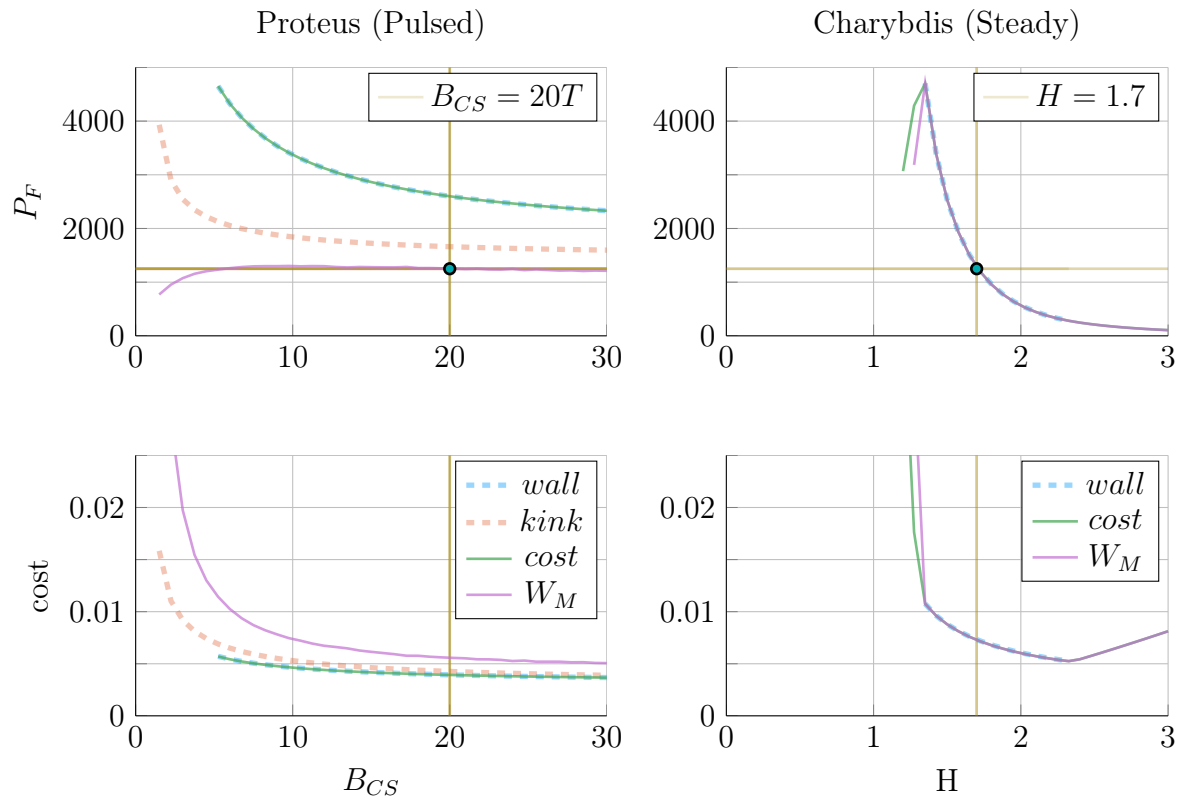


Figure 6-7: How to Build a Fusion Reactor

As is convention in fusion engineering, a good design only relies on one miracle. For steady-state reactors, we assume we can get better confinement – by increasing H . While in the pulsed case, the miracle is assuming strong magnets for the central solenoid – B_{CS} .

6.2.1 Navigating around Charybdis

The Charybdis reactor is the steady-state twin developed for this paper. As mentioned, its parameters are similar to the ARC design. This is shown in Fig. 6-8, where the two $R_0 - B_0$ curves are almost interchangeable. Before moving on, it proves useful to note that the optimum place to build on these curves is where the two portions intersect – as it minimizes costs.

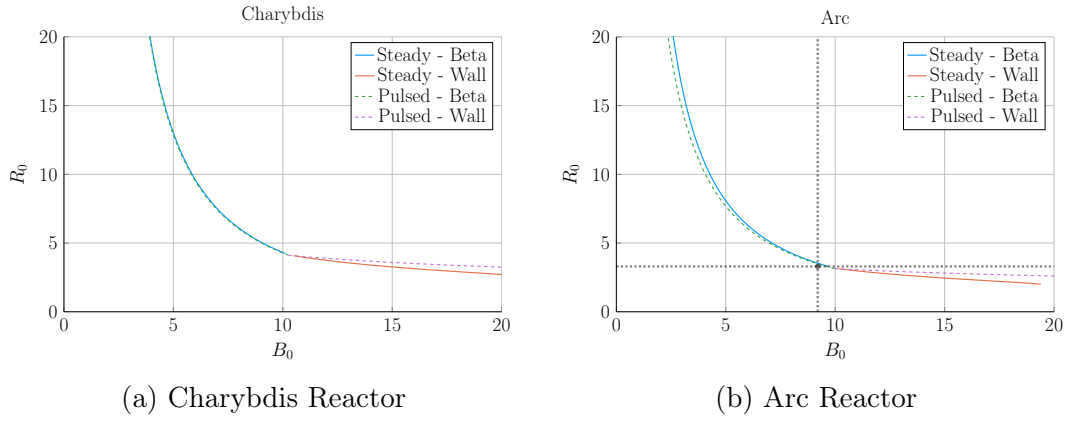


Figure 6-8: Steady State Prototype Comparison

Table 6.6: Charybdis Variables

(a) Input Variables

Input	Value
H	1.7
Q	25.0
N_G	0.9
ϵ	0.3
κ_{95}	1.8
δ_{95}	0.35
ν_n	0.4
ν_T	1.1
l_i	0.5579
A	2.5
Z_{eff}	1.75
f_D	0.9
τ_{FT}	1.6e9
B_{CS}	12.0

(b) Output Variables

Output	Value
R_0	4.13
B_0	10.28
I_P	8.98
\bar{n}	1.47
\bar{T}	15.81
β_N	0.028
q_{95}	6.089
P_W	3.003
f_{BS}	0.723
f_{CD}	0.277
f_{ID}	0.0
V	225.5
P_F	1294
η_{CD}	0.291

6.2.2 Pinning down Proteus

The pulsed twin reactor, Proteus, highlights the effects of a high field central solenoid. When compared to the Pulsed Demo design, the $R_0 - B_0$ curve looks far more favorable – i.e. each machine built at a certain magnet strength would be more compact (and cheaper). An interesting facet of Proteus is that it exhibits all three used limits: kink safety factor, Troyon beta, and wall loading.

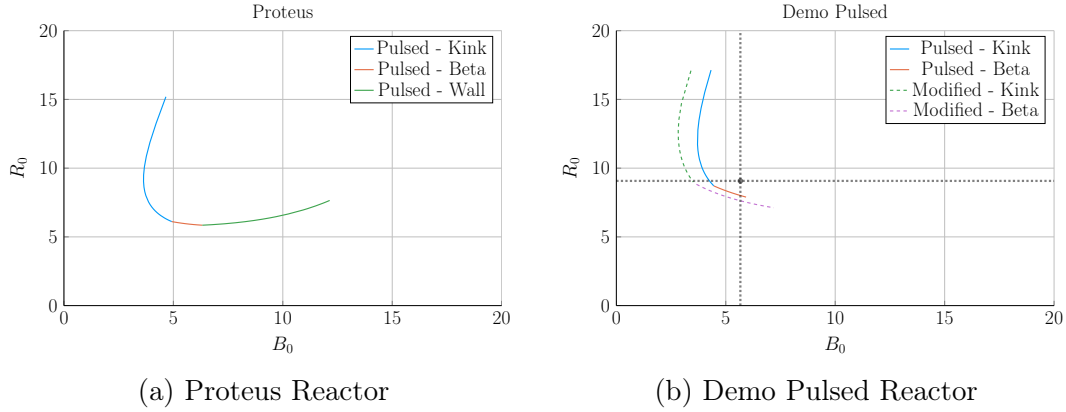


Figure 6-9: Pulsed Prototype Comparison

Table 6.7: Proteus Variables

(a) Input Variables

Input	Value
H	1.0
Q	25.0
N_G	0.9
ϵ	0.3
κ_{95}	1.8
δ_{95}	0.35
ν_n	0.4
ν_T	1.1
l_i	0.6328
A	2.5
Z_{eff}	1.75
f_D	0.9
τ_{FT}	7200
B_{CS}	20.0

(b) Output Variables

Output	Value
R_0	6.11
B_0	4.93
I_P	15.54
\bar{n}	1.16
\bar{T}	11.25
β_N	0.028
q_{95}	2.5
P_W	1.763
f_{BS}	0.2675
f_{CD}	0.0
f_{ID}	0.7325
V	732.6
P_F	1667
η_{CD}	0.0

1898 6.3 Learning from the Data

1899 Now that the model has been properly vetted and prototypes designed, we can explore
1900 how pulsed and steady-state tokamaks scale. Fitting with the Dickens theme, there
1901 will be three mostly independent results. The first result will explore how to minimize
1902 costs for a reactor by choosing optimum design points. The next will be an argument
1903 for how to properly utilize the HTS magnet technology in component design. Lastly,
1904 we will take a cursory look at the other parameters capable of lowering machine costs.

1905 6.3.1 Picking a Design Point

1906 With more than twenty design parameters, finding the most efficient reactor is a
1907 fool’s errand. Intuition building aside, finding good reactors becomes much more fea-
1908 sible when only focusing on ~~dynamic~~~~floating~~ variables – i.e. when keeping ~~static~~~~fixed~~
1909 variables constant. This method, for example, is how all the $R_0 - B_0$ curves have
1910 been produced this chapter. Once these curves are produced, it is up to the user to
1911 choose which reactor on them to build. However, the guiding metric usually involves
1912 lowering some cost, either: capital cost or cost-per-watt.

1913 Regardless of reactor type, most efficient tokamaks operate near the beta limit – where
1914 plasma pressure is greatest. Besides being a regime highly sensitive to magnetic field
1915 strength, the beta limit is a constraint that occurs on every reactor (seen by the
1916 authors). This beta limit is usually nested between the kink limit to lower B_0 values
1917 and wall loading to higher ones. Understanding these regimes is the first step towards
1918 building an intuition favoring efficient machines – see Fig. 6-10.

1919 Now that the beta limit curve has been designated as the most efficient regime to
1920 operate in (usually), the goal is to select which reactor on it is the best one to build.
1921 Starting with the easier of the two, the optimum design point for steady-state reactors
1922 is the point where wall loading first starts to dominate design. Here, engineering
1923 concerns cause the reactor to start increasing in size and cost – which is bad. This
1924 conclusion is justified by the cost curves for all five reactors in Fig. 6-11. As these

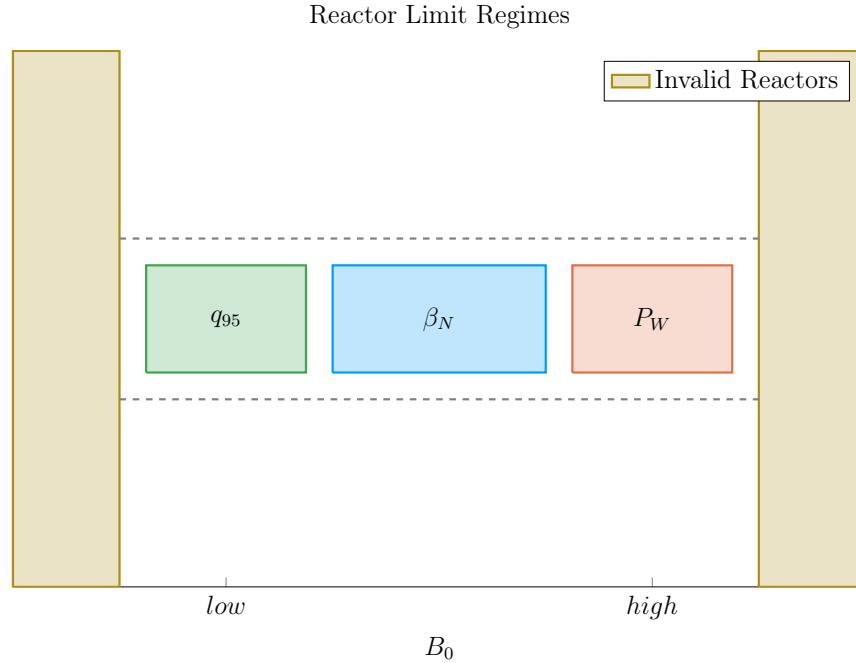


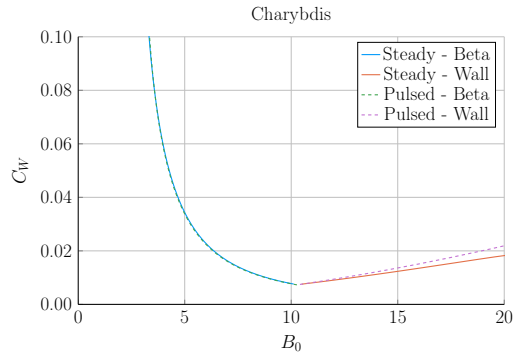
Figure 6-10: Limit Regimes as function of B_0

show, it is also where these reactor designers pinned down their tokamaks.*

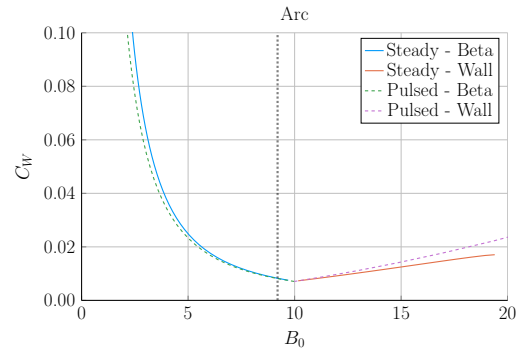
The problem of selecting an optimum design is more difficult for the pulsed case. This is mainly due to the kink limit regime being actually achievable. Following the conclusion from steady-state reactors would be an oversimplification because there are actually two costs relevant to a reactor: capital cost and cost-per-watt. These beta-wall reactors are actually the points often best for minimizing cost-per-watt (i.e. your rate of return). The new beta-kink reactors, then, lead to cheap to build machines – as they minimize capital cost. These conclusions are shown in Fig. 6-12.

Summarizing the conclusions of this subsection, the beta limit is usually the best constraint to operate at. For lowering the cost-per-watt, a reactor should always be run at the highest magnetic field strength (B_0) that satisfies the beta limit. This most often occurs when wall loading takes over (for steady-state reactors) or reactors start being physically unrealizable (for pulsed ones). Building cheap to build reactors – i.e. minimizing capital cost – then actually proved to make pulsed design one of trade-offs.

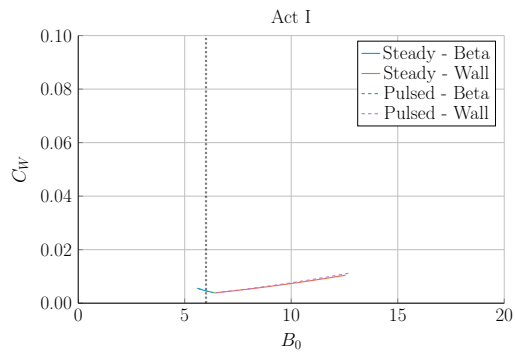
*Simply stated, the optimum reactor for steady-state tokamaks is one that just barely satisfies the beta and wall loading limit simultaneously – i.e. where the two curves intersect.



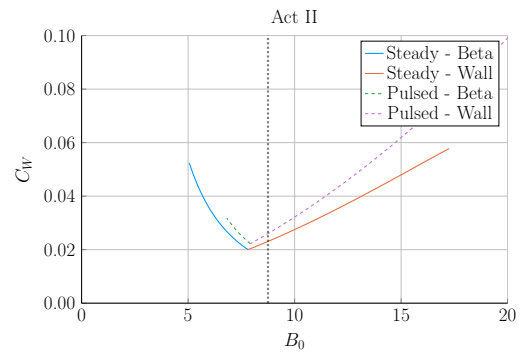
(a) Charybdis



(b) Arc

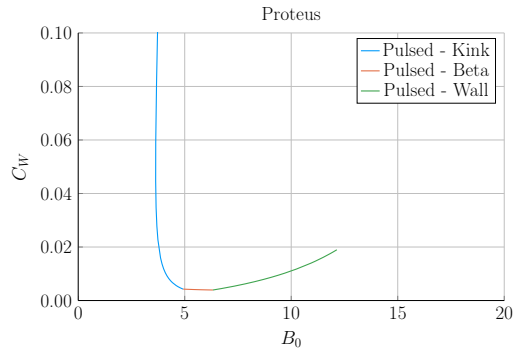


(c) Act I

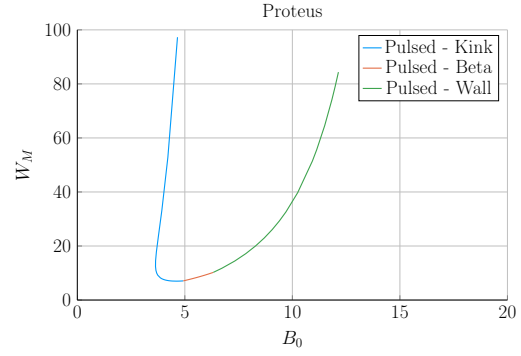


(d) Act II

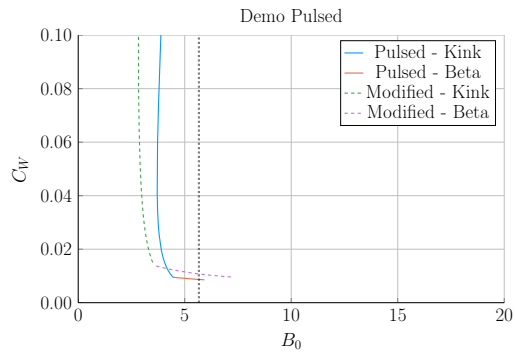
Figure 6-11: Steady State Cost Curves



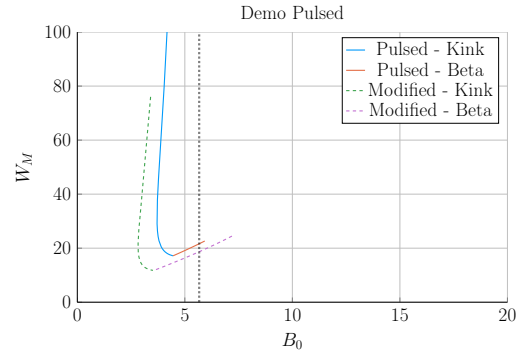
(a) Proteus Cost-per-Watt



(b) Proteus Capital Cost



(c) Demo Pulsed Cost-per-Watt



(d) Demo Pulsed Capital Cost

Figure 6-12: Pulsed Cost Curves

1939 This is because the beta-kink curve intersection produces a low capital cost reactor,
1940 but at the price of operating at a subpar cost-per-watt. Designers should therefore
1941 balance the two cost metrics.

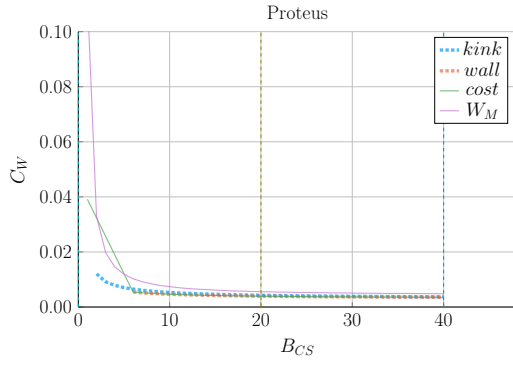
1942 6.3.2 Utilizing High Field Magnets

1943 The main conclusion for this paper is that high field magnets are the way to go to
1944 build an efficient, compact fusion reactor. In line with the MIT ARC effort, these
1945 high fields will be built with high-temperature superconducting (HTS) tape. This
1946 innovation is set to double the strength of conventional magnets. The real question
1947 is how best to use this technology.

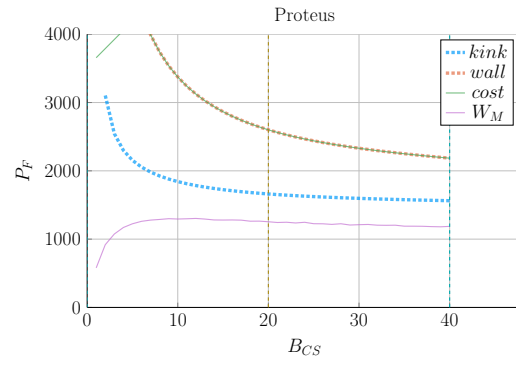
1948 At a very simple level, there are two main places strong magnets can be employed:
1949 the toroidal fields (B_0) and the central solenoid (B_{CS}). The easier mode of operation
1950 to start with is steady-state. This is because steady-state tokamaks do not rely on
1951 a central solenoid for the profitability of their machines. Further, the cost curves
1952 in Fig. 6-11 show that all these designs would benefit from toroidal fields (B_0) not
1953 achievable with conventional magnets – which can only reach around 10 T on a good
1954 day.

1955 The more interesting result is that pulsed reactors gain no real benefit from using
1956 HTS toroidal field magnets. Within the modern paradigm (i.e. D-T fuel, H-Mode,
1957 etc), pulsed reactors never have to exceed the limits of inexpensive, copper magnets.
1958 The place HTS can really help is with the central solenoid, which governs how long a
1959 pulse can last. Further, the effect of improving the central solenoid saturates within
1960 the range accessible to HTS tape. Again, HTS would be more than adequate for the
1961 modern paradigm. These conclusions are shown in Figs. 6-13 and 6-14.

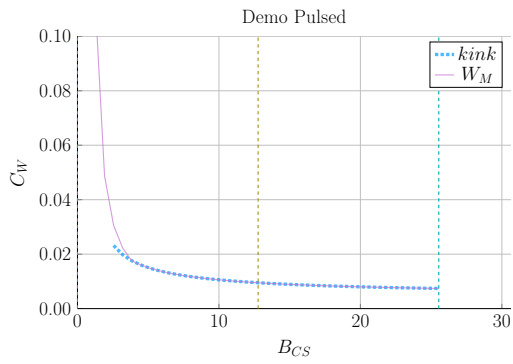
1962 Rehashing this section, HTS tape is the best way to lower the cost of fusion reactors
1963 at a commercial scale. For steady-state reactors, HTS works best in the toroidal field
1964 coils (B_0), while the tape would fare better in the central solenoid (B_{CS}) of pulsed
1965 reactors. Further, both effects saturate within the range of this HTS tape, rendering



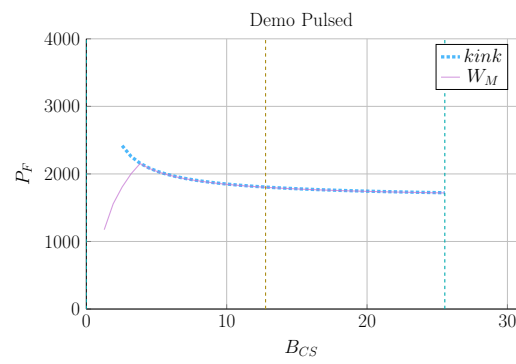
(a) Proteus Cost-per-Watt



(b) Proteus Fusion Power

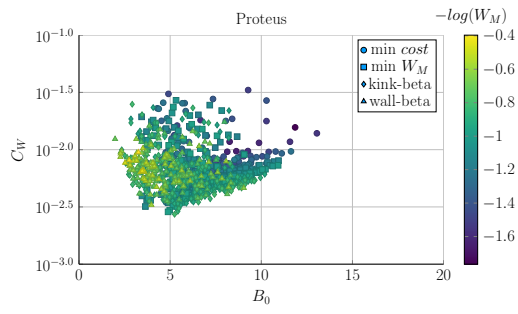


(c) Demo Pulsed Cost-per-Watt

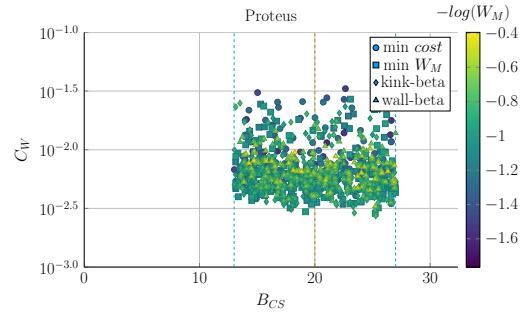


(d) Demo Pulsed Fusion Power

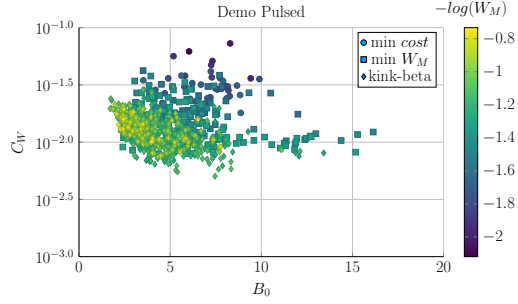
Figure 6-13: Pulsed B_{CS} Sensitivity



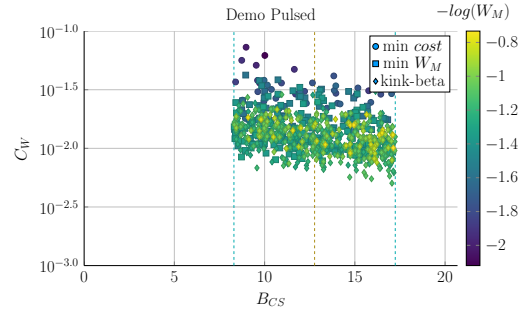
(a) Proteus B_0 Sampling



(b) Proteus B_{CS} Sampling



(c) Demo Pulsed B_0 Sampling



(d) Demo Pulsed B_{CS} Sampling

Figure 6-14: Pulsed Monte Carlo Sampling

1966 more sophisticated magnetic technology unnecessary. HTS is truly the answer to
1967 affordable fusion energy.

1968 6.3.3 Looking at Design Alternatives

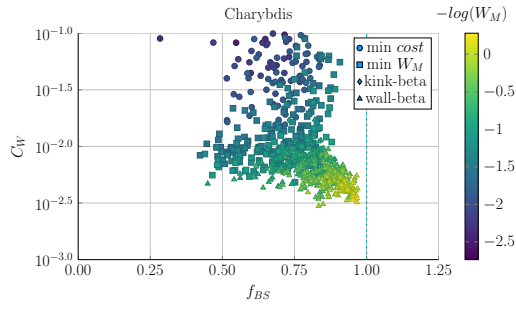
1969 Even in this relatively simple fusion model, there are more than twenty ~~static~~fixed/input
1970 variable knobs a designer can tune to improve reactor feasibility. Many have prac-
1971 tical limits, such as being physically realizable or fitting within the ELMy H-Mode
1972 database. Thus, the goal of this subsection is to investigate some of the more inter-
1973 esting results. Although many more plots are available in the appendix.

1974 Capitalizing the Bootstrap Current

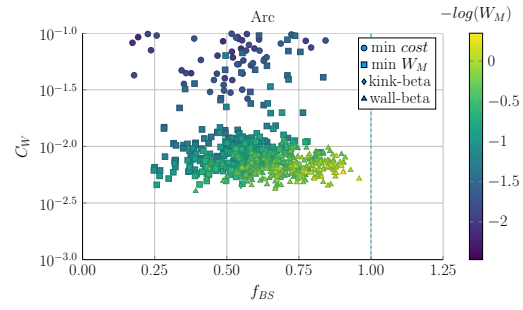
1975 Besides artificially enhancing a plasmas confinement with the H-factor, steady-state
1976 reactor designers may also heavily rely on high bootstrap currents. This is because
1977 bootstrap current is the portion of current you do not have to pay for. The research
1978 camp most focused on this miracle is General Atomic's DIII-D in San Diego. This
1979 miracle relies on tailoring current profiles to be extremely hollow.

1980 Quickly reasoning this camp's thought process are two sets of plots. The first plot
1981 (Fig. 6-15) highlights how the cheapest possible steady-state designs have bootstrap
1982 fractions approaching unity – they use almost no current drive. This makes sense as
1983 current drive is extremely cost prohibitive (i.e. why people consider pulsed tokamaks).

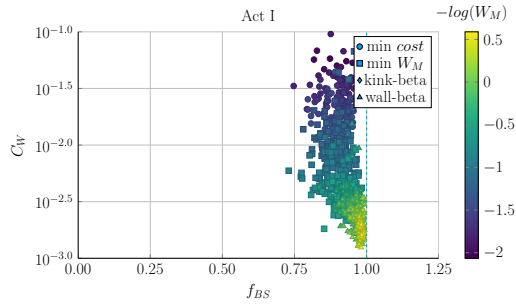
1984 The next plot is the parameter that determines a current profile's peak radius: l_i . As
1985 can be seen, the current peak approaches the outer edge of the plasma as l_i decreases.
1986 This in turn boosts the bootstrap fraction closer to one – leading to inexpensive
1987 reactors.



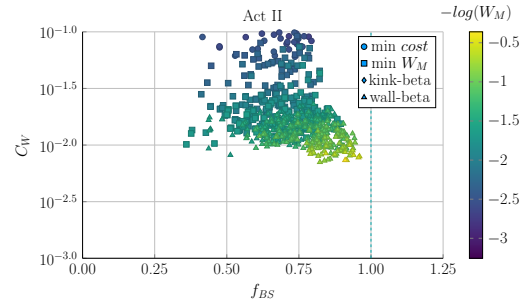
(a) Charybdis l_i Sampling



(b) Arc l_i Sampling

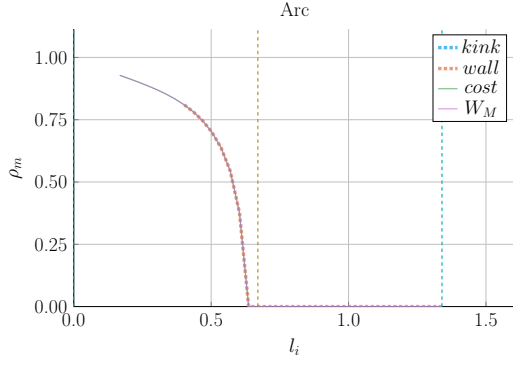


(c) Act I l_i Sampling

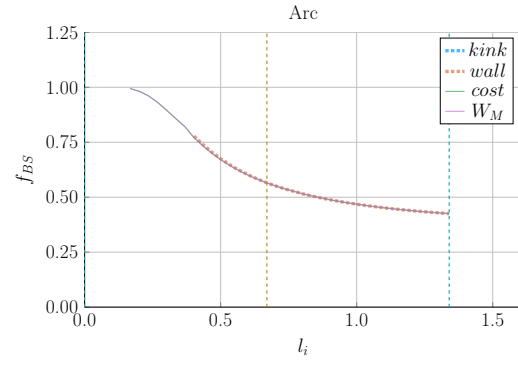


(d) Act II l_i Sampling

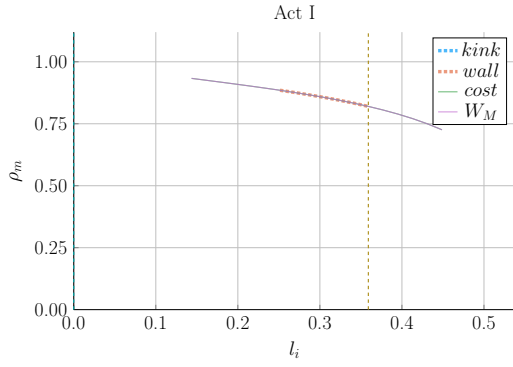
Figure 6-15: Bootstrap Current Monte Carlo Sampling



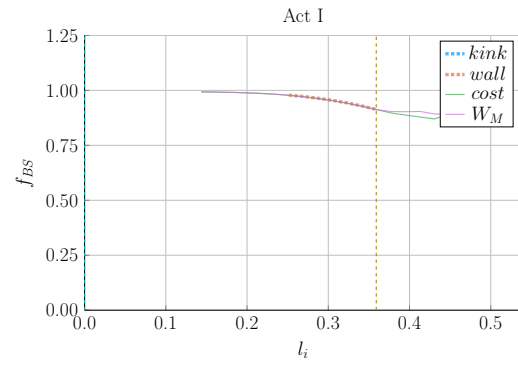
(a) Arc Peak Radius



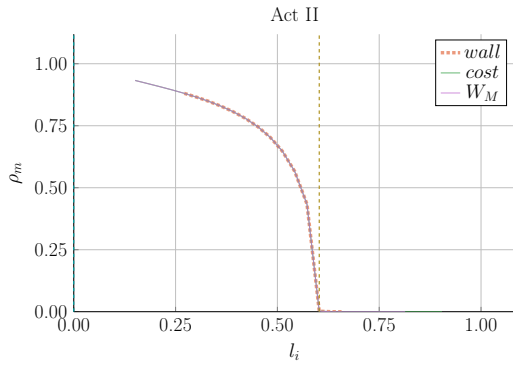
(b) Arc Bootstrap Fraction



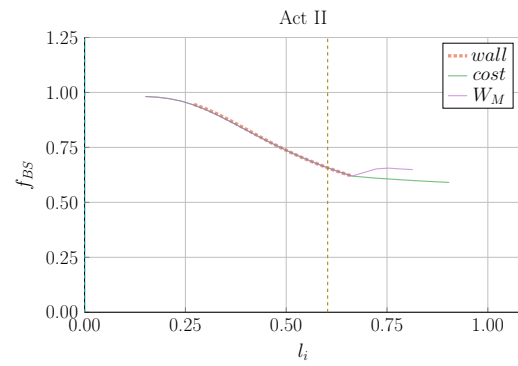
(c) Act I Peak Radius



(d) Act I Bootstrap Fraction



(e) Act II Peak Radius



(f) Act II Bootstrap Fraction

Figure 6-16: Internal Inductance Sensitivities

1988 Contextualizing the H-Factor

1989 From before, increasing the H-factor always led to more cost effective steady-state
1990 reactors. This is because the enhanced confinement allows for smaller machines.
1991 This was already heavily explored in Fig. 6-2. These plots also show that steady
1992 state reactors would not be physically possible using a default H factor of one! In
1993 other words, steady-state tokamaks require some technical advancement before they
1994 can ever be used as fusion reactors. The same cannot be said for pulsed machines.
1995 For pulsed reactors, increasing H always reduces capital cost, but may actually in-
1996 crease the cost-per-watt. The reason for this is because fusion powers are much
1997 smaller in pulsed machines. This interesting result demonstrates the unusual behav-
1998 iors of highly non-linear systems: masterclass intuition may not match model results.

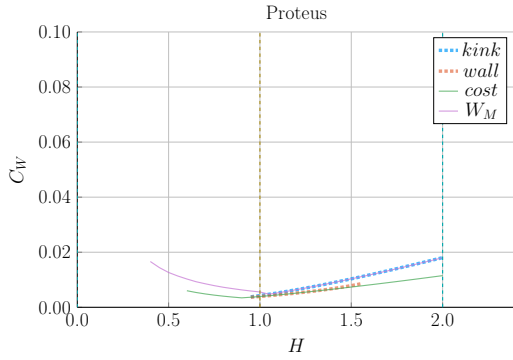
1999 Showcasing the Current Drive Efficiency

2000 The last exploration is less about building an efficient machine and more about under-
2001 standing the self-consistent current drive efficiency in steady-state tokamaks. Using
2002 the Ehst-Karney model²⁰ coupled with Jeff's textbook⁷ leads to a remarkably simple
2003 and accurate solver. The model captures the physics almost spot on for the different
2004 designs.*

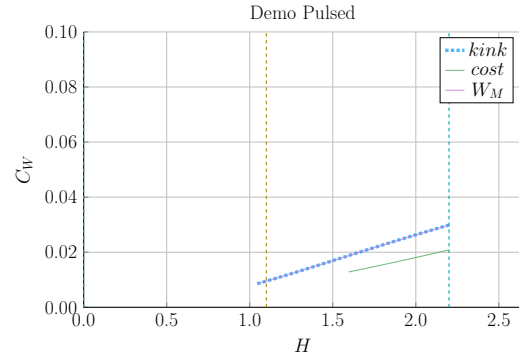
2005 In a similar fashion as the bootstrap fraction results, the variable that most captures
2006 how to directly maximize η_{CD} is the LHCD laser launch angle, θ_{wave} . When below
2007 90° it is considered outside launch, whereas up to 135° it is considered inside launch.
2008 Notably, these curves are not monotonic, there is an optimum launching angle.

2009 It should be noted that the launch angle was not found to have a major impact. This
2010 may be a due to an oversimplification of the model.

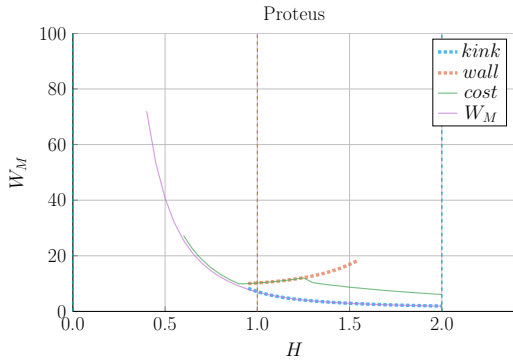
*It did, however, not converge for the DEMO steady reactor. This is probably due to lack of self-consistency for η_{CD} in their systems framework.



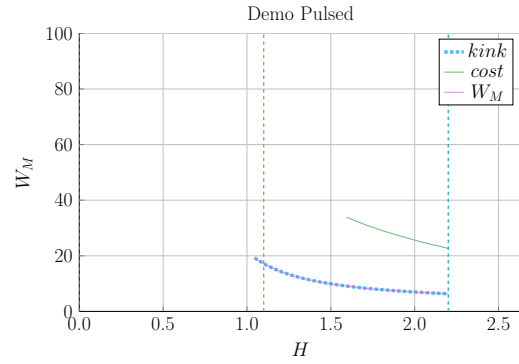
(a) Proteus Cost-per-Watt



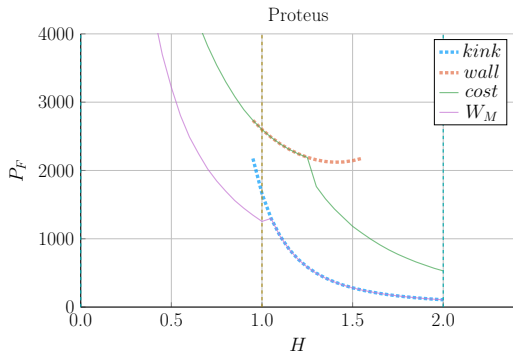
(b) Demo Pulsed Cost-per-Watt



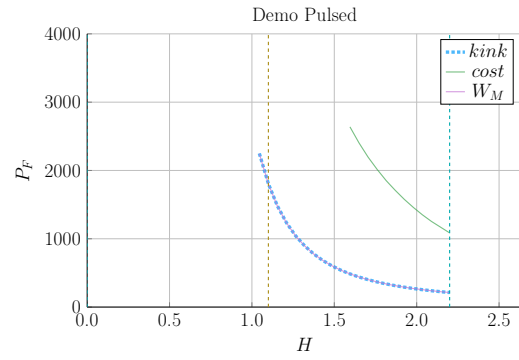
(c) Proteus Capital Cost



(d) Demo Pulsed Capital Cost

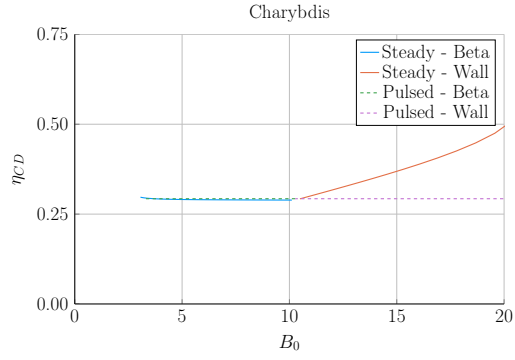


(e) Proteus Fusion Power

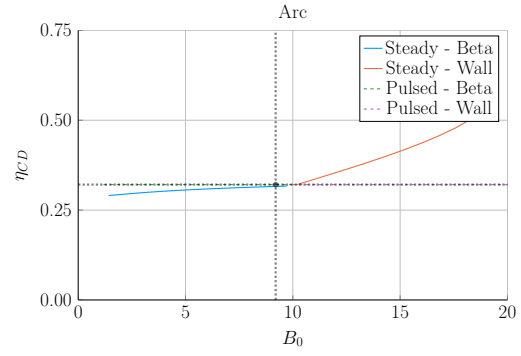


(f) Demo Pulsed Fusion Power

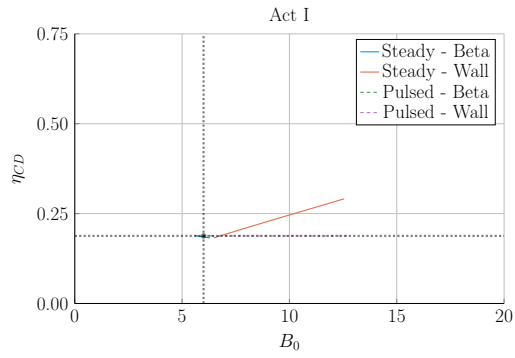
Figure 6-17: Pulsed H Sensitivities



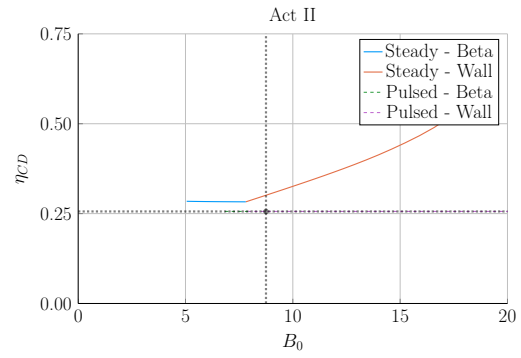
(a) Charybdis



(b) Arc

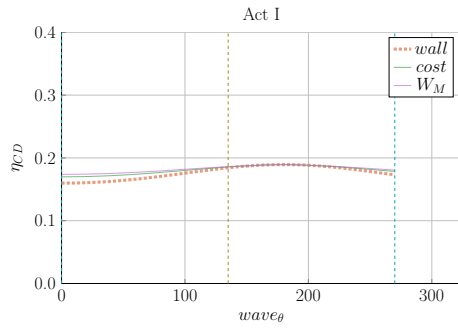


(c) Act I

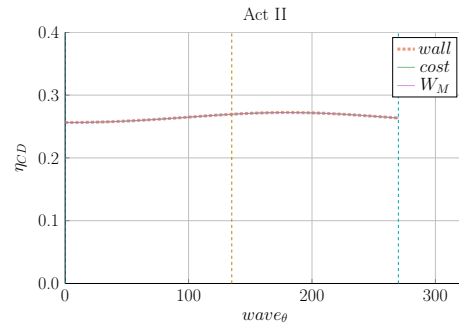


(d) Act II

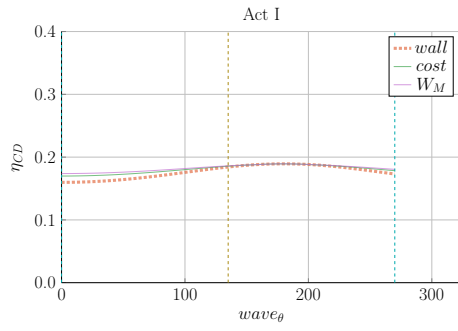
Figure 6-18: Steady State Current Drive Efficiency



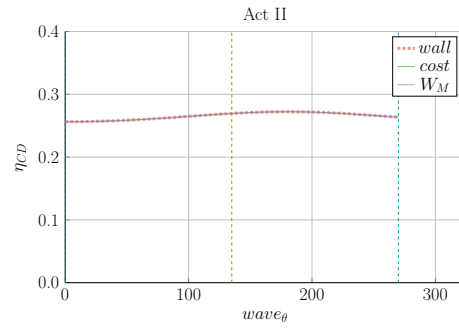
(a) Charybdis



(b) Arc



(c) Act I



(d) Act II

Figure 6-19: Current Drive Efficiency vs Launch Angle

2011 Chapter 7

2012 Planning Future Work

2013 This model may run and produce interesting results, but there is always more to do.

2014 This chapter explores three potential fusion reactors that could help guide real world
2015 designs. It then goes into a laundry list of possible model improvements.

2016 The three reactors covered are: a stellarator (Ladon), a steady-state/pulsed hybrid
2017 (Janus), and a tokamak capable of reaching H, L, and I modes (Daedalus).

2018 7.1 Incorporating Stellarator Technology – Ladon

2019 A stellarator is, at a basic level, a tokamak helically twisted along the length of its
2020 major circle. For a long time they were dismissed because of the difficulty involved in
2021 building spiraled magnets. Recent technological improvements, though, have eased
2022 this situation – as seen with the Wendelstein 7-X device in Germany. The problem
2023 now is engrained in the missing scaling laws stemming from a lack of machines and,
2024 more fundamentally, data points.

2025 Optimistically, expanding this model would just involve developing a new confinement
2026 time scaling law and replacing the Greenwald density limit. The reason the Greenwald
2027 density limit is no longer important is because stability is much easier to maintain in
2028 a stellarator. Most likely, the density limit will now be governed by Bremsstrahlung

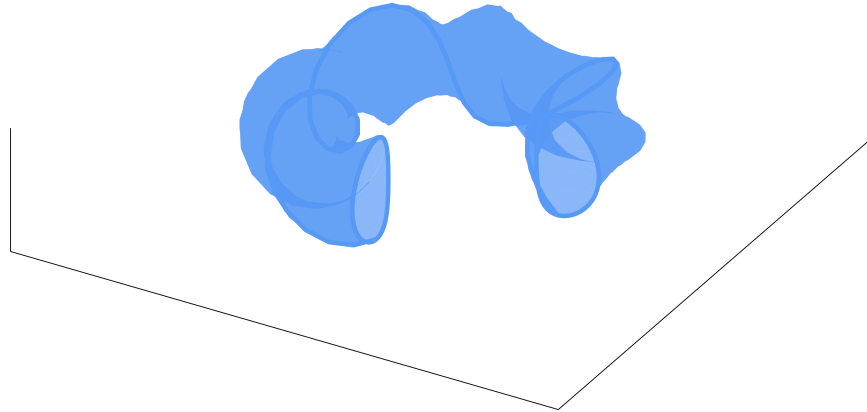


Figure 7-1: Cut-Away of Stellarator Reactor

2029 radiation. If this were the case, each equation would need to be redivided using it.
 2030 Ladon would be the reactor built using this enhancement.

2031 7.2 Making a Hybrid Reactor – Janus

2032 The next interesting reactor would be a hybrid tokamak incorporating pulsed and
 2033 steady-state operation, codenamed: Janus. Fundamentally, this would mean current
 2034 would come from both LHCD (steady-state) and inductive (pulsed) sources. This was
 2035 actually used in Demo Pulsed, but the current drive was not handled self-consistently.
 2036 Coupling these two current sources could reduce reliance on bootstrap current and
 2037 lead to much more compact machines.

2038 The arguments against this are mainly technical: why build two difficult auxiliary
 2039 systems when one is needed – especially when they probably work against each other.
 2040 Although rational, the argument implicitly assumes a current is achievable through
 2041 only one source (i.e. either through LHCD or from a central solenoid). Using two
 2042 may allow for stronger plasma currents.

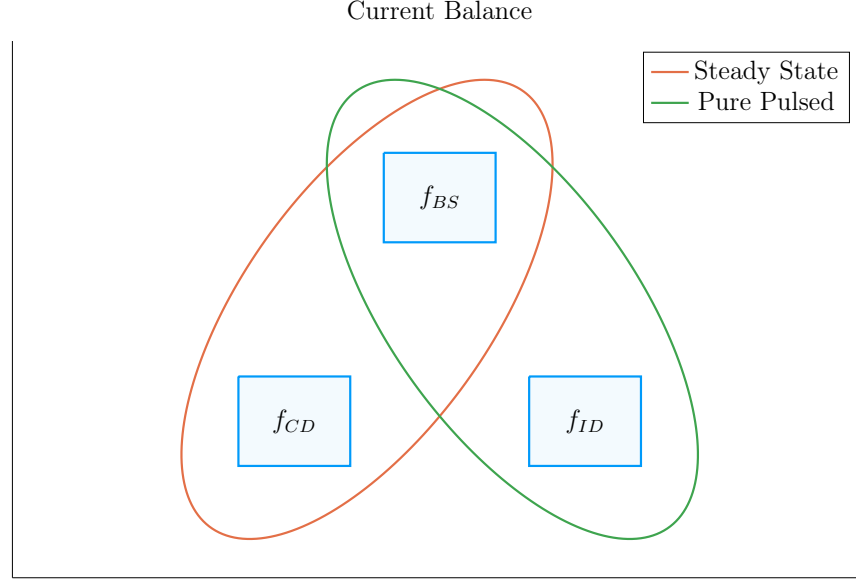


Figure 7-2: Current Balance in a Tokamak

In a tokamak, there needs to be a certain amount of current – and that current has to come from somewhere. All good reactors have an adequate bootstrap current. What provides the remaining current is what distinguishes steady state from pulsed operation.

2043 7.3 Bridging Confinement Scalings – Daedalus

2044 The final potential reactor – Daedalus – is designed to collect as many scaling laws
 2045 as possible. As a baseline, it should be able to run in H-Mode, L-Mode, and I-Mode.
 2046 Because L-Mode is available on any machine, the first step is building under H-Mode.
 2047 The goal then is to find reactors that can also reach I-Mode – thus improving the
 2048 scaling law's fit and making the actual reactor more cost effective.

2049 Presented below are the three confinement scaling laws, as well as the generalized
 2050 formula. As should be noted, the I-Mode scaling currently lacks a true radial de-
 2051 pendence – as it has only been found on two machines. This is one reason Daedalus
 2052 would be so valuable.

$$\tau_E^G = K_\tau H \frac{I_P^{\alpha_I} R_0^{\alpha_R} a^{\alpha_a} \kappa^{\alpha_\kappa} \bar{n}^{\alpha_n} B_0^{\alpha_B} A^{\alpha_A}}{P_L^{\alpha_P}} \quad (3.26)$$

$$\tau_E^H = 0.145 H \frac{I_P^{0.93} R_0^{1.39} a^{0.58} \kappa^{0.78} \bar{n}^{0.41} B_0^{0.15} A^{0.19}}{P_L^{0.69}} \quad (3.29)$$

$$\tau_E^L = 0.048 H \frac{I_P^{0.85} R_0^{1.2} a^{0.3} \kappa^{0.5} \bar{n}^{0.1} B_0^{0.2} A^{0.5}}{P_L^{0.5}} \quad (7.1)$$

$$\tau_E^I = \frac{0.014 H}{0.68^{\lambda_R} \cdot 0.22^{\lambda_a}} \cdot \frac{I_P^{0.69} R_0^{\lambda_R} a^{\lambda_a} \kappa^{0.0} \bar{n}^{0.17} B_0^{0.77} A^{0.0}}{P_L^{0.29}} \quad (7.2)$$

$$\lambda_R + \lambda_a = 2.2 \quad (7.3)$$

A final point to make is reemphasizing that the I-Mode scaling law is not battle-tested. It is the target of ongoing research at the MIT PSFC.

7.4 Addressing Model Shortcomings

Before moving on to the final conclusions, we will give a quick recap of the more audacious simplifications used within this fusion systems framework. These include: approximating temperature profiles as simple parabolas, neglecting all radiation except Bremsstrahlung, and handling flux sources at too basic a level.

7.4.1 Including Pedestal Temperature Profiles

The most dubious simplification in the code at this point is modeling temperature profiles as parabolas. Although these parabolas work for densities and L-Mode plasma temperatures, the same cannot be said about H-Mode temperatures. This is because they have a distinct pedestal region on the outer edge of the plasma.

The usage of pedestal temperatures – discussed in the appendix – improves two aspects of the model: the fusion power and the bootstrap current. These were shown in the results to be over-calculated and underestimated, respectively. Pedestals, having a lower core temperature, would decrease the total fusion power. As well, they would boost bootstrap current due to the quick drop near the plasma’s edge (i.e. they have

2073 a large derivative there).

2074 These improvements could easily be added to the code, because temperature was
2075 addressed as a difficult parameter to handle from the beginning.

2076 **7.4.2 Expanding the Radiation Loss Term**

2077 The next area that would be improved by more sophisticated theory would be the
2078 radiation loss term. From before, it was pointed out that the Bremsstrahlung ra-
2079 diation was the dominant term within the plasma core and, therefore, provided a
2080 first-order approximation. Drawing the radiation losses closer to real world values
2081 would involve adding line radiation and synchrotron radiation. The former of which
2082 would be needed as high-Z impurities become more important.

2083 **7.4.3 Taking Flux Sources Seriously**

2084 The final oversimplification in the model deals with the flux sources involved in a
2085 pulsed reactor – existing at almost every level. First, the derivation of flux balance
2086 started with a simple transformer between a solenoid primary and a plasma secondary.
2087 Even this initial step is probably too simple.

2088 After we developed an equation for flux balance, we compared it to ones in the
2089 literature (i.e. PROCESS) to build confidence in the model. To draw this equation
2090 closer to theirs, we then added a PF coil contribution a posteriori. This implicitly
2091 ignored coupling between most of the components. Thus leading to another source
2092 of error for the model. Moreover, this formula for PF coil contribution was much
2093 simpler than ones found in other fusion systems codes.

2094 Even though this model may be extremely simple, it does remarkably well at matching
2095 more sophisticated codes – and does so at a much faster pace. These suggestions were
2096 all just ways to draw results closer to real world values.

2097 Chapter 8

2098 Concluding Reactor Discussion

2099 The goal of this document was to develop a simple fusion systems model that can
2100 work for both pulsed and steady-state tokamaks. The main conclusion was that the
2101 best way to build a more efficient, compact reactor is to invest in strong magnets –
2102 as MIT is doing with high-temperature superconducting (HTS) tape. Further it was
2103 shown that to best utilize materials, the tape should be incorporated into the toroidal
2104 field coils for steady-state machines and in the central solenoid for pulsed ones.

2105 Although some skepticism should be allotted to these conclusions, it was shown that
2106 this simple algebraic solver matched sophisticated multiyear research studies with
2107 speed and ease. This model may not provide an engineer’s rigor in measuring cost,
2108 but the same can be said for any code or theory. The fusion system is as nonlinear
2109 a problem as they come, but we still managed to build a framework that can hone
2110 even a well-trained physicist’s intuition.

2111 The final point to make is that this model actually predicts that HTS technology can
2112 provide the optimum magnetic field strength for a reactor. Once HTS doubles the
2113 maximum achievable teslas, the law of diminishing returns heavily kicks in. This of
2114 course assumes H-Mode D-T plasmas at the Greenwald density limit.

Appendix A

Presenting ~~Static~~Fixed Variables

Table A.1: List of ~~Static~~Fixed Variables

Name	Value
is_pulsed	is reactor pulsed or steady-state (for η_{CD} consistency or multiple current roots)
H	h factor for ELMy H-mode scaling
Q	Physics Gain (P_F/P_H)
ϵ	inverse aspect ratio
κ_{95}	elongation at 95 flux surface
δ_{95}	triangularity at 95 flux surface
ν_n	parabolic density peaking factor
ν_T	parabolic temperature peaking factor
Z_{eff}	effective charge
f_D	dilution factor
A	average mass number (in amus)
l_i	internal inductance (interchangeable with ρ_m)
ρ_m	normalized radius of current peak (interchangeable with l_i)
N_G	Greenwald density fraction
η_T	thermal efficiency of the reactor
η_{RF}	efficiency of the RF antenna
τ_{FT}	time of flattop of reactor pulse
B_{CS}	strength of magnetic field in central solenoid
$(\beta_N)_{max}$	max allowed normalized beta normal
$(q_{95})_{max}$	min allowed safety factor
$(P_W)_{max}$	maximum allowed wall loading power per surface area

2117 Appendix B

2118 Simulating with Fussy.jl

2119 Fussy.jl is a 0-D fusion systems code written using the Julia language. The reason for
2120 choosing Julia over say Matlab and Python was due to metaprogramming concerns
2121 and its tight-knit computational community, respectively. Incorporating the model
2122 used throughout this paper, the code is quick to run and matches more sophisticated
2123 frameworks with high fidelity.

2124 This chapter will be broken down into three steps. The first is getting a user up
2125 and running with the code. Once the user gets to this point, hopefully they will
2126 wonder how the code is structured. This will be the second step. The final step
2127 will be explaining the various functions callable on reactor objects – the atomic data
2128 structure for Fussy.jl.

2129 B.1 Getting the Code to Work

2130 The hardest step of any codebase is getting it up and running. These instructions
2131 should get a user to a point where they are a few internet searches away from a
2132 working copy of Fussy.jl. As an aide, you can view an interactive collection of Fussy.jl
2133 Jupyter notebooks at the following website:

2134 www.fusion.codes

2135 Although `fusion.codes` is a nice tool for viewing this document’s results, it is a little
2136 slow for producing new data – and it also lacks a method for storing it. Therefore,
2137 an advanced user should first download a copy of Julia from:

2138 julialang.org/downloads

2139 Currently the `Fussy.jl` codebase is written using `v0.6`, but should be `v1.0` compatible
2140 by 2019. Using Julia nomenclature, `Fussy.jl` is a Julia package. It can be cloned using
2141 Julia conventions from the following Github repository:

2142 <https://github.com/djsegal/Fussy.jl.git>

2143 Once the `Fussy.jl` package has been cloned into your Julia package library, you should
2144 be able to access it through the Julia REPL or a Jupyter notebook. You can now
2145 reproduce every plot in this text. A quick test to see if your code works is:

2146

```
2147 using Fussy
2148 cur_reactor = Reactor(15)
2149
2150 @assert cur_reactor.T_bar == 15
```

2151 B.2 Sorting out the Codebase

2152 Assuming the user got to this section, the code works and now you want to know
2153 what you can do with it. The place to start is in the `src` folder, again viewable online
2154 at:

2155 git.io/tokamak

2156 Within the `src` folder are several subfolders as well as a few files (e.g. `Fussy.jl` and
2157 `defaults.jl`). In an attempt to not bore the reader, we will be painting with thick
2158 brushstrokes. Further, the `methods` subfolder will be the topic of the next section –
2159 as most involve calls on a reactor object.

2160 **B.2.1 Typing out Structures**

2161 The place to start in any modeling framework is its data structures. These type
2162 definitions allow the building of nested hierarchies of constructed objects. The most
2163 atomic of these is the Reactor struct, but several other ones allow for solving broader
2164 scoped questions (i.e. Scans, Sensitivities, and Samplings.)

2165 **The Reactor Structure**

2166 Reactors are the most atomic data structure in this fusion systems model. They
2167 store all the fields needed to represent a reactor as it exists in reactor space. This
2168 obviously includes its temperature, current, and radius, but also includes derived
2169 quantities, such as the cost-per-watt and bootstrap fraction. They can be initialized,
2170 solved, updated, and honed. Most other data structures are just wrappers to hold
2171 these reactors – they are described next.

2172 **The Scan Structure**

2173 A Scan object is a collection of reactors made from scanning a list of temperatures.
2174 For example, a scan of five temperatures from 5 keV to 25 keV would result in several
2175 arrays of five reactors. Most often, one of these lists would correspond to beta reactors,
2176 one to kink reactors, and one to wall loading reactors. There may then be fewer than
2177 five reactors in a list if some of the reactors are invalid or fundamentally unsolvable.
2178 This is the data structure that produces the various comparison plots in the results.

2179 **The Sensitivity Structure**

2180 Sensitivity studies are how computationalists test the effect of changing a variable
2181 over multiple values – i.e. do a 20% sensitivity around the H factor. Like Scans,
2182 Sensitivities store various lists of reactors, each corresponding to an interesting data
2183 point. These include limit reactors where the beta limit and kink limit are just

2184 satisfied or when the beta limit and wall loading are just satisfied. Additionally, they
2185 include the minimum capital cost reactors and the minimum cost-per-watt ones.

2186 **The Sampling Structure**

2187 The Sampling struct was created to do simple Monte Carlo runs over a reactor's
2188 ~~static~~~~fixed~~ values. While sensitivities only allow one variable to change at a time,
2189 samplings randomly assign a list of variables to some neighborhood of possible values.
2190 These are how the scatter plots are made. Succinctly, where sensitivity studies show
2191 local changes to variables, Monte Carlo samplings show global trends in reactor design.

2192 **The Equation Structure**

2193 In order to store the various equations from Table 5.1 is the Equation Struct. It stores
2194 the γ exponents for: R_0 , B_0 , and I_P . – as well as the function representing $G(\bar{T})$.
2195 Repeated these are the unknowns in:

$$R_0^{\gamma_R} \cdot B_0^{\gamma_B} \cdot I_P^{\gamma_I} = G(\bar{T}) \quad (5.2)$$

2196 Concretely, there are 16 objects that use this struct – one for each equation (e.g. for
2197 fusion power, the beta limit, and temperature assignment).

2198 **The Equation Set Structure**

2199 The step up from the Equation struct are the Equation Sets. These collections of
2200 three equations allow R_0 , B_0 , and maybe I_P to be substituted out of the current
2201 balance root-solving equation. This is where Eqs. (5.3) to (5.9) come into play.

2202 B.2.2 Referencing Input Decks and Solutions

2203 With more than twenty ~~static~~~~fixed~~ variables in the model, the range of tokamak
2204 reactors is basically infinite. To help users build a net of designs to explore reactor
2205 space are seven input decks. These are the ones given in the results: Arc, Act I
2206 /II, Demo Steady/Pulsed, Proteus and Charybdis. Coupled with the non-prototype
2207 reactors are solution reactors that store various quantities from the original papers
2208 (e.g. P_F , f_{BS} , R_0). These are how the comparison tables were constructed.

2209 B.2.3 Acknowledging Utility Functions

2210 For the uninitiated, utility functions are grab bag functions that do not really belong
2211 in a codebase – but do anyway. This sentiment does not mean they are worthless,
2212 just not fusion related at all. In Fussy.jl, the most notable are a normalized integral
2213 calculator, a filter that includes numeric tolerances, and a robust root solver.

2214 Although since incorporated into the official Roots.jl package, `find_roots` allows
2215 finding an arbitrary number of roots within a bounded range. This was needed
2216 because many roots can be found at various levels of the reactor solving problem –
2217 i.e. for I_P , \bar{T} , η_{CD} , etc.

2218 B.2.4 Mentioning Base Level Files

2219 In addition to subdirectories within the `src` folder are three files: Fussy.jl, abstracts.jl,
2220 and defaults.jl. Fussy.jl is the package’s main file that actually stores the Fussy
2221 module. While, abstracts.jl stores various abstract structures that help clean up
2222 other files.

2223 Finally, defaults.jl stores various default values that are important to the codebase.
2224 For example, this is where the various scaling law exponents are stored. It is also
2225 where the bounding values for the different root solving problems live. These include
2226 minimum and maximum values for: I_P , \bar{T} , η_{CD} .

2227 Now that a majority of the files have been discussed, we can turn to the reactor
2228 methods. These constitute most of the interesting functionality within the codebase.

2229 B.3 Delving into Reactor Methods

2230 The reactor is the most atomic data structure in this model. It therefore makes
2231 sense that it has many instance methods. These include all the coefficients, fluxes,
2232 powers, etc. It also includes methods that solve a reactor, perform a match on some
2233 field's value, or converge η_{CD} to self-consistency. The various subdirectories within
2234 the `src/methods/reactors` folder will now be discussed.

2235 Calculations

2236 The calculation subdirectory of reactor methods are used to set various important
2237 values in the solver. For ~~dynamicfloating~~ variables, these include: \bar{n} , R_0 , B_0 , and
2238 I_P . This folder also includes the calculation of the Bosch-Hale reactivity and the
2239 Ehst-Karney current drive efficiency.

2240 Coefficients and Composites

2241 The coefficients and composites directories correspond to the model's ~~staticfixed~~ and
2242 ~~dynamicfloating~~ coefficients, respectively. For clarity, ~~staticfixed~~ coefficients, includ-
2243 ing K_n and K_{CD} , were labeled with a K. Whereas, ~~dynamicfloating~~ coefficients then
2244 started with G's – i.e. G_{PB} and G_V .

2245 Fluxes and Powers

2246 Within flux balance and power balance were around a dozen terms or sub-terms.
2247 Although not directly used in the conservation equations, sub-terms are used to com-
2248 pare the model to ones from the literature. For clarity, fluxes include: Φ_{CS} , Φ_{PF} ,
2249 Φ_{RU} , Φ_{FT} , Φ_{res} , and Φ_{ind} . The powers, then, include: P_F , P_{BR} , P_κ , P_L , P_W , etc.

2250 Profiles

2251 The next collection of reactor methods are the various profiles. Most obviously, these
2252 include radial plasma profiles for density, temperature, and current. However, this
2253 folder also includes the magnetic field strength as a function of radius – as was used
2254 within current drive efficiency calculations.

2255 Geometries

2256 Additionally, there are many geometric relations. These include the various tokamak
2257 thicknesses: a, b, c, d – as well as the radius and height of the central solenoid. This
2258 group also includes the volume, perimeter, surface area, and cross-sectional area. It
2259 also includes the many subscripted fields. For example, the elongation (i.e. κ_{95})
2260 includes the following alternative definitions: κ_X , κ_P , and κ_T

2261 Formulas

2262 The final set of reactor methods are formulas that do not really fit anywhere else.
2263 If a method is not related to geometry, power, calculations, etc, it ends up here.
2264 For example, this group includes: β_N , f_{BS} , C_W , and τ_E . Total, there are around 25
2265 formulas – as of the writing of this document.

2266 B.4 Demonstrating Code Usage

2267 Now that the Fussy.jl package has been described in detail, the final step is showing a
2268 simple example that can recreate a figure from the results chapter. This will closely
2269 match the Jupyter notebook available at:

2270 www.git.io/fussy_sensitivity

2271 Our goal will be to make a cost curve for the ARC reactor as a function of H – a so
2272 called sensitivity study plot.

2273 B.4.1 Initializing the Workspace

2274 The first step for any Fussy.jl Jupyter notebook is loading the required packages – i.e.
2275 the Fussy.jl and Plots.jl packages. This can be done using the following commands:

```
2276     addprocs(6)
2277
2278     @everywhere using Fussy
2279     using Plots
```

2280 The Plots.jl package may take a minute to load – similar to Matlab’s initial boot
2281 time. If the kernel raises an error about Plots.jl not being installed, use the following
2282 lines:

```
2283     import Pkg
2284     Pkg.add("Plots")
```

2285 B.4.2 Running a Study

2286 Now that the necessary packages have been loaded, we can move on to actually
2287 running the sensitivity study. We will split this command into two steps to make it
2288 more explicit.

2289 The first step will be making several variables that store: boolean flags, numbers, and
2290 symbols – which are like strings, but prefaced with a colon (:) instead of surrounded
2291 by double quotes (").

```
2292     cur_param = :H
2293     cur_deck = :arc
2294     is_pulsed = false
2295     is_consistent = true
2296     cur_sensitivity = 1.0
```

*The `addprocs` and `@everywhere` commands are to parallelize the code. This is because `addprocs(6)` activates 6 worker processes and `@everywhere Fussy.jl` adds Fussy.jl to the main kernel and worker processes.

2297 `cur_num_points = 41`

2298 These six variables almost completely describe a sensitivity study. The first two
2299 saw we are using the Arc reactor deck and running a sensitivity over the H-factor
2300 parameter. Next, the two boolean values refer to the reactor (1) being treated as
2301 pulsed or steady-state and (2) whether to handle η_{CD} self-consistently.* Ergo, what
2302 these two flags do is make sure ARC is being handled as a steady-state reactor with
2303 a self-consistent η_{CD} . The last two variables are then ways to change the sensitivity
2304 of the study (with 1.0 \rightarrow 100%) and the number of reactors it will produce (i.e. 41).
2305 Now all six of these variables can be piped into a call to the **Study** struct to start
2306 running the sensitivity study:

```
2307     cur_study = Study(  
2308         cur_param,  
2309         deck = cur_deck,  
2310         is_pulsed = is_pulsed,  
2311         is_consistent = is_consistent,  
2312         sensitivity = cur_sensitivity,  
2313         num_points = cur_num_points  
2314     )
```

2315 Note here that the equal signs inside the parentheses are called keyword arguments,
2316 which are common to most modern programming languages. After executing the
2317 command, the code will need to run for a few minutes.

2318 B.4.3 Extracting Results

2319 At this point, a user should have a completed sensitivity study they wish to plot.
2320 To make the plot useful, the study data structure first has to be unpacked and its
2321 contents cleaned. This is the goal of this subsection.

2322 First and foremost, a study has four families of reactors within it: beta-wall (i.e.

*Note that, currently, a pulsed reactor cannot be self-consistent in η_{CD} – it therefore causes an error.

2323 "wall"), beta-kink (i.e. "kink"), minimum capital cost (i.e. "W_M"), and minimum
2324 cost-per-watt (i.e. "cost"). Therefore, we will extract these reactor lists into a new
2325 dictionary data structure:

```
2326     cur_dict = Dict()  
2327  
2328     cur_dict["Beta-Wall"] = cur_study.wall_reactors  
2329     cur_dict["Beta-Kink"] = cur_study.kink_reactors  
2330  
2331     cur_dict["Min Cost per Watt"] = cur_study.cost_reactors  
2332     cur_dict["Min Capital Cost"] = cur_study.W_M_reactors
```

2333 Next, we will want to filter out all the invalid reactors that constitute non-physically
2334 realizable ones. These would likely be reactors that could fit in your hand or take up
2335 a whole city block.

```
2336     for (cur_key, cur_value) in cur_dict  
2337         cur_dict[cur_key] = filter(  
2338             cur_reactor -> cur_reactor.is_valid,  
2339             deepcopy(cur_value)  
2340         )  
2341     end
```

2342 B.4.4 Plotting Curves

2343 Our goal is now to turn our unpacked, clean reactor lists into plots – i.e. measuring
2344 costs-per-watt as a function of H. For simplicity, this will lack a lot of the features
2345 shown in the Jupyter notebook from the beginning of the section. Additionally, we
2346 will be doing it in an iterative process made possible by the Plots.jl framework.

2347 The first step is simply making a plot object

```
2348     cur_plot = plot()
```

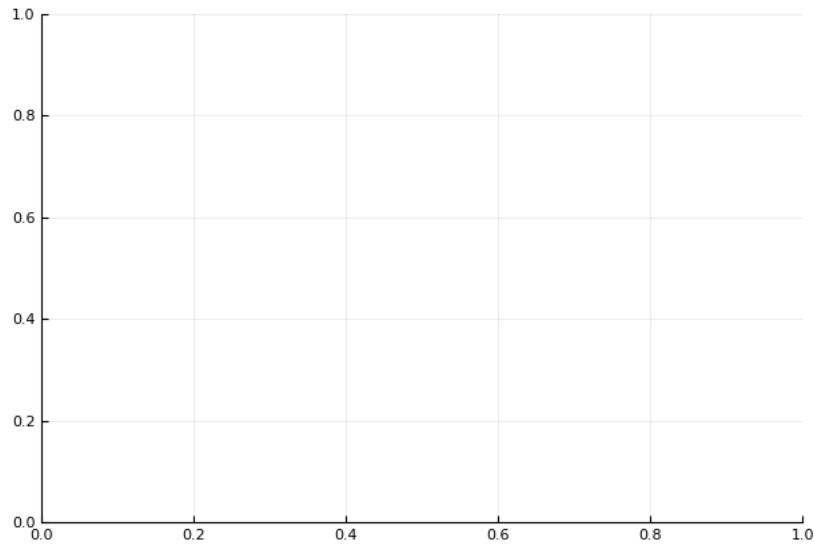


Figure B-1: A Blank Plot

A simple 2-D plot with no labels or data.

2349 After execution, this should produce the plank 2-D plot shown in Fig. B-1.

2350 Next we will add a simple title and labels for the axes:

```
2351     title!("Arc")
```

```
2352
```

```
2353     xlabel!("H")
```

```
2354     ylabel!("Cost")
```

2355 The exclamation marks ensure this title and the labels are added to the `cur_plot`.

2356 Upon execution, you should see a plot with this information (Fig. B-2).

2357 Now we will loop over the dictionary of reactors and add them one at a time.

```
2358     for (cur_key, cur_value) in cur_dict
```

```
2359         cur_x = map(cur_reactor -> cur_reactor.H, cur_value)
```

```
2360         cur_y = map(cur_reactor -> cur_reactor.cost, cur_value)
```

```
2361         plot!(cur_x, cur_y, label=cur_key)
```

```
2362     end
```

```
2363     plot!()
```

2364 This results in the not very useful plot shown in Fig. B-3. Note that each label is

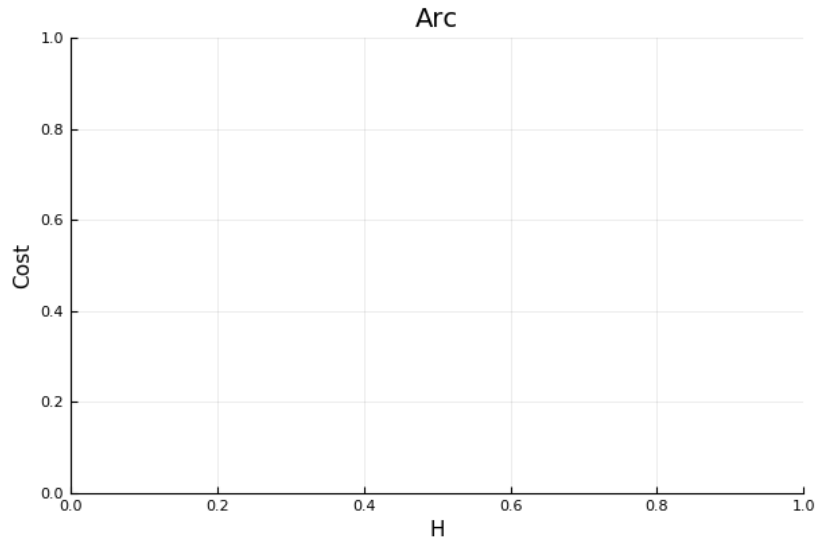


Figure B-2: An Empty Plot

A simple 2-D plot with labels, but no data.

2365 exactly the key assigned to it in `cur_dict`.

2366 The final step is adding proper limits to make what is going on obvious to the reader:

2367 `ylims!(0, 0.03)`

2368 The addition of which can be seen in Fig. B-4.

2369 This completes the example. At this point, you should now be able to use every
2370 feature of `Fussy.jl`. Good luck!

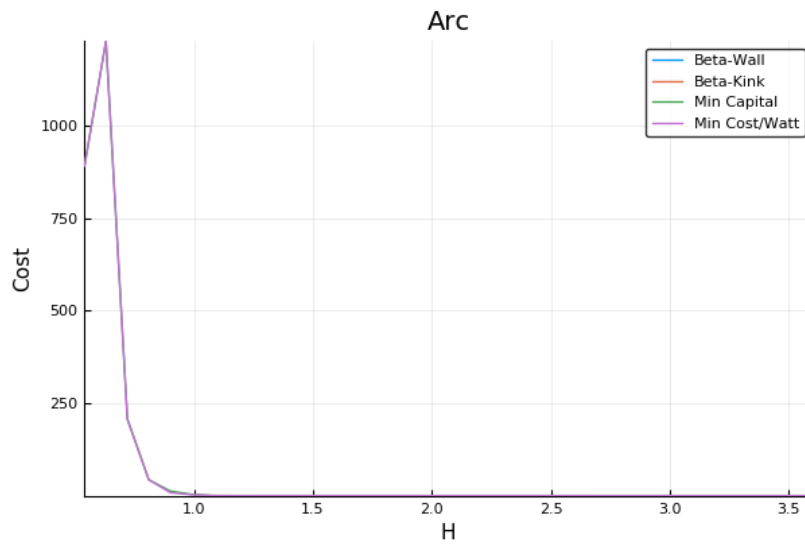


Figure B-3: An Unscaled Plot

A simple 2-D plot with Bad Limits.

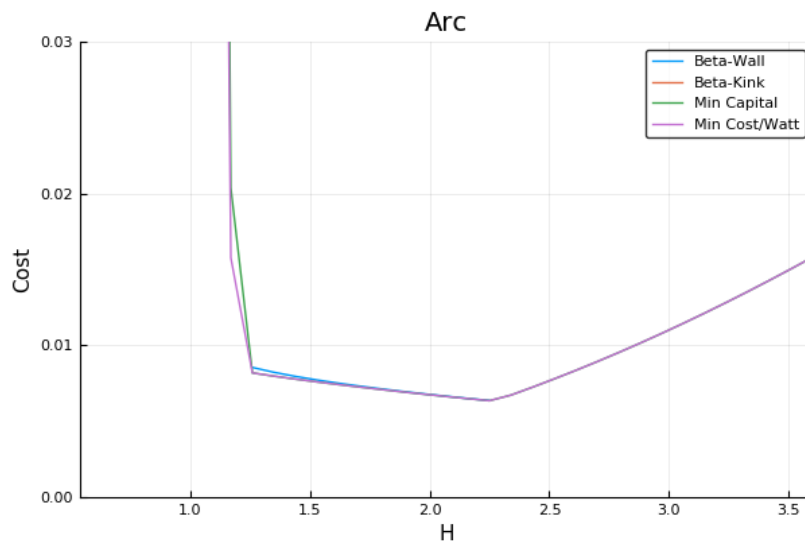


Figure B-4: A Scaled Plot

An example plot showing cost as a function of the H factor.

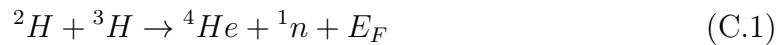
2371 Appendix C

2372 Discussing Fusion Power

2373 C.1 Fusion Power – P_F

2374 This requires a more first-principles approach than those used up until now. As such,
2375 a quick background is given to motivate the parameters it adds – i.e. the dilution
2376 factor (f_D) and the Bosch-Hale fusion reactivity (σv).

2377 The natural place to start when talking about fusion is the binding-energy per nucleon
2378 plot (see Fig. C-1). As can be seen, the function reaches a maximum value around the
2379 element Iron (A=56). What this means at a basic level is: elements lighter than iron
2380 can *fuse* into a heavier one (i.e. hydrogens into helium), whereas heavier elements
2381 can *fission* into lighter ones (e.g. uranium into krypton and barium). This is what
2382 differentiates fission (uranium-fueled) reactors from fusion (hydrogen-fueled) ones.
2383 For fusion reactors, the most common reaction in a first-generation tokamak will be:



2384

$$E_F = 17.6 \text{ MeV} \quad (\text{C.2})$$

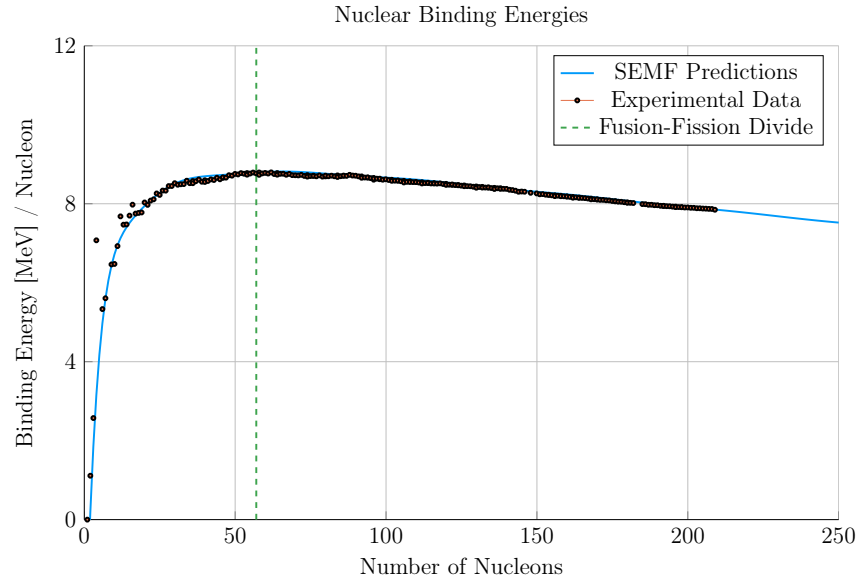


Figure C-1: Comparing Nuclear Fusion and Fission

The binding energy per nucleon is what differentiates nuclear fusion from fission. Nuclei heavier than Iron fission (e.g. Uranium), while light ones – such as Hydrogen – fuse.

2385 What this reaction describes is two isotopes of hydrogen – i.e. deuterium and tritium
 2386 – fusing into a heavier element, helium, while simultaneously ejecting a neutron. The
 2387 entire energy of the fusion reaction (E_F) is then divvied up 80-20 between the neutron
 2388 and helium, respectively. Quantitatively, the helium (hereafter referred to as an alpha
 2389 particle) receives 3.5 MeV.

2390 The final point to make before returning to the fusion power derivation is the main
 2391 difference between the two fusion products: helium (i.e. the alpha particle) and the
 2392 neutron. First, neutrons lack a charge – they are neutral. This means they cannot
 2393 be confined with magnetic fields. As such, they simply move in straight lines until
 2394 they collide with other particles. As the structure of a tokamak is mainly metal, the
 2395 neutron is much more likely to collide there than the gaseous plasma, which is orders
 2396 of magnitude less dense. Conversely, alpha particles are charged – when stripped of
 2397 their electrons – and can therefore be kept within the plasma using magnets. What
 2398 this means practically is that of the 17.6 MeV that comes from every fusion reaction,
 2399 only 3.5 MeV remains inside the plasma (within the helium particle species).

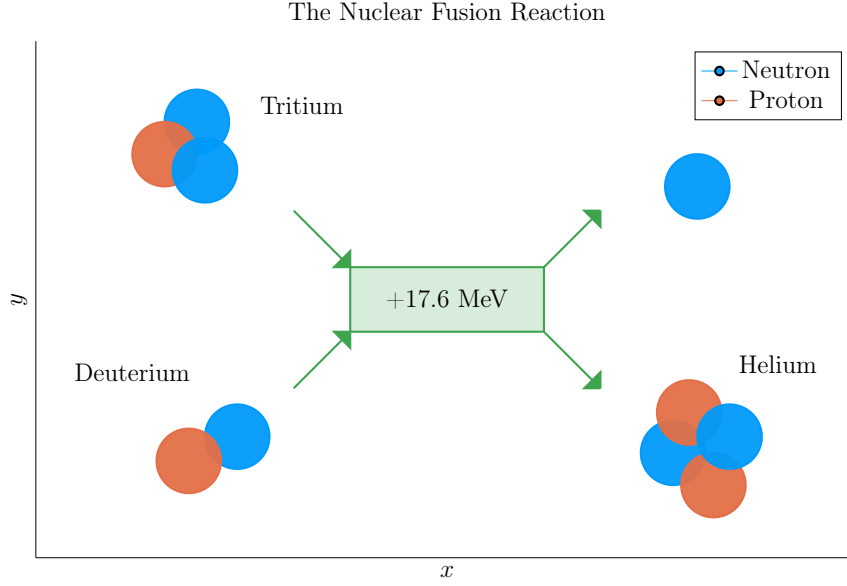


Figure C-2: The D-T Fusion Reaction

In a first generation tokamak reactor, the main source of energy will come from two hydrogen isotopes fusing into a helium particle – and ejecting a 14.1 MeV neutron.

As mentioned before, this fusion power is divided up 80-20 between the neutron and alpha particle. These relations will be used shortly. For now, they can be described mathematically as:

$$P_{\alpha} = 0.2 \cdot P_F \quad (\text{C.3})$$

$$P_n = 0.8 \cdot P_F \quad (\text{C.4})$$

C.2 Reactivity – $\langle \sigma v \rangle$

When discussing reactivity, the place to start is talking about fusion power,

$$P_F = \int E_F n_D n_T \langle \sigma v \rangle d\mathbf{r} \quad (\text{C.5})$$

For the tokamak geometry given, volume integrals can be reduced to 0-D forms.

2408 An arbitrary $F(\rho)$ has that:

$$F_V = 4 \pi^2 R_0 a^2 \kappa g \int_0^1 F(\rho) \rho d\rho \quad (\text{C.6})$$

2409 Given that $E_F = 17.6$ MeV and,

$$n_D = n_T = f_D \frac{n_e}{2} = \frac{f_D}{2} \cdot (\bar{n} (1 + \nu_n) (1 - \rho^2)^{\nu_n}) \quad (\text{C.7})$$

2410 Fusion power can be expressed as,

$$P_F = K_F \cdot (\bar{n}^2 R_0^3) \cdot (\sigma v) \quad [MW] \quad (\text{C.8})$$

2411

$$(\sigma v) = 10^{21} (1 + \nu_n)^2 \int_0^1 (1 - \rho^2)^{2\nu_n} \langle \sigma v \rangle \rho d\rho \quad (\text{C.9})$$

2412

$$K_F = 278.3 (f_D^2 \epsilon^2 \kappa g) \quad (\text{C.10})$$

2413 The Bosch-Hale parametrization of the volumetric reaction rates is then given by,^{28,29}

$$\langle \sigma v \rangle = C_1 \cdot \theta \cdot \exp(-3\xi) \cdot \sqrt{\frac{\xi}{m_\mu c^2 T^3}} \quad [\text{m}^3/\text{s}] \quad (\text{C.11})$$

2414

$$\theta = T \cdot \left(1 - \frac{T(C_2 + T(C_4 + TC_6))}{1 + T(C_3 + T(C_5 + TC_7))} \right)^{-1} \quad (\text{C.12})$$

2415

$$\xi = \left(\frac{B_G^2}{4\theta} \right)^{1/3} \quad (\text{C.13})$$

2416 Where approximate DT volumetric reaction rate ($10 \lesssim T \text{ [keV]} \lesssim 20$)

$$\langle \sigma v \rangle_{\text{DT}} = 1.1 \times 10^{-24} \cdot T^2 \quad [\text{m}^3/\text{s}] \quad (\text{C.14})$$

2417 In our model, each appearance of T is set to the profile defined earlier.

Bosch-Hale parametrization coefficients for volumetric reaction rates

	${}^2\text{H}(\text{d,n}){}^3\text{He}$	${}^2\text{H}(\text{d,p}){}^3\text{H}$	${}^3\text{H}(\text{d,n}){}^4\text{He}$	${}^3\text{He}(\text{d,p}){}^4\text{He}$
B_G [keV $^{1/2}$]	31.3970	31.3970	34.3827	68.7508
$m_\mu c^2$ [keV]	937 814	937 814	1 124 656	1 124 572
C_1	5.43360×10^{-12}	5.65718×10^{-12}	1.17302×10^{-9}	5.51036×10^{-10}
C_2	5.85778×10^{-3}	3.41267×10^{-3}	1.51361×10^{-2}	6.41918×10^{-3}
C_3	7.68222×10^{-3}	1.99167×10^{-3}	7.51886×10^{-2}	-2.02896×10^{-3}
C_4	0.0	0.0	4.60643×10^{-3}	-1.91080×10^{-5}
C_5	-2.96400×10^{-6}	1.05060×10^{-5}	1.35000×10^{-2}	1.35776×10^{-4}
C_6	0.0	0.0	-1.06750×10^{-4}	0.0
C_7	0.0	0.0	1.36600×10^{-5}	0.0
Valid range (keV)	$0.2 < T_i < 100$	$0.2 < T_i < 100$	$0.2 < T_i < 100$	$0.5 < T_i < 190$

 Tabulated Bosch-Hale reaction rates [m 3 s $^{-1}$]

T (keV)	${}^2\text{H}(\text{d,n}){}^3\text{He}$	${}^2\text{H}(\text{d,p}){}^3\text{H}$	${}^3\text{H}(\text{d,n}){}^4\text{He}$	${}^3\text{He}(\text{d,p}){}^4\text{He}$
1.0	9.933×10^{-29}	1.017×10^{-28}	6.857×10^{-27}	3.057×10^{-32}
1.5	8.284×10^{-28}	8.431×10^{-28}	6.923×10^{-26}	1.317×10^{-30}
2.0	3.110×10^{-27}	3.150×10^{-27}	2.977×10^{-25}	1.399×10^{-29}
3.0	1.602×10^{-26}	1.608×10^{-26}	1.867×10^{-24}	2.676×10^{-28}
4.0	4.447×10^{-26}	4.428×10^{-26}	5.974×10^{-24}	1.710×10^{-27}
5.0	9.128×10^{-26}	9.024×10^{-26}	1.366×10^{-23}	6.377×10^{-27}
8.0	3.457×10^{-25}	3.354×10^{-25}	6.222×10^{-23}	7.504×10^{-26}
10.0	6.023×10^{-25}	5.781×10^{-25}	1.136×10^{-22}	2.126×10^{-25}
12.0	9.175×10^{-25}	8.723×10^{-25}	1.747×10^{-22}	4.715×10^{-25}
15.0	1.481×10^{-24}	1.390×10^{-24}	2.740×10^{-22}	1.175×10^{-24}
20.0	2.603×10^{-24}	2.399×10^{-24}	4.330×10^{-22}	3.482×10^{-24}

Appendix D

Selecting Plasma Profiles

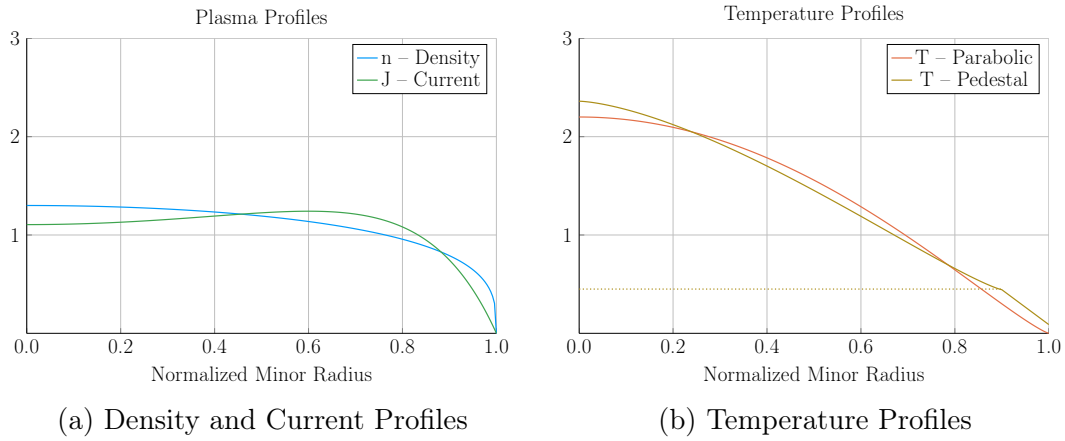


Figure D-1: Radial Plasma Profiles

The three most fundamental properties of a fusion plasma are its temperature, density, and current. These profiles allow the model to reduce from three dimensions to half of one.

D.1 Density – n

The Density is important to us. We use it in the Greenwald density limit, so it should be clean in both line-averaged and volume-averaged forms. Because of its flat profile, a parabola is a good approximation for H-mode pulses:

$$n(\rho) = \bar{n} \cdot (1 + \nu_n) \cdot (1 - \rho^2)^{\nu_n} \quad (\text{D.1})$$

2424 The line average density is related to \bar{n} through:

$$\hat{n} = \bar{n} \cdot \left(\frac{\pi^{1/2}}{2} \right) \cdot \frac{\Gamma(\nu_n + 2)}{\Gamma(\nu_n + 3/2)} \quad (\text{D.2})$$

2425 The convenience of this function comes from how the volumetric average comes out.

2426 To relate this to the volume integral, we use:

$$\bar{x} = \frac{1}{V} \int x(\rho) dV \quad (\text{D.3})$$

2427 For a normalized radial profile that does not depend on angle,

$$V = \int_0^1 \rho d\rho = 1/2 \quad (\text{D.4})$$

2428 Then, when $x = n$,

$$\bar{n} = 2 \int_0^1 n(\rho) \rho d\rho = \bar{n} \quad (\text{D.5})$$

2429 Additionally, the Greenwald Density limit that we will use throughout,

$$\hat{n} = N_G \cdot \left(\frac{I_M}{\pi a^2} \right) \quad (\text{D.6})$$

2430 can now be written in the following form:

$$\bar{n} = K_n \cdot \left(\frac{I_M}{R_0^2} \right) \quad (\text{D.7})$$

2431

$$K_n = \frac{2 N_G}{\epsilon^2 \pi^{3/2}} \cdot \left(\frac{\Gamma(\nu_n + 3/2)}{\Gamma(\nu_n + 2)} \right) \quad (\text{D.8})$$

2432 D.2 Temperature – T

2433 The Temperature is the swept variable in our model framework. Therefore, it's the
 2434 one we can allow people to be the most cavalier with. Additionally, as temperature
 2435 profiles are highly peaked, their pedestal region is sometimes wrongfully neglected
 2436 with a parabola.

$$T(\rho) = \bar{T} \cdot (1 + \nu_T) \cdot (1 - \rho^2)^{\nu_T} \quad (\text{D.9})$$

2437 Therefore, our model sometimes treats the system as if it had a pedestal region. This
 2438 is mainly for the bootstrap current and fusion power, which were previously known
 2439 to misalign and overshoot, respectively.

$$T(\rho) = \begin{cases} T_{para} , & x \in [0, \rho_{ped}] \\ T_{line} , & x \in (\rho_{ped}, 1] \end{cases} \quad (\text{D.10})$$

2440 Where the piecewise functions are given by,

$$T_{para} = T_{ped} + (T_0 - T_{ped}) \cdot \left(1 - \left(\frac{\rho}{\rho_{ped}} \right)^{\lambda_T} \right)^{\nu_T} \quad (\text{D.11})$$

2441

$$T_{line} = T_{sep} + (T_{ped} - T_{sep}) \cdot \left(\frac{1 - \rho}{1 - \rho_{ped}} \right) \quad (\text{D.12})$$

2442 This temperature profile is related to the volume-averaged temperature through,

$$\bar{T} \cdot V = \int_0^{\rho_{ped}} T_{para}(\rho) \rho d\rho + \int_{\rho_{ped}}^1 T_{line}(\rho) \rho d\rho \quad (\text{D.13})$$

2443 Starting with the second integral,

$$\int_{\rho_{ped}}^1 T_{line}(\rho) \rho d\rho = \frac{1}{3} \cdot (1 - \rho_{ped}) \cdot ((T_{sep} + T_{ped}/2) + \rho_{ped} \cdot (T_{ped} + T_{sep}/2)) \quad (D.14)$$

The first integral can be handled by breaking it into to,

$$\begin{aligned} \int_0^{\rho_{ped}} T_{para}(\rho) \rho d\rho &= T_{ped} \cdot \int_0^{\rho_{ped}} \rho d\rho + \\ &\quad (T_0 - T_{ped}) \cdot \int_0^{\rho_{ped}} \left(1 - \left(\frac{\rho}{\rho_{ped}}\right)^{\lambda_T}\right)^{\nu_T} \cdot \rho d\rho \end{aligned} \quad (D.15)$$

2444 The first sub-integral is then,

$$T_{ped} \cdot \int_0^{\rho_{ped}} \rho d\rho = \frac{T_{ped} \rho_{ped}^2}{2} \quad (D.16)$$

2445 Utilizing the following transformation,

$$u = \frac{\rho}{\rho_{ped}} \quad (D.17)$$

$$2446 \quad d\rho = \rho_{ped} du \quad (D.18)$$

$$2447 \quad u(\rho = \rho_{ped}) = 1 \quad (D.19)$$

2448 The second sub-integral becomes (assuming independence from T_0 and T_{ped}),

$$(T_0 - T_{ped}) \cdot \rho_{ped}^2 \cdot \int_0^1 (1 - u^{\lambda_T})^{\nu_T} \cdot u du \quad (D.20)$$

2449 Where:

$$\int_0^1 (1 - u^{\lambda_T})^{\nu_T} \cdot u du = \frac{\Gamma(1 + \nu_T) \Gamma\left(\frac{2}{\lambda_T}\right)}{\lambda_T \cdot \Gamma\left(1 + \nu_T + \frac{2}{\lambda_T}\right)} \quad (D.21)$$

2450 We are now in a position to solve for T_0 in terms of \bar{T} :

$$T_0 = T_{ped} + \frac{\bar{T} - K_{TU}}{K_{TD}} \quad (D.22)$$

2451

$$K_{TU} = T_{ped} \rho_{ped}^2 + \frac{(1 - \rho_{ped})}{3} \cdot ((2T_{sep} + T_{ped}) + \rho_{ped} \cdot (2T_{ped} + T_{sep})) \quad (D.23)$$

2452

$$K_{TD} = \rho_{ped}^2 \cdot \left(\frac{2}{\lambda_T} \right) \cdot \frac{\Gamma(1 + \nu_T) \Gamma\left(\frac{2}{\lambda_T}\right)}{\Gamma\left(1 + \nu_T + \frac{2}{\lambda_T}\right)} \quad (D.24)$$

2453 Which although not pretty, can be plugged into the original equation.

2454 D.3 Pressure – p

2455 The first point to make is that we are not using the same temperature profile for
 2456 the pressure as for the temperature. This is because it would lead to hypergeometric
 2457 functions that are not worth the headache.

2458 As most of the pressure is at the center, we use simple parabolic profile. This leads
 2459 to:

$$\bar{p} = 0.1581 (1 + f_D) \frac{(1 + \nu_n)(1 + \nu_T)}{1 + \nu_n + \nu_T} \bar{n} \bar{T} \quad [atm] \quad (D.25)$$

2460 D.4 Bootstrap Current – f_{BS}

2461 We start with,

$$f_{BS} = \frac{I_{BS}}{I_P} = \frac{2\pi a^2 \kappa}{I_P} \int_0^1 J_B \rho d\rho \quad (D.26)$$

2462 Expanding the previous equation using the following relations,

$$J_B = -4.85 \cdot R_0 \epsilon^{1/2} \cdot \left(\frac{\rho^{1/2} n T}{d\psi/d\rho} \right) \cdot \left(\frac{dn/d\rho}{n} + 0.54 \cdot \frac{dT/d\rho}{T} \right) \quad (D.27)$$

2463

$$\frac{d\psi}{d\rho} = \frac{\mu_0 R_0 I_P}{\pi} \cdot \left(\frac{\kappa}{1 + \kappa^2} \right) \cdot b_p(\rho) \quad (D.28)$$

2464 Yields:

$$f_{BS} = -K_{BS} \int_0^1 (1 - \rho^2)^{\nu_n} \cdot \left(\frac{\rho^{3/2}}{b_p(\rho)} \right) \cdot \left(\frac{T}{n} \cdot \frac{dn}{d\rho} + 0.54 \cdot \frac{dT}{d\rho} \right) d\rho \quad (D.29)$$

2465

$$K_{BS} = K_n \cdot \left(\frac{2\pi^2 \cdot 4.85 \cdot \epsilon^{5/2}}{\mu_0} \right) \cdot (1 + \nu_n) \cdot (1 + \kappa^2) \quad (D.30)$$

2466 Here, b_p comes from:

$$b_p(\rho) = \frac{-e^{\gamma\rho^2}(\gamma\rho^2 - 1 - \gamma) - 1 - \gamma}{\rho(e^\gamma - 1 - \gamma)} \quad (D.31)$$

2467 And the value of γ comes from the the normalized internal inductance:

$$l_i = \frac{4\kappa}{1 + \kappa^2} \int_0^1 b_p^2 \frac{d\rho}{\rho} \quad (D.32)$$

2468 With our profiles,

$$- \left(\frac{T}{n} \cdot \frac{dn}{d\rho} \right) = 2\nu_n \cdot \left(\frac{T \cdot \rho}{1 - \rho^2} \right) \quad (D.33)$$

2469 While treating temperature differently results in,

$$- \left(\frac{dT}{d\rho} \right)_{para} = \left(\frac{T_0 - T_{ped}}{\rho_{ped}^{\lambda_T}} \right) \cdot (\nu_T \lambda_T) \cdot \rho^{\lambda_T - 1} \cdot \left(1 - \left(\frac{\rho}{\rho_{ped}} \right)^{\lambda_T} \right)^{\nu_T - 1} \quad (D.34)$$

2470

$$- \left(\frac{dT}{d\rho} \right)_{line} = \left(\frac{T_{ped} - T_{sep}}{1 - \rho_{ped}} \right) \quad (D.35)$$

2471 Where we will be using the new symbol definition,

$$\partial T = - \left(\frac{dT}{d\rho} \right) \quad (D.36)$$

Which ultimately allows us to write,

$$f_{BS} = K_{BS} \int_0^1 H_{BS} d\rho \quad (D.37)$$

$$H_{BS} = (1 - \rho^2)^{\nu_n - 1} \cdot \left(\frac{\rho^{3/2}}{b_p(\rho)} \right) \cdot \left(2\nu_n \cdot \rho \cdot T + 0.54 \cdot (1 - \rho^2) \cdot \partial T \right) \quad (D.38)$$

2472 Where the values of T are determined through,

$$T_{para} = T_{ped} + (T_0 - T_{ped}) \cdot \left(1 - \left(\frac{\rho}{\rho_{ped}} \right)^{\lambda_T} \right)^{\nu_T} \quad (D.39)$$

2473

$$T_{line} = T_{sep} + (T_{ped} - T_{sep}) \cdot \left(\frac{1 - \rho}{1 - \rho_{ped}} \right) \quad (D.40)$$

2474 And the values of ∂T are:

$$\partial T_{para} = \left(\frac{T_0 - T_{ped}}{\rho_{ped}^{\lambda_T}} \right) \cdot (\nu_T \lambda_T) \cdot \rho^{\lambda_T - 1} \cdot \left(1 - \left(\frac{\rho}{\rho_{ped}} \right)^{\lambda_T} \right)^{\nu_T - 1} \quad (D.41)$$

2475

$$\partial T_{line} = \left(\frac{T_{ped} - T_{sep}}{1 - \rho_{ped}} \right) \quad (D.42)$$

2476 D.5 Volume Averaged Powers

2477 The first thing to consider in a fusion reactor is power balance.

2478 It is what separates a profitable device from a toaster. It's given by:

$$P_\alpha + P_H = P_\kappa + P_B \quad (D.43)$$

2479

$$P_\alpha = \frac{P_F}{5} \quad (\text{D.44})$$

2480

$$P_H = \frac{P_F}{Q} \quad (\text{D.45})$$

2481

$$P_\kappa = \frac{3}{2\tau_E} \int p \, d\mathbf{r} \quad [3D] \quad (\text{D.46})$$

2482

$$P_B = 5.35e3 \, Z_{eff} \int n_{\bar{n}}^2 \sqrt{T} \, d\mathbf{r} \quad [3D] \quad (\text{D.47})$$

2483 As mentioned before, P_F is handled by (σv) and therefore the lefthand-side uses the
 2484 pedestal temperature profiles. However, for the same reasons as discussed earlier, the
 2485 righthand-side (P_κ and P_B) need to use the parabolic temperature profiles.

2486 Using the parabolic profiles (for n and T) gives for the Bremsstrahlung radiation,

$$P_B = K_B \cdot \left(R_0^3 \bar{n}^2 \sqrt{\bar{T}} \right) \quad [MW] \quad (\text{D.48})$$

2487

$$K_B = 0.1056 \cdot Z_{eff} \cdot (\epsilon^2 \kappa g) \cdot \frac{(1 + \nu_n)^2 (1 + \nu_T)^{1/2}}{1 + 2\nu_n + 0.5\nu_T} \quad (\text{D.49})$$

2488 And a similar exercise for the thermal conduction losses results in:

$$P_\kappa = K_\kappa \cdot \left(\frac{R_0^3 \bar{n} \bar{T}}{\tau_E} \right) \quad [MW] \quad (\text{D.50})$$

2489

$$K_\kappa = 0.4744 \cdot (1 + f_D) \cdot (\epsilon^2 \kappa g) \cdot \frac{(1 + \nu_n)(1 + \nu_T)}{1 + \nu_n + \nu_T} \quad (\text{D.51})$$

2490 Appendix E

2491 Determining Plasma Flux Surfaces

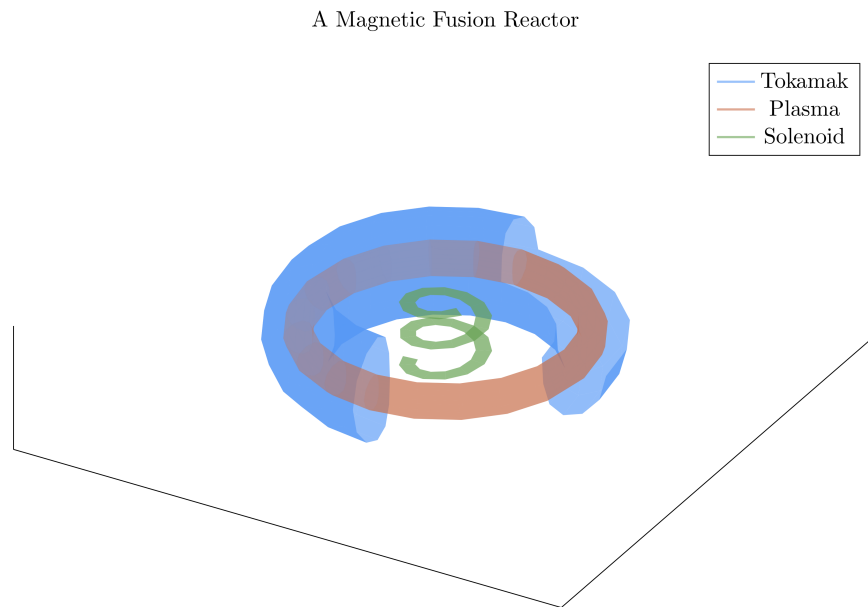


Figure E-1: Cut-Away of Tokamak Reactor

The three main components of a magnetic fusion reactor are: the tokamak structure, the plasma fuel, and the spring-like solenoid at the center.

2492 E.1 Flux Surface Coordinates

2493 We begin with the shape of the outer plasma surface (i.e. the 95% flux surface)
2494 written in terms of normalized coordinates x and y as follows – with α being an

2495 angle-like coordinate:

$$R = R_0 + ax(\alpha) \quad (E.1)$$

2496

$$Z = ay(\alpha) \quad (E.2)$$

2497

$$0 \leq \alpha \leq 2\pi \quad (E.3)$$

2498 The surface representation can now be written as:

$$x(\alpha) = c_0 + c_1 \cos(\alpha) + c_2 \cos(2\alpha) + c_3 \cos(3\alpha) \quad (E.4)$$

2499

$$y(\alpha) = \kappa \sin(\alpha) \quad (E.5)$$

2500 The constraints determining c_j – for $j = 1, 2, 3$ – are chosen as:

$$x(0) = 1 \quad (E.6)$$

2501

$$x(\pi) = -1 \quad (E.7)$$

2502

$$x\left(\frac{\pi}{2}\right) = -\delta \quad (E.8)$$

2503

$$x_{\alpha\alpha}(\pi) = 0.3 \cdot (1 - \delta^2) \quad (E.9)$$

2504 The last constraint, which is related to the surface curvature at $\alpha = \pi$, is chosen to
2505 make sure that the surface is always convex. A trial and error empirical fit resulted
2506 in the choice $x_{\alpha\alpha}(\pi) = 0.3 \cdot (1 - \delta^2)$. The constraint relations are easily evaluated and
2507 then solved, leading to values for the c_j ,

$$c_0 = -\frac{\delta}{2} \quad (E.10)$$

2508

$$c_1 = g \quad (E.11)$$

2509

$$c_2 = \frac{\delta}{2} \quad (E.12)$$

2510

$$c_3 = 1 - g \quad (E.13)$$

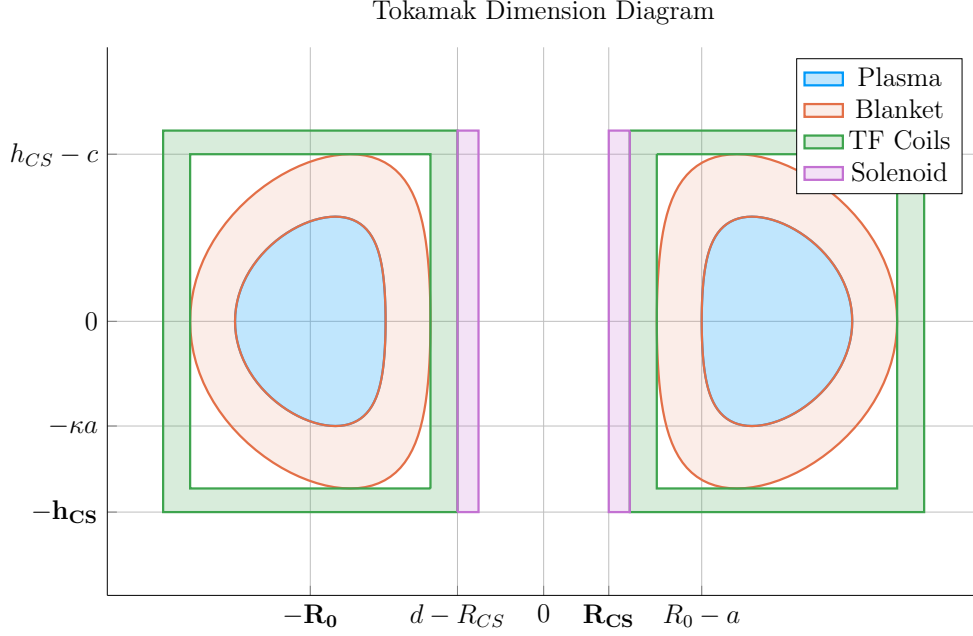


Figure E-2: Dimensions of Tokamak Cross-Section

Here, g is a shaping parameter approximately equal to one:

$$g = \frac{9 - 2\delta - 0.3 \cdot (1 - \delta^2)}{8} \quad (\text{E.14})$$

E.2 Cross-sectional Area and Volume

The plasma cross-sectional area and volume can be evaluated by straightforward calculations,

$$\begin{aligned} A &= \int \int dR dZ = a^2 \int \int dx dy = a^2 \int_0^{2\pi} x \frac{dy}{d\alpha} d\alpha \\ &= \pi a^2 \kappa g \end{aligned} \quad (\text{E.15})$$

$$\begin{aligned} V &= \int \int \int R dR dZ d\Phi = 2\pi a^2 \int \int R dx dy \\ &= 2\pi a^2 R_0 \int_0^{2\pi} \left(x + \epsilon \frac{x^2}{2} \right) \frac{dy}{d\alpha} d\alpha \approx 2\pi a^2 R_0 \int_0^{2\pi} x \frac{dy}{d\alpha} d\alpha \\ &= 2\pi^2 R_0 a^2 \kappa g \end{aligned} \quad (\text{E.16})$$

2516 The second form of the volume integral makes use of the small inverse aspect ratio
 2517 expansion, $\epsilon \ll 1$, which is a good approximation and used throughout the analysis.

2518 E.3 Surface and Volume Integrals

2519 Eqs. (E.4) and (E.5) are simple formulas describing the shape of the outer plasma
 2520 surface. We next modify the model so that it gives a plausible description of the
 2521 interior flux surfaces as well. The idea is to introduce a normalized flux label, which
 2522 is radial-like in behavior. This label is denoted by ρ and $\rho \in [0, 1]$ with $\rho = 1$ being
 2523 the outer plasma surface (i.e. the 95% surface) and $\rho = 0$ being the magnetic axis.
 2524 Additional trial and error results in the following representation for the flux surfaces,

$$x(\rho, \alpha) = \sigma(1 - \rho^2) + c_0\rho^4 + c_1\rho \cos(\alpha) + c_2\rho^2 \cos(2\alpha) + c_3\rho^3 \cos(3\alpha) \quad (\text{E.17})$$

2525

$$y(\rho, \alpha) = \kappa\rho \sin(\alpha) \quad (\text{E.18})$$

2526 with σ being the shift of the magnetic axis. Usually, $\sigma \sim 0.1$ for a high field tokamak.
 2527 Lastly, we note that in the course of the work it will be necessary to integrate functions
 2528 of ρ over the volume and cross-sectional area of the plasma. Specifically we will need
 2529 to evaluate:

$$Q_V = \int \int \int Q(\rho) R dR dZ d\Phi \approx 2\pi R_0 a^2 \int \int Q(\rho) dx dy \quad (\text{E.19})$$

2530

$$Q_A = \int \int Q(\rho) dR dZ = a^2 \int \int Q(\rho) dx dy \quad (\text{E.20})$$

2531 Here, $Q(\rho)$ is an arbitrary function of ρ such as pressure or temperature. In the large
 2532 aspect ratio limit, both integrals require the evaluation of the same quantity:

$$K = \int \int Q(\rho) dx dy \quad (\text{E.21})$$

2533 To evaluate this integral, we need to convert from x, y coordinates to ρ, α coordinates.

2534 Using the Jacobian of the transformation leads to

$$K = \int \int Q(\rho)(x_\rho y_\alpha - x_\alpha y_\rho) d\rho d\alpha \quad (\text{E.22})$$

2535 Here,

$$\begin{aligned} x_\rho y_\alpha - x_\alpha y_\rho = & \kappa \sin(\alpha) \cdot (c_1 \rho \sin(\alpha) + 2c_2 \rho^2 \sin(2\alpha) + 3c_3 \rho^3 \sin(3\alpha)) \\ & + \kappa \rho \cos(\alpha) \cdot \left[\right. \\ & \quad - 2\rho\sigma + 4\rho^3 c_0 + c_1 \cos(\alpha) \\ & \quad + 2c_2 \rho \cos(2\alpha) + 3c_3 \rho^2 \cos(3\alpha) \\ & \left. \right] \end{aligned} \quad (\text{E.23})$$

2536 Since Q is only a function of ρ , the α integral can be carried out analytically. The
 2537 only term that survives the averaging are the ones containing c_1 . A simple integration
 2538 over α then yields the desired results:

$$Q_V = 4\pi^2 R_0 a^2 \kappa g \int_0^1 Q(\rho) \rho d\rho \quad (\text{E.24})$$

2539

$$Q_S = 2\pi a^2 \kappa g \int_0^1 Q(\rho) \rho d\rho \quad (\text{E.25})$$

2540

2541 Appendix F

2542 Expanding on the Bootstrap Current

2543 The bootstrap current fraction – f_{BS} – is an important parameter that enters in
2544 the design of tokamak reactors. It must be calculated with reasonable accuracy to
2545 determine how much external current drive is required. The value of f_{BS} thus has
2546 a strong impact on the overall fusion energy gain. Obtaining reasonable accuracy
2547 requires a moderate amount of analysis, which is presented in a following section.
2548 The results are summarized below.

2549 F.1 Summarized Results

2550 The analysis is based on an expression for the bootstrap current valid for arbitrary
2551 cross section assuming (1) equal temperature electrons and ions $T_e = T_i = T$, (2) large
2552 aspect ratio $\epsilon \ll 1$, and (3) negligible collisionality $\nu_* \rightarrow 0$. Under these assumptions
2553 the bootstrap current $\mathbf{J}_{BS} \approx J_{BS} \mathbf{e}_\phi$ has the form

$$J_{BS} = -3.32 f_T R_0 n T \left(\frac{1}{n} \frac{dn}{d\psi} + 0.054 \frac{1}{T} \frac{dT}{d\psi} \right) \quad (\text{F.1})$$

2554 Here, $f_T \approx 1.46(r/R_0)^{1/2}$ is an approximate expression for the trapped particle frac-
2555 tion and ψ is the poloidal flux.

2556 The analysis next section shows that Eq. (F.1) leads to an expression for the bootstrap
 2557 fraction, assuming for simplicity elliptical flux surfaces, that can be written as:

$$f_{BS} = \frac{I_{BS}}{I} = \frac{2\pi a^2 \kappa}{I} \int_0^1 J_{BS} \rho d\rho = \frac{K_{BS}}{K_n} \frac{\bar{n} \bar{T} R_0^2}{I_P^2} \quad (\text{F.2})$$

2558

$$K_{BS} = 4.879 \cdot K_n \cdot \left(\frac{1 + \kappa^2}{2} \right) \cdot \epsilon^{5/2} \cdot H_{BS} \quad (\text{F.3})$$

2559

$$H_{BS} = (1 + \nu_n)(1 + \nu_T)(\nu_n + 0.054\nu_T) \int_0^1 \frac{\rho^{5/2} (1 - \rho^2)^{\nu_n + \nu_T - 1}}{b_p} d\rho \quad (\text{F.4})$$

2560

$$b_p(\rho) = \frac{-e^{\gamma \rho^2} (\gamma \rho^2 - 1 - \gamma) - 1 - \gamma}{\rho (e^\gamma - 1 - \gamma)} \quad (\text{F.5})$$

2561

$$\bar{J}_\phi(\rho) = -\frac{I}{\pi a^2 \kappa} \left[\frac{\gamma^2 (1 - \rho^2) e^{\gamma \rho^2}}{e^\gamma - 1 - \gamma} \right] \quad (\text{F.6})$$

2562 In this expression b_p is a normalized form of the poloidal magnetic field derived from
 2563 a prescribed model for the *total* flux surface averaged current density profile $\bar{J}_\phi(\rho)$.
 2564 The $\bar{J}_\phi(\rho)$ profile, in analogy with the density and temperature profiles, is not self-
 2565 consistent but is chosen to have a plausible experimental shape characterized by the
 2566 parameter γ . The profile can have either an on-axis ($\gamma < 1$) or off-axis peak ($\gamma > 1$).
 2567 The normalized internal inductance l_i and radial location of the current peak ρ_m are
 2568 related to the value of γ by:

$$\frac{4\kappa}{1 + \kappa^2} \int_0^1 b_p^2 \frac{d\rho}{\rho} \quad (\text{F.7})$$

2569

$$\rho_m = \begin{cases} \left(\frac{\gamma}{\gamma - 1} \right)^{1/2}, & \gamma > 1 \\ 0, & \gamma < 1 \end{cases} \quad (\text{F.8})$$

2570 F.2 Detailed Analysis

2571 The starting point for the analysis is the general expression for the bootstrap current
 2572 in a tokamak with arbitrary cross section.³⁰ This expression can be simplified by

2573 assuming (1) equal temperature electrons and ions $T_e = T_i = T$, (2) large aspect ratio
 2574 $\epsilon \ll 1$, and (3) negligible collisionality $\nu_* \rightarrow 0$. The bootstrap current $\mathbf{J}_{BS} \approx J_{BS} \mathbf{e}_\phi$
 2575 reduces to

$$J_{BS} = -3.32 f_T R_0 n T \left(\frac{1}{n} \frac{dn}{d\psi} + 0.054 \frac{1}{T} \frac{dT}{d\psi} \right) \quad (\text{F.9})$$

2576 Several values of the trapped particle fraction f_T have been given in the literature.³¹
 2577 For simplicity we use a form valid for large aspect ratio. This is a slightly optimistic
 2578 value but saves a large amount of detailed calculation. It can be written as,

$$f_T \approx 1.46 (r/R_0)^{1/2} = 1.46 \epsilon^{1/2} \rho^{1/2} \quad (\text{F.10})$$

2579 Here, as in the main text, ρ is a radial-like flux surface label that varies between
 2580 $0 \leq \rho \leq 1$. In other words $\psi = \psi(\rho)$. Under these assumptions the bootstrap current
 2581 reduces to:

$$J_{BS} = -4.85 R_0 \epsilon^{1/2} \left(\frac{\rho^{1/2} n T}{d\psi/d\rho} \right) \left(\frac{1}{n} \frac{dn}{d\rho} + 0.054 \frac{1}{T} \frac{dT}{d\rho} \right) \quad (\text{F.11})$$

2582 Since we have specified profiles for $n(\rho)$ and $T(\rho)$ all that remains in order to be able
 2583 to evaluate $J_{BS}(\rho)$ is to determine $\psi' = d\psi/d\rho$. Keep in mind that at this point, in
 2584 spite of the approximations that have been made, the expression for $J_{BS}(\rho)$ is still
 2585 valid for arbitrary cross section.

2586 The analysis that follows shows how to calculate ψ' for an arbitrary cross section
 2587 including finite aspect ratio. As an example an explicit expression for large aspect
 2588 ratio, finite elongation ellipse is obtained. Consider the Grad-Shafranov equation for
 2589 the flux: $\Delta^* \psi = -\mu_0 R J_\psi$. We integrate this equation over the volume of an arbitrary
 2590 flux surface making use of Gauss' theorem, which leads to:

$$\int_S \frac{\mathbf{n} \cdot \nabla \psi}{R^2} dS = -\mu_0 \int_V \frac{J_\phi}{R} d\mathbf{r} \quad (\text{F.12})$$

2591 Next, assume that the coordinates of the flux surface can be expressed in terms of ρ
 2592 and an angular-like parameter α with $0 \leq \alpha \leq 2\pi$. In other words, the flux surface

2593 coordinates can be written as $R = R(\rho, \alpha) = R_0 + ax(\rho, \alpha)$ and $Z = Z(\rho, \alpha) =$
 2594 $ay(\rho, \alpha)$. The functions $R(\rho, \alpha)$ and $Z(\rho, \alpha)$ are assumed to be known. The term on
 2595 the left hand side can be evaluated by noting that

$$dl = dlt \quad (\text{F.13})$$

2596

$$dl = (R_\alpha^2 + Z_\alpha^2)^{1/2} d\alpha \quad (\text{F.14})$$

2597

$$\mathbf{t} = \frac{R_\alpha \mathbf{e}_R + Z_\alpha \mathbf{e}_Z}{(R_\alpha^2 + Z_\alpha^2)^{1/2}} \quad (\text{F.15})$$

2598

$$\mathbf{n} = \mathbf{e}_\phi \times \mathbf{t} = \frac{Z_\alpha \mathbf{e}_R - R_\alpha \mathbf{e}_Z}{(R_\alpha^2 + Z_\alpha^2)^{1/2}} \quad (\text{F.16})$$

2599

$$dS = Rd\phi dl = 2\pi R(R_\alpha^2 + Z_\alpha^2)^{1/2} d\alpha \quad (\text{F.17})$$

2600 It then follows that

$$\mathbf{n} \cdot \nabla \psi = \frac{1}{(R_\alpha^2 + Z_\alpha^2)^{1/2}} \left(Z_\alpha \frac{\partial \psi}{\partial R} - R_\alpha \frac{\partial \psi}{\partial Z} \right) = \frac{1}{(R_\alpha^2 + Z_\alpha^2)^{1/2}} \frac{d\psi}{d\rho} Z_\alpha \rho_R - R_\alpha \rho_Z \quad (\text{F.18})$$

2601 We can rewrite the last term by noting that

$$\begin{aligned} dR = R_\rho d\rho + R_\alpha d\alpha &\rightarrow d\rho = (Z_\alpha dR - R_\alpha dZ) / (R_\rho Z_\alpha - R_\alpha Z_\rho) \\ dZ = Z_\rho d\rho + Z_\alpha d\alpha &\rightarrow d\alpha = (-Z_\rho dR + R_\rho dZ) / (R_\rho Z_\alpha - R_\alpha Z_\rho) \end{aligned} \quad (\text{F.19})$$

2602 from which follows

$$\begin{aligned} \rho_R &= \frac{Z_\alpha}{(R_\rho Z_\alpha - R_\alpha Z_\rho)} \\ \rho_Z &= -\frac{R_\alpha}{(R_\rho Z_\alpha - R_\alpha Z_\rho)} \end{aligned} \quad (\text{F.20})$$

2603 the normal gradient reduces to

$$\mathbf{n} \cdot \nabla \psi = \frac{R_\alpha^2 + Z_\alpha^2}{(R_\rho Z_\alpha - R_\alpha Z_\rho)} \frac{d\psi}{d\rho} \quad (\text{F.21})$$

2604 Using this relation we see that the left hand side of Eq. (F.12) can now be written as:

$$\int_S \frac{\mathbf{n} \cdot \nabla \psi}{R^2} dS = 2\pi \frac{d\psi}{d\rho} \int_0^{2\pi} \frac{R_\alpha^2 + Z_\alpha^2}{(R_\rho Z_\alpha - R_\alpha Z_\rho)} \frac{d\alpha}{R} \quad (\text{F.22})$$

2605 Consider now the right hand side of Eq. (F.12). The critical assumption is that the
 2606 current density is approximated by its flux surface averaged value, $J_\phi(\rho, \alpha) \approx \bar{J}_\phi(\rho)$.
 2607 This is obviously not self-consistent with the Grad-Shafranov equation. Even so, it
 2608 should suffice for present purposes where we only need to evaluate global volume
 2609 integrals. Also, in the same spirit as prescribing $n(\rho)$ and $T(\rho)$ we assume that $\bar{J}_\phi(\rho)$
 2610 is also prescribed. Under these assumptions the right hand side of Eq. (F.12) simplifies
 2611 to:

$$\begin{aligned} -\mu_0 \int_V \frac{J_\phi}{R} d\mathbf{r} &= -2\pi\mu_0 \int_A J_\phi dA \\ &= -2\pi\mu_0 \int_0^\rho d\rho \int_0^{2\pi} J_\phi (R_\rho Z_\alpha - R_\alpha Z_\rho) d\alpha \\ &\approx -2\pi\mu_0 \int_0^\rho d\rho \left[\bar{J}_\phi \int_0^{2\pi} (R_\rho Z_\alpha - R_\alpha Z_\rho) d\alpha \right] \end{aligned} \quad (\text{F.23})$$

2612 Combining the results in Eqs. (F.22) and (F.23) leads to the required general expres-
 2613 sion for $d\psi/d\rho$,

$$\frac{d\psi}{d\rho} \int_0^{2\pi} \frac{R_\alpha^2 + Z_\alpha^2}{(R_\rho Z_\alpha - R_\alpha Z_\rho)} \frac{d\alpha}{R} = -\mu_0 \int_0^\rho d\rho \left[\bar{J}_\phi \int_0^{2\pi} (R_\rho Z_\alpha - R_\alpha Z_\rho) d\alpha \right] \quad (\text{F.24})$$

2614 Next, to help specify a plausible choice for \bar{J}_ϕ it is useful to define the kink safety
 2615 factor and the actual local safety factor. The kink safety factor is defined by

$$q_* = \frac{2\pi a^2 B_0}{\mu_0 R_0 I} \left(\frac{1 + \kappa^2}{2} \right) \quad (\text{F.25})$$

2616 where

$$I = \int J_o dA = \int_0^1 d\rho \left[\bar{J}_o \int_0^{2\pi} (R_\rho Z_\alpha - R_\alpha Z_\rho) d\alpha \right] \quad (\text{F.26})$$

2617 This leads to

$$\frac{1}{q_*} = \frac{\mu_0 R_0}{2\pi a^2 B_0} \left(\frac{2}{1 + \kappa^2} \right) \int_0^1 d\rho \left[\bar{J}_\phi \int_0^{2\pi} (R_\rho Z_\alpha - R_\alpha Z_\rho) d\alpha \right] \quad (\text{F.27})$$

2618 Similarly, the local safety factor can be expressed as

$$q(\rho) = \frac{F(\rho)}{2\pi} \int \frac{dl}{RB_p} \quad (\text{F.28})$$

2619 Here, $F(\rho) = RB_o$. Substituting $RB_p = \mathbf{n} \cdot \nabla \psi$ then yields

$$q(\rho) = \frac{F(\rho)}{2\pi \psi'} \int_0^{2\pi} \frac{1}{R} (R_\rho Z_\alpha - R_\alpha Z_\rho) d\alpha \quad (\text{F.29})$$

2620 with $\psi' = d\psi/d\rho$.

2621 For present purposes we can obtain relatively simple analytic expressions for all the
 2622 quantities of interest by assuming the flux surfaces are concentric ellipses, character-
 2623 ized by $R = R_0 + a\rho \cos \alpha$ and $Z = \kappa a\rho \sin \alpha$. We assume low β so that $F(\rho) \approx R_0 B_0$.
 2624 This model accounts for elongation but neglects the effects of triangularity and finite
 2625 aspect ratio. The derivatives in Eqs. (F.24), (F.27) and (F.29) can now be easily
 2626 evaluated. Also, after some trial and error we chose $\bar{J}_\phi(\rho)$ to be a plausible profile
 2627 which is peaked off-axis at $\rho = \rho_m$.

$$\bar{J}_\phi(\rho) = -\frac{I}{\pi a^2 \kappa} \left[\frac{\gamma^2 (1 - \rho^2) e^{\gamma \rho^2}}{e^\gamma - 1 - \gamma} \right] \quad (\text{F.30})$$

2628 Here, $\gamma = 1/(1 - \rho_m^2)$.

2629 These profiles are substituted into Eq. (F.24) after which each of the integrals can be
 2630 evaluated analytically. A straightforward calculation yields:

$$\begin{aligned}
\rho \frac{d\psi}{d\rho} &= -2\mu_0 R_0 a^2 \left(\frac{\kappa^2}{1 + \kappa^2} \right) \int_0^\rho \bar{J}_\phi \rho d\rho \\
&= \frac{\mu_0 R_0 I}{\pi} \left(\frac{\kappa}{1 + \kappa^2} \right) \frac{(1 + \gamma - \gamma \rho^2) e^{\gamma \rho^2} - 1 - \gamma}{e^\gamma - 1 - \gamma}
\end{aligned} \tag{F.31}$$

2631 The safety factors are given by

$$\begin{aligned}
\frac{1}{q_*} &= \frac{\psi'(1)}{\kappa a^2 B_0} \\
\frac{q(\rho)}{q_*} &= \frac{\rho \psi'(1)}{\psi'(\rho)}
\end{aligned} \tag{F.32}$$

2632 Eq. (F.31) is now substituted into the expression for the bootstrap current given by
2633 Eq. (F.11). The resulting expression can then be integrated over the plasma cross
2634 section to yield the bootstrap fraction. A straightforward calculation leads to:

$$f_{BS} = \frac{I_{BS}}{I} = \frac{2\pi a^2 \kappa}{I} \int_0^1 J_{BS} \rho d\rho = \frac{K_{BS}}{K_n} \frac{\bar{n} \bar{T} R_0^2}{I_P^2} \tag{F.33}$$

2635

$$K_{BS} = 4.879 \cdot K_n \cdot \left(\frac{1 + \kappa^2}{2} \right) \cdot \epsilon^{5/2} \cdot H_{BS} \tag{F.34}$$

2636

$$H_{BS} = (1 + \nu_n)(1 + \nu_T)(\nu_n + 0.054\nu_T) \int_0^1 \frac{\rho^{5/2} (1 - \rho^2)^{\nu_n + \nu_T - 1}}{b_p} d\rho \tag{F.35}$$

2637

$$b_p(\rho) = \frac{-e^{\gamma \rho^2} (\gamma \rho^2 - 1 - \gamma) - 1 - \gamma}{\rho (e^\gamma - 1 - \gamma)} \tag{F.36}$$

2638 This is the desired result.

Bibliography

- [1] P J Knight and M D Kovari. A User Guide to the PROCESS Fusion Reactor Systems Code, 2016.
- [2] Martin Greenwald. Density limits in toroidal plasmas, 2002.
- [3] M Kovari, R Kemp, H Lux, P Knight, J Morris, and D J Ward. " PROCESS " : A systems code for fusion power plants—Part 1: Physics. *Fusion Engineering and Design*, 89(12):3054–3069, 2014.
- [4] Meszaros et al. Demo I Input File.
- [5] W Biel, M Beckers, R Kemp, R Wenninger, and H Zohm. Systems code studies on the optimization of design parameters for a pulsed DEMO tokamak reactor, 2016.
- [6] C E Kessel, M S Tillack, F Najmabadi, F M Poli, K Ghantous, N Gorelenkov, X R Wang, D Navaei, H H Toudeshki, C Koehly, L El-Guebaly, J P Blanchard, C J Martin, L Mynsburge, P Humrickhouse, M E Rensink, T D Rognlien, M Yoda, S I Abdel-Khalik, M D Hageman, B H Mills, J D Rader, D L Sadowski, P B Snyder, H. St. John, A D Turnbull, L M Waganer, S Malang, and A F Rowcliffe. The ARIES advanced and conservative tokamak power plant study. *Fusion Science and Technology*, 67(1):1–21, 2015.
- [7] Jeffrey P Freidberg. *Plasma Physics and Fusion Energy*, volume 1. 2007.
- [8] Stephen O Dean. Fusion Power by Magnetic Confinement Program Plan. Technical Report 4, 1998.
- [9] DOE. FY 1987 Congressional Budget Request. Technical report.
- [10] DOE. FY 2019 Congressional Budget Request. Technical report.
- [11] Marsha Freeman. The True History of The U.S. Fusion Program. Technical report, 2009.
- [12] D. G. Whytea, A E Hubbard, J W Hughes, B Lipschultz, J E Rice, E S Marmor, M Greenwald, I Cziegler, A Dominguez, T Golfinopoulos, N Howard, L. Lin,

2666 R. M. McDermottb, M Porkolab, M L Reinke, J Terry, N Tsujii, S Wolfe, S Wuk-
2667 itch, and Y Lin. I-mode: An H-mode energy confinement regime with L-mode
2668 particle transport in Alcator C-Mod. *Nuclear Fusion*, 50(10), 2010.

2669 [13] J. W. Connor, T Fukuda, X Garbet, C Gormezano, V Mukhovatov, M Wakatani,
2670 M. Greenwald, A. G. Peeters, F. Ryter, A. C.C. Sips, R. C. Wolf, E. J. Doyle,
2671 P. Gohil, C. M. Greenfield, J. E. Kinsey, E. Barbato, G. Bracco, Yu Baranov,
2672 A. Becoulet, P. Buratti, L. G. Ericsson, B. Esposito, T. Hellsten, F. Imbeaux,
2673 P. Maget, V. V. Parail, T Fukuda, T. Fujita, S. Ide, Y. Kamada, Y. Sakamoto,
2674 H. Shirai, T. Suzuki, T. Takizuka, G. M.D. Hogewei, Yu Esipchuk, N. Ivanov,
2675 N. Kirneva, K. Razumova, T. S. Hahm, E. J. Synakowski, T. Aniel, X Garbet,
2676 G. T. Hoang, X. Litaudon, J. Weiland, B. Unterberg, A. Fukuyama, K. Toi,
2677 S. Lebedev, V. Vershkov, and J. E. Rice. A review of internal transport barrier
2678 physics for steady-state operation of tokamaks, apr 2004.

2679 [14] K C Shaing, A Y Aydemir, W A Houlberg, and M C Zarnstorff. Theory
2680 of Enhanced Reversed Shear Mode in Tokamaks. *Physical Review Letters*,
2681 80(24):5353–5356, 1998.

2682 [15] David J. Griffiths. *Introduction to electrodynamics*.

2683 [16] D C McDonald, J G Cordey, K Thomsen, C Angioni, H Weisen, O J W F
2684 Kardaun, M Maslov, A Zabolotsky, C Fuchs, L Garzotti, C Giroud, B Kurzan,
2685 P Mantica, A G Peeters, and J Stober. Scaling of density peaking in H-mode
2686 plasmas based on a combined database of AUG and JET observations. *Nucl.*
2687 *Fusion*, 47:1326–1335, 2018.

2688 [17] T Onjun, G Bateman, A H Kritz, and G Hammett. Models for the pedestal
2689 temperature at the edge of H-mode tokamak plasmas. *Physics of Plasmas*, 9(10),
2690 2002.

2691 [18] G Saibene, L D Horton, R Sartori, and A E Hubbard. Physics and scaling of the
2692 H-mode pedestal The influence of isotope mass, edge magnetic shear and input
2693 power on high density ELMy H modes in JET Physics and scaling of the H-mode
2694 pedestal. *Control. Fusion*, 42:15–35, 2000.

2695 [19] J Jacquinet,) Jet, S Putvinski,) Jct, G Bosia, Jct), A Fukuyama, U) Okayama,
2696 R Hemsworth, Cea Cadarache), S Konovalov, Rrc Kurchatov), W M Nevins,
2697 Lnl), F Perkins, K A Rasumova, Rrc-) Kurchatov, F Romanelli, Enea-) Frascati,
2698 K Tobita, Jaeri), K Ushigusa, J W Van, U Dam, V Texas), Rrc Vdovin,
2699 S Kurchatov), R Zweben, Erm Koch, Kms-) Brussels, J.-G Wégrowe, Cea-)
2700 Cadarache, V V Alikaev, B Beaumont, A Bécoulet, S Bern-Abei, Pppl), V P
2701 Bhatnagar, Ec Brussels), S Brémond, and M D Carter. Chapter 6: Plasma
2702 auxiliary heating and current drive. *ITER Physics Basis Editors Nucl. Fusion*,
2703 39, 1999.

2704 [20] D A Ehst and C F F Karney. Approximate formula for radiofrequency current
2705 drive efficiency with magnetic trapping, 1991.

- [21] Tobias Hartmann, Thomas Hamacher, Hon-Prof rer nat Hartmut Zohm, and Hon-Prof rer nat Sibylle Günter. Development of a Modular Systems Code to Analyse the Implications of Physics Assumptions on the Design of a Demonstration Fusion Power Plant.
- [22] B Labombard, E Marmar, J Irby, T Rognlien, and M Umansky. ADX: a high field, high power density, advanced divertor and RF tokamak Nuclear Fusion. Technical report, 2017.
- [23] J P Freidberg, F J Mangiarotti, and J Minervini. Designing a tokamak fusion reactor - How does plasma physics fit in? *Physics of Plasmas*, 22(7):070901, 2015.
- [24] B. N. Sorbom, J. Ball, T. R. Palmer, F. J. Mangiarotti, J. M. Sierchio, P. Bonoli, C. Kasten, D. A. Sutherland, H. S. Barnard, C. B. Haakonsen, J. Goh, C. Sung, and D. G. Whyte. ARC: A compact, high-field, fusion nuclear science facility and demonstration power plant with demountable magnets. *Fusion Engineering and Design*, 100:378–405, nov 2015.
- [25] S P Hirshman and G H Neilson. External inductance of an axisymmetric plasma. *Physics of Fluids*, 29(3):790–793, 1986.
- [26] D P Schissel and B B Mcharg. Data Analysis Infrastructure at the Diii-D National Fusion Facility. (October), 2000.
- [27] Jeff P Freidberg, Antoin Cerfon, and Jungpyo Lee. Tokamak elongation: how much is too much? I Theory. *arXiv.org*, pages 1–34, 2015.
- [28] H Bosch and G M Hale. Improved formulas for fusion cross-sections and thermal reactivities. 611.
- [29] Zachary S Hartwig and Yuri A Podpaly. Magnetic Fusion Energy Formulary. Technical report, 2014.
- [30] John Wesson and David J Campbell. *Tokamaks*, volume 149. Oxford University Press, 2011.
- [31] C. E. Kessel. Bootstrap current in a tokamak. *Nuclear Fusion*, 34(9):1221–1238, 1994.